IDŐJÁRÁS

QUARTERLY JOURNAL OF THE HUNGAROMET
HUNGARIAN METEOROLOGICAL SERVICE

CONTENTS

VOL. 128 * NO. 4 * OCTOBER – DECEMBER 2024

IDŐJÁRÁS

Quarterly Journal of the HungaroMet Hungarian Meteorological Service

Editorial Office: Kitaibel P.u. 1, H-1024 Budapest, Hungary
P.O. Box 38, H-1525 Budapest, Hungary
E-mail: journal.idojaras@met.hu

Indexed and abstracted in Science Citation Index Expanded™ and Journal Citation Reports/Science Edition
Covered in the abstract and citation database SCOPUS®
Included in EBSCO's database

Subscription by mail:
IDŐJÁRÁS, P.O. Box 38, H-1525 Budapest, Hungary
E-mail: journal.idojaras@met.hu

DOI:10.28974/idojaras.2024.4.1

IDŐJÁRÁS

Quarterly Journal of the HungaroMet Hungarian Meteorological Service
Vol. 128, No. 4, October – December, 2024, pp. 399–423

Potential of remote sensing techniques for integrated spatio-temporal monitoring and analysis of drought in the Sana River basin, Bosnia and Herzegovina

Luka Sabljić [1,*], **Tin Lukić** [2], **Slobodan B. Marković**[2,3,4,5], and **Davorin Bajić** [1]

[1]*University of Banja Luka,*
Faculty of Natural Sciences and Mathematics
Mladena Stojanovića 2, 78000 Banja Luka, Bosnia and Herzegovina

[2]*University of Novi Sad,*
Faculty of Natural Sciences,
Department of Geography, Tourism and Hotel Management
Trg Dositeja Obradovića 3, 21000 Novi Sad, Serbia

[3]*Serbian Academy of Sciences and Arts,*
Kneza Mihaila 35, 11000 Belgrade, Serbia

[4]*University of Technology,*
Institute of Physics – Centre for Science and Education,
Division of Geochronology and Environmental Isotopes,
Konarskiego 22b, 44100 Gliwice, Poland

[5]*University of Montenegro,*
Faculty of Philosophy,
Danila Bojovića bb, 81400 Nikšić, Montenegro

[*]*Corresponding author E-mail: luka.sabljic@pmf.unibl.org*

(Manuscript received in final form February 19, 2024)

Abstract— The subject of the research paper is the exploration of the potential of remote sensing techniques for enhanced spatio-temporal monitoring and analysis of drought impacts within the Sana River basin area in Bosnia and Herzegovina (B&H). The aim is to identify meteorological, hydrological, agricultural, and socio-economic drought occurrences by processing remote sensing "products". An integral part of this aim involves calculating the standardized precipitation index (SPI), temperature condition index (TCI), vegetation condition index (VCI), and vegetation health index (VHI). Meteorological drought monitoring was carried out using the Climate Hazards Group InfraRed Precipitation with Station Data (CHIRPS) dataset processed through the Google Earth Engine (GEE) platform. A 42-year period (1981–2023) was compared with reference years

(2016 and 2017). The occurrence of meteorological drought (lack of precipitation) was identified, and SPI was calculated. The period with reduced precipitation and negative SPI values during 2016 and 2017 coincided with the pattern of decreasing water levels in the main stream of the Sana River, confirming the impact of meteorological drought on the occurrence of hydrological drought. Agricultural drought monitoring was conducted using Moderate Resolution Imaging Spectroradiometer (MODIS) satellite data, namely MOD13Q1 and MOD11A2, to calculate TCI, VCI, and VHI. The results indicate negligible drought occurrence for 2016, while extreme agricultural drought was observed in the basin area for 2017. The consequences of agricultural drought on the occurrence of socio-economic drought were examined. The results show an extreme decrease in yields of wheat, barley, corn, potatoes, pears, and plums during 2017 compared to 2016. The research contributes to a better spatio-temporal understanding of drought phenomena, and the presented data and results are significant for numerous practical issues related to monitoring, mitigation, and/or prevention of negative consequences of drought in river basin areas.

Key-words: drought, hazard, remote sensing, geographic information systems, mapping, Sana River basin, Bosnia and Herzegovina.

1. Introduction

Drought is an exceptionally complex natural disaster (*Xie* and *Li*, 2020a). According to *Hao* and *Singh* (2015) and *Dong et al.* (2022), drought is one of the most common natural disasters in terrestrial ecosystems, characterized by wide coverage, frequent occurrences, and negative impacts, which directly or indirectly cause significant economic losses at regional and global levels. Drought leads to widespread exhaustion of natural and artificial water resources over an extended period (*Rossi*, 2000). Over the past few decades, under the influence of climate change, the impact of drought on agriculture, economy, and society has intensified (*Council*, 1992; *Wilhite et al.*, 2007; *Orimoloye*, 2022). Drought leads to a negative impact on agricultural productivity, desertification, forest degradation, and other socio-economic problems (*Li et al.*, 2020a,b; *Xie* and *Li*, 2020b).

Depending on the type of drought, its impacts vary in space and time (*Žurovec et al*., 2017). According to *Wilhite* (1985), the following types of droughts exist: meteorological, hydrological, agricultural, and socio-economic. Meteorological droughts are closely related to reduced or lack of precipitation (*Wilhite*, 2000; *Gabrić* and *Plavšić*, 2019). According to *Liu et al.* (2023), meteorological drought, caused by insufficient precipitation, high temperatures, and significant evapotranspiration, can lead to water shortages, manifested through soil moisture deficits. Traditional monitoring of meteorological drought relies on meteorological data from meteorological stations (MS) (*Robock et al.*, 2000; *Hashim* et al., 2016). However, in areas with disparate distribution of MS, access to long-term and reliable data for monitoring meteorological drought is limited (*Tan et al*., 2017; *Tian et al.*, 2018). Uneven spatial distribution of MS and discontinuous precipitation data trends are characteristic of developing countries,

such as Bosnia and Herzegovina (B&H). Consequently, there is a shortage of research concerning meteorological droughts within the borders of B&H, particularly related to specific geographic environments. The lack of an adequate number and uneven distribution of MS can be overcome by an alternative approach using satellite meteorological data. According to *Ezzine et al.* (2014) and *Tang et al*. (2020), satellite meteorological data offer the possibility of identifying conditions for drought occurrence on various surfaces, as well as suitability for monitoring large-scale droughts in real-time with high accuracy and implementation. *Zhu et al.* (2019) highlight the abundance of various satellite precipitation data and their wide application in meteorological drought analysis (*Gao et al*., 2018; *Tladi et al.*, 2022; *Feng et al.*, 2023; *Kourtis et al*., 2023; *Torres-Vázquez et al.*, 2023; *Zhang et al*., 2023; *Oukaddour* et al., 2024). According to the authors of this study, satellite meteorological data have not been used to investigate meteorological drought in the territory of B&H thus far. According to *Wilhite* (2000), meteorological drought can act as a "trigger" for the occurrence of other types of droughts. *Lee et al.* (2022) emphasize that this type of drought directly influences the occurrence of hydrological drought. The mentioned drought is traditionally detected through field observations of river flow, surface or groundwater levels, providing direct evidence of water scarcity (*Nalbantis* and *Tsakiris*, 2009; *Zhu et al.*, 2016).

According to *Spinoni et al.* (2018), there is an established consensus about recent trends of meteorological and hydrological droughts in Europe: in the last decades, southern Europe experienced increasing drought frequency and severity (*Briffa et al*., 2009; *Vicente-Serrano* et al., 2014; *Gudmundsson* and *Seneviratne*, 2015; *Spinoni et al.*, 2015a,b), with the Mediterranean region as a hotspot (*Hoerling et al.*, 2012), especially in spring and summer (*Spinoni et al*., 2017). Drought has been present several times in the territory of B&H during the past two decades (*Žurovec et al*., 2017). During the period from 2000 to 2021, extreme drought occurred eight times: in 2003, 2007, 2011, 2012, 2013, 2015, 2016, and 2017 (*Trbić et al*., 2022). *Trbić et al*. (2013) emphasize that in the future, a greater number of hot/tropical days, along with reduced precipitation and the occurrence of dryness or aridity, will increase the likelihood of drought in the territory of B&H. In this regard, the negative impacts of droughts observed in the past may be significant for the future, making areas where more frequent severe droughts are expected a very important subject of research (*Spinoni et al*., 2018).

Meteorological and hydrological droughts, intensified by high temperatures, contribute to soil moisture deficits, thereby causing agricultural drought (*Liu et al*., 2016). *Wilhite* (2000) emphasizes that due to soil moisture deficits, agriculture is the first economic sector affected by drought, especially if the period of moisture deficiency is accompanied by high temperatures and windy conditions. By processing remote sensing "products" in the form of satellite imagery, it is possible to generate various indices for monitoring agricultural drought. Specifically, *Yoon et al*. (2020) highlight that for the identification, monitoring,

and analysis of agricultural droughts, remote sensing-based indices have proven to be the most helpful supplementary data due to their simplicity, low cost of synoptic display, and reliability. The use of indices such as the normalized difference vegetation index (NDVI), temperature condition index (TCI), and vegetation condition index (VCI) for identifying agricultural drought is globally recognized (*Nicholson* and *Farrar*, 1994; *Kogan*, 1995a; *Seiler et al*., 2000; *Wang* et al., 2001). The uniqueness of these indicators lies in their autonomy from various environmental conditions (*Anyamba et al*., 2001; *Ji* and *Peters*, 2003), allowing for effective monitoring of agricultural drought in any geographic environment. Agricultural drought has a significant impact on reducing agricultural production and yields, leading to the manifestation of socio-economic drought, which, according to *Wilhite* and *Glantz* (1985), involves considering the effects that the mentioned drought has on the supply and demand of economic goods such as fruits, vegetables, grains, and meat.

The primary objective of this study is to improve drought monitoring in the Sana River basin (B&H) through the utilization of remote sensing techniques. This involves conducting integrated spatio-temporal analysis and exploring potential mitigation strategies. A fundamental part of this goal involves identifying meteorological and hydrological droughts, mapping agricultural drought as a causal consequence, and examining environmental impacts through the identification and monitoring of socio-economic drought. The research is based on the application of modern technologies such as Geographic Information Systems (GIS) and remote sensing. The presented methodology is significant for identifying and understanding drought as a natural disaster. The research results can be beneficial to relevant institutions in policy-making and planning activities in the areas of monitoring, prevention, and/or mitigation of the harmful effects of drought in the geographic environment.

2. Study area

The study area comprises the river basin of the Sana River, which stretches across the northwest of B&H [44.18° N – 45.09°N; 16.29° E – 17.09° E] (*Fig. 1*). The Sana River originates from three karstic sources on the border of the municipalities of Ribnik and Mrkonjić Grad. The mentioned river is a tributary of the Una River and belongs to the larger river basin of the Sava River with a surface participation of 3.55%. The length of the Sana River is 146 km, its source is located at an altitude of 414 m a. s. l., and its mouth at 122 m a. s. l. It is characterized by the Posavina variant of the pluvio-nival water regime, which is characterized by high water levels in April, and lower levels in August (*Gnjato*, 2018). Based on data from the hydrological station (HS) Prijedor (1961–2014), the highest flow rates on the Sana River were recorded in the spring season (119.7 m^3/s), and the lowest in the summer season (42.6 m^3/s). The total area of the river

basin according to the HydroSHEDS database (https://www.hydrosheds.org/) is 3470 km^2. The average elevation of the river basin is 505 m, while the average slope is 10.9°. Based on data from MS Novi Grad, Prijedor, Sanski Most, and Ribnik (1981–2023), the average annual precipitation in the river basin area is 1043.42 mm, while the average annual temperature is 11.09 °C. According to the Köppen-Geiger climate classification (*Kottek* et al., 2016), the Sana River basin belongs to the Cfb climate type, which is characterized by moderately cold winters and warm summers.

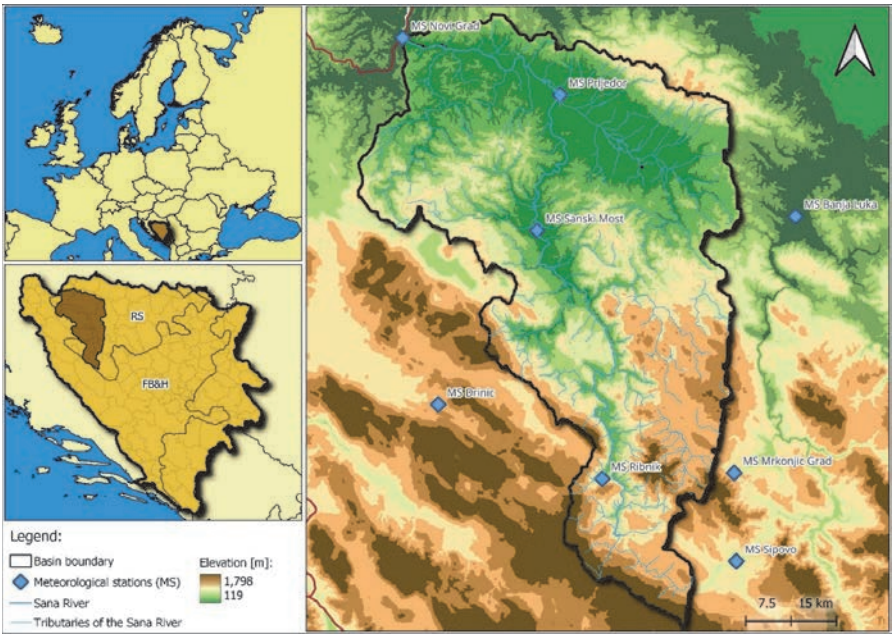

Fig. 1. Location of the study area with meteorological stations used in this study.

The Sana River basin extends across both entities in B&H: Republic of Srpska (RS) and the Federation of Bosnia and Herzegovina (FB&H). It partially or entirely covers the following municipalities in RS: Novi Grad, Kostajnica, Prijedor, Oštra Luka, Banja Luka, Ribnik, Mrkonjić Grad, Krupa on Una, as well as municipalities in FB&H: Bosanska Krupa, Sanski Most, and Ključ. According to the latest population census in B&H from 2013, these municipalities had a combined population of 454,000 inhabitants (*Agency for*

Statistics of Bosnia and Herzegovina, 2016), which also represents the total population in the basin area. Based on the Corine Land Cover database from 2018 (https://land.copernicus.eu/), concerning land use within the study area, built-up areas occupy 38.68 km^2, arable land covers 1514.09 km^2, forested areas cover 1830.82 km^2, and water bodies cover 21.79 km^2. The significant participation of arable land, accounting for 43.64% of the basin area, indicates that agriculture as the primary economic sector is exceptionally significant for the economic development of this geographical environment.

3. Methods and data

Monitoring drought in the research is based on processing remote sensing "products" in the form of satellite imagery. The Google Earth Engine (GEE) platform, based on cloud technology, was used for processing. In order to identify the period of meteorological drought within the research, satellite precipitation estimate data called Climate Hazards Group InfraRed precipitation with Station data (CHIRPS) were used. The mentioned data are of a global nature, with relatively high spatial resolution ($0.05^o \times 0.05^o \sim 5.3$ km) and long-term temporal coverage (1981 – almost real-time) (*Funk et al*., 2015). Before using CHIRPS data, they were validated based on data from the meteorological stations. The validity of CHIRPS data based on MS data has been confirmed in several studies (*Katsanos et al*., 2016; *Hsu et al.,* 2021; *Alsilibe et al*., 2023), and they have been used in drought analyses (*Rivera et al*., 2018; *Habitou et al*., 2020). At the study area level, CHIRPS data were previously validated in a research by *Sabljić et al.* (2023). According to the methodology of the mentioned authors, the validity assessment process involved comparing the average precipitation amount of CHIRPS and meteorological data from MS Prijedor and Sanski Most (1992–2022). In this research, and according to the mentioned methodology, during the validity assessment process, meteorological data from a larger number of MS stations were additionally taken into account, and a longer time period was observed (1981–2023). Meteorological data were obtained from the Republic Hydro-Meteorological Institute of the Republic of Srpska (RHMIRS) and the Federal Hydro-Meteorological Institute of the Federation of Bosnia and Herzegovina (FHMIFB&H). Meteorological data from MS stations located within the basin area were considered, as well as data from MS stations located in its immediate vicinity (*Table 1*). The reason for including MS stations located outside the basin boundaries is explained by the lack of such stations at higher elevations within the basin.

Table 1. MS stations whose data were used in the validity assessment process

Row number	Name	Location	Time period	Elevation (m)
1	Novi Grad	45°05’ N; 16°37’ E	1981–2023	122
2	Prijedor	44°97' N; 16°71' E	1981–2023	133
3	Banja Luka	44°79’ N; 17°20’ E	1981–2020	150
4	Sanski Most	44°46’ N; 16°42’ E	1981–2022	158
5	Ribnik	44°40’ N; 16°81’ E	2000–2023	293
6	Šipovo	44°28’ N; 17°09’ E	1999–2023	454
7	Mrkonjić Grad	44°41’ N; 17°08’ E	1981–2023	570
8	Drinić	44°50’ N; 16°46’ E	1981–2023	722

Meteorological drought is characterized by a lack of precipitation, and to establish its occurrence, a comparison is made between the 42-year average precipitation (1981–2023) and the average precipitation of reference years (2016 and 2017). Therefore, following the recommendations of the World Meteorological Organization, the meteorological element covering one full climatological cycle was observed (*Lukić et al.*, 2021). The aim of this process is to identify the time period during the reference years when the precipitation was below the 42-year average. The time period during which a lower amount of precipitation than the average is observed is characterized by the occurrence of meteorological drought.

The occurrence of meteorological drought was further analyzed by calculating the standardized precipitation index (*SPI*). This indicator, presented by *McKee et al.* (1993), represents the deviation *z* from the mean value in units of standard deviation. In the research, *SPI* was calculated based on CHIRPS precipitation data at the location of each pixel composite period for each year during the reference period (*Fig. 2*). The formula for calculating *SPI* is as follows:

$$SPI_{ijk} = \frac{\left(P_{ijk} - \overline{P_{ij}}\right)}{\sigma_{ij}}, \quad (1)$$

where SPI_{ijk} is the *z*-value for the pixel (*i*) during timeframe (*j*) for year (*k*), P_{ijk} is the precipitation value for pixel (*i*) during timeframe (*j*) for year (*k*), P_{ij} is the mean for pixel (*i*) during timeframe (*j*) over *n* years, and σ_{ij} is the standard deviation of pixel (*i*) during week (*j*) over *n* years.

Meteorological drought acts as a trigger for the occurrence of other types of droughts. Hydrological drought arises from meteorological drought (lack of precipitation), often developing slowly and lasting for months, with serious consequences for ecosystems, the environment, agricultural production, and water resource systems (*Van Loon*, 2015). Within the scope of the study, the impact of meteorological drought on the occurrence of hydrological drought was established

through the analysis of the water level of the main stream of the Sana River. The average mean water level on the main stream of the Sana River was calculated, incorporating data from the HS Prijedor and Sanski Most for the studied time period (2001–2019). The average mean water level of the 18-year period was compared with the average mean water level of the reference years (2016 and 2017). Months during which a lower average mean water level than the 18-year average was evident are characterized by the occurrence of hydrological drought.

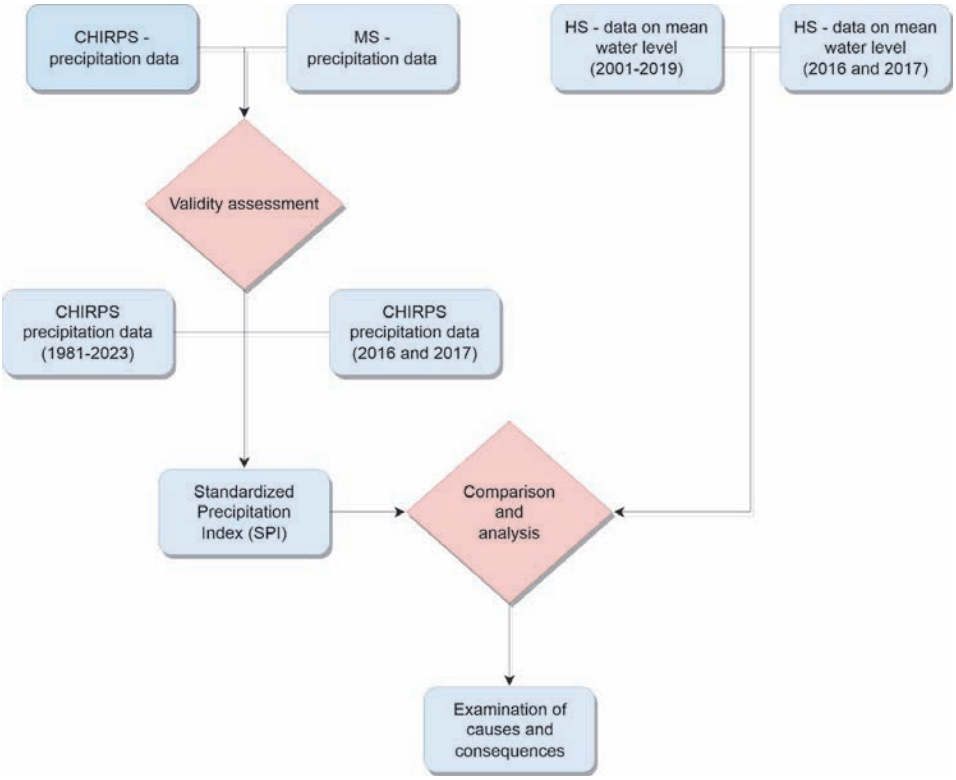

Fig. 2. Methodology for processing and monitoring meteorological and hydrological droughts.

The time periods characterized by clear differences in the amount of received precipitation, negative *SPI* values, as well as periods with significant decreases in the water level of the main stream of the Sana River, represent the basic temporal data for the process of identification and mapping of agricultural drought at the

study area level. The process of mapping agricultural drought is based on the computation of *TCI* and *VCI*, and the results of these indices are used to calculate *VHI* (*Fig. 3*). The mentioned indices are computed by processing remote sensing data in the form of satellite data through the GEE platform. In this regard, Moderate Resolution Imaging Spectroradiometer (MODIS) satellite data were used, specifically: MOD13Q1 and MOD11A2. An overview of the characteristics of these satellite data is provided in *Table 2* (*Didan*, 2021; *Wan et al*., 2021).

Table 2. Overview of MOD13Q1 and MOD11A2 satellite data characteristics

COLLECTION		**GRANULE – MOD13Q1**	
Characteristic	**Description**	**Characteristic**	**Description**
Collection	Terra MODIS	Number of science dataset (SDS) layers	12
Temporal resolution	Multi-Day	Columns/Rows	4800 × 4800
Temporal extent	2000-02-18 – now	Pixel size	250 m
Spatial extent	Global	**GRANULE – MOD11A2**	
Coordinate system	Sinusoidal	**Characteristic**	**Description**
Datum	N/A	Number of science dataset (SDS) layers	12
File format	HDF-EOS	Columns/Rows	1200 × 1200
Geographic dimensions	1200 ×1200 km	Pixel size	1000 m

TCI represents the initial indicator of water stress and drought. It was developed by *Kogan* (1995a) using the thermal bands of the Advanced Very High Resolution Radiometer (AVHRR) to determine vegetation stress caused by temperature, as well as stress induced by excessive moisture. The input satellite data for calculating *TCI* is the MOD11A2 satellite data. The formula for calculating *TCI* according to the previously mentioned author is:

$$TCI_j = \frac{(TCI_j - TCI_{min})}{(TCI_{max} - TCI_{min})} \times 100\ , \tag{2}$$

where TCI_{max} and TCI_{min} are the maximum and minimum values of *TCI* in a multi-year dataset. *j* is the *TCI* value of the current month in the calculation.

VCI is applied when assessing the status of agricultural drought. Its component is *NDVI*. It was developed by *Kogan* (1995a, 1997). *VCI* estimates the current *NDVI* by comparing it with a range of values observed during previous years. The input data for its calculation is the MOD13Q1 satellite data. The result of *VCI* is expressed in numerical values, where lower values indicate poorer vegetation conditions, while higher values indicate better vegetation conditions.

According to *Kogan* (1997) and *Bento et al.* (2018), the calculation of *VCI* for each pixel and period during the reference years is based on the formula:

$$VCI_j = \frac{(NDVI_j - NDVI_{min})}{(NDVI_{max} - NDVI_{min})} \times 100\ , \tag{3}$$

where $NDVI_{max}$ and $NDVI_{min}$ are the maximum and minimum values of NDVI in a multi-year dataset. *j* is the *NDVI* value for the current month in the calculation.

VHI represents an index used in monitoring agricultural drought. According to *Bhuiyan et al*. (2006), *VHI* takes into account local biophysics (soil and slope) as well as climatic conditions, making it highly applicable in monitoring drought in various agrometeorological regions. *Prasad et al.* (2006) and *Kogan et al.* (2012) emphasized that the results of *VHI* are highly correlated with crop yields, particularly during critical phases of crop growth. To be successfully calculated, its computation requires the integration of the results of the two previously mentioned sub-indices: *VCI* and *TCI*, and the final formula for calculation is:

$$VHI = \alpha \times VCI + (1 - \alpha) \times TCI\ , \tag{4}$$

where α is the "weight" for measuring the contribution of *VCI* and *TCI* in assessing drought status. Generally, the value of α is set to 0.5 due to challenges arising in differentiating the contributions of surface temperature and *NDVI* during vegetation stress measurements.

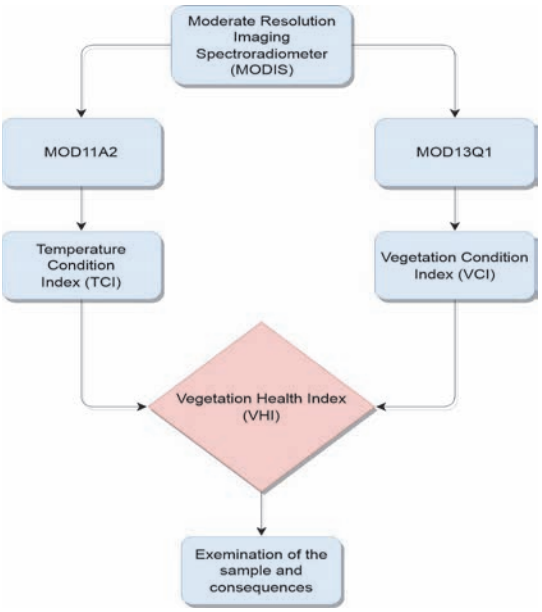

Fig. 3. Data processing methodology for identifying and mapping agricultural drought.

The results of the mentioned indices (*TCI*, *VCI*, and *VHI*) range from -1 to 1. Negative values indicate the occurrence of drought, while positive values indicate the absence of drought. In the study, following recommendations (*Kogan*, 1990, 1995b) and previous research (*Monteleone et al.*, 2020; *Zeng et al.*, 2022), the standardization of these indices was performed through their reclassification into values from 0 to 100, in an equal number of drought categories (*Table 3*).

Table 3. Categorization of drought types

Row number	Value	Drought type
1	< 10	Extreme drought
2	< 20	Severe drought
3	< 30	Moderate drought
4	< 40	Mild drought
5	>= 40	No drought

The consequences of identified agricultural drought are examined through the occurrence and analysis of socio-economic drought. This type of drought was identified by analyzing statistical data on crop yields during the reference period. The data were obtained from the Institute of Statistics Republic of Srpska (ISRS) and Federal Institute of Statistics of the Federation of Bosnia and Herzegovina (FISFB&H). Data on yields at the municipal level within the Sana River basin were considered, including: Bosanska Krupa, Ključ, Sanski Most, Banja Luka, Novi Grad, Kostajnica, Prijedor, Oštra Luka, Ribnik, and Mrkonjić Grad. Yield data were compared for the reference years (2016 and 2017) for the following crops: wheat, maize, barley, potatoes, apples, pears, and plums, and the causes and consequences of this type of drought were examined.

4. Results and discussion

The validation of CHIRPS satellite precipitation data was performed according to the previously described methodology. A comparison of the average precipitation quantity between CHIRPS and the MS indicates a high degree of validity of the satellite data (*Fig. 4*). December is characterized by 89.40% agreement between satellite and real data. Five out of twelve months (April, May, September, October, and November) are characterized by >90% agreement, while six out of twelve months (January, February, March, June, July, and August) are characterized by >95% agreement between satellite and real data.

Fig. 4. Evaluation of meteorological data validity (1981–2023).

The average annual precipitation (1981–2023) aligns with the data obtained from the MS stations at a rate of 94.95%, while the total precipitation matches at a rate of 98.19%. Previous research (*Sabljić et al*., 2023) assessing the validity of the average annual precipitation (1992–2022) for the Sana River basin resulted in a match of 92.63%, as well as 92.38% for total precipitation. Considering the inclusion of a greater number of MS stations at different altitudes, as well as the observation over a longer time period, led to more accurate results in the validation process of satellite precipitation data. Taking into account that HM data relates to seven points in space representing MS stations, while satellite data covers the entire area, along with the spatial resolution factor of satellite data, it is concluded that satellite data is valid for the research and monitoring of meteorological drought.

According to the methodology described earlier, to identify meteorological drought, a comparison was made between the average precipitation for a 42-year period (1981–2023) and the average precipitation for the years 2016 and 2017 (*Fig. 5*). During the year 2016, lower precipitation amounts (*Fig. 5a*) were identified in April (-15.27 mm), September (-19.7 mm), October (-5.85 mm), and December (-85.67 mm). On the other hand, during the year 2017, lower precipitation amounts (*Fig. 5b*) were identified in May (-9.21 mm), June (-22.57 mm), July (-20.92 mm), August (-30.85 mm), and October (-12.75 mm).

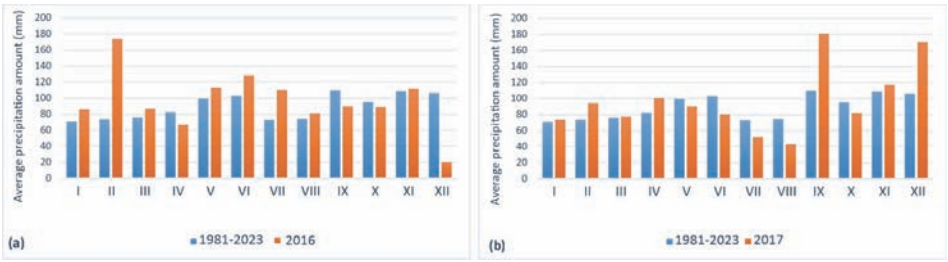

Fig. 5. Comparison of average precipitation amounts per month (1992–2022) with the reference years (2016 and 2017)

To confirm the occurrence of meteorological drought, the *SPI* was calculated. The input meteorological data for *SPI* calculation are previously validated CHIRPS data. *SPI* was calculated for the years 2016 and 2017 (*Fig. 6*). The *SPI* values for 2016 range from -1.73 to 2.69, and for 2017, they range from -0.85 to 1.25. According to *McKee et al.* (1993), drought occurs when the *SPI* value is less than 0. During 2016, *SPI* <0 was identified in April (-0.75), August (-0.14), September (-0.21), October (-0.24), and December (-1.73). For 2017, *SPI* <0 was identified in May (-0.31), June (-0.63), July (-0.85), August (-0.81), and October (-0.31).

Fig. 6. Monthly *SPI* values (2016 and 2017).

To identify hydrological drought, a comparison of the average water level for 18-year period (2001–2019) with the average water level of 2016 and 2017

was conducted (*Fig. 7*). During 2016, at the location of the hydrological station in Prijedor (*Fig. 7a*), lower average water levels were identified in January (-12 cm), April (-72.7 cm), June (-27.1 cm), September (-4.1 cm), and December (-94.9 cm). In the same year, at the location of the hydrological station in Sanski Most (*Fig. 7b*), lower average water levels were identified in January (-21.1 cm), March (-4.5 cm), April (-55.2 cm), June (-31.6 cm), July (-0.4 cm), August (-2.7 cm), September (-11.3 cm), November (-1.6 cm), and December (-62.3 cm). During 2017, at the location of the hydrological station in Prijedor (*Fig. 7c*), lower average water levels were identified in January (-80.5 cm), June (-45.7 cm), July (-12.4 cm), August (-12.1 cm), and October (-7.4 cm). Similarly, in the same year, at the location of the hydrological station in Sanski Most (*Fig. 7d*), lower average water levels were identified in January (-58.1 cm), March (-6.5 cm), April (-23.2 cm), May (-13.4 cm), June (-35.6 cm), July (-41.4 cm), August (-41.7 cm), September (-31.3 cm), October (-24.5 cm), and November (-19.6 cm).

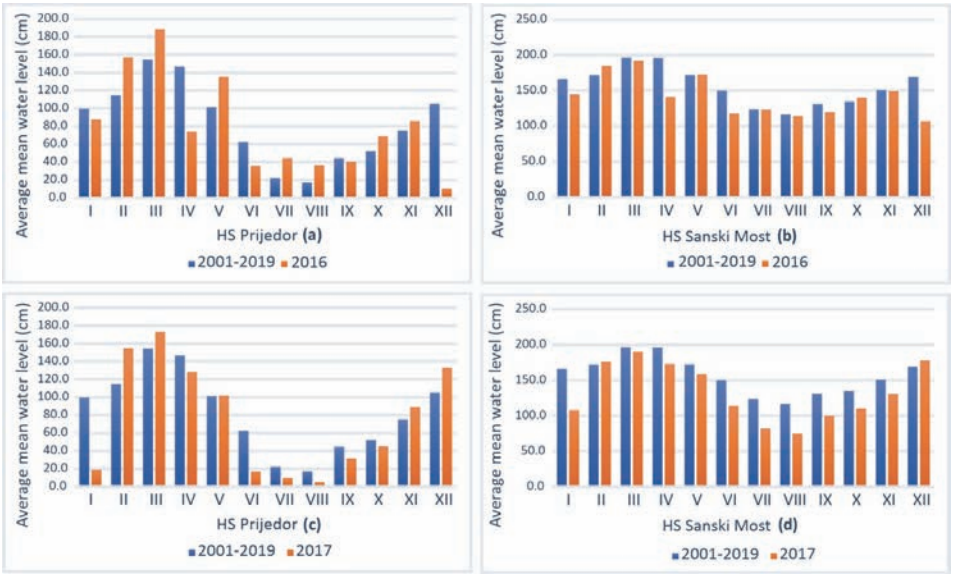

Fig. 7. Comparison of average mean water level (2001–2019) with the reference years (2016 and 2017) at the Prijedor and Sanski Most hydrological stations.

According to the results of *Ducić et al.* (2014), frequent occurrences of severe and extreme meteorological droughts have been evident in B&H during the last decades. There has been an increasing number of dry days, while the number of days with intense rainfall has also increased (*Trbić et al.*, 2013, 2014;

Popov et al., 2019). The occurrence of these phenomena in B&H, coupled with rising temperatures, leads to more intense and extreme droughts, especially during the summer period (*Trbic et al*., 2022). During the past decade (2001–2010), *Žurovec et al.* (2011) identified 24 months as dry in central B&H. In the recent past, *Điderlija et al.* (2023) identified a lack of precipitation, negative *SPI*, and high temperatures during 2017 in the Sarajevo canton area of B&H. Similarly, in the basin of the Sana River, during 2016 and 2017, deficiencies in precipitation and negative *SPI* were observed at the monthly level, indicating the occurrence of meteorological drought. Considering the time series, these occurrences were not temporally continuous during 2016, and therefore did not show characteristics of severe meteorological drought. In contrast, during 2017, reduced precipitation and negative *SPI* were identified continuously over a four-month period (from May to August). The occurrence of meteorological drought with this duration can have serious consequences for the geographical environment and the occurrence of other types of droughts. According to the results of *Čadro et al.* (2017), in the time period from 1961 to 2010, the occurrence of hydrological drought was noted several times in the lower course of the Sana River. Within the results of this research, there is a clear temporal coincidence of periods with lower precipitation and lower water levels in the main course of the Sana River during 2016 and 2017. This phenomenon indicates that meteorological drought influenced the occurrence of hydrological drought. Taking into account the presented results regarding the occurrence of meteorological and hydrological droughts during 2016 and 2017, as well as the agricultural potential of this geographical environment (*Korjenić*, 2012), it is assumed that these occurrences could have significantly affected the occurrence of agricultural, as well as socio-economic drought during the reference years.

The identification, mapping, and monitoring of agricultural drought at the study area level were conducted by calculating the *TCI*, *VCI*, and *VHI* indicators. Taking into account the planting and harvesting calendar of major crops in B&H (*Bajić et al*., 2022), agricultural drought monitoring with the calculation of these indicators was performed with an instantaneous assessment in July of the reference years.

Monitoring agricultural drought involved creating maps categorizing drought according to *TCI* and *VCI* values (*Fig. 8*). The initial results of *TCI* and *VCI* (*Fig. 8a-d)* range numerically from -1 to 1. According to *Karnieli et al.* (2006), negative *TCI* values indicate vegetation stress. In this regard, high temperatures can worsen vegetation dryness, leading to elevated vegetation stress levels. Similarly, negative *VCI* values indicate stress and poor vegetation conditions. Conversely, positive values of these indices represent healthy or "unstressed" vegetation, indicating areas free from agricultural drought. Spatially, negative *TCI* values (< 0) during 2016 (*Fig. 8a*) prevail in the southern part of the river basin, while during 2017 (*Fig. 8b*), they dominantly cover the entire river basin area, indicating pronounced drought. On the other hand, negative *VCI* values (<0) during 2016 (*Fig. 8c*) are negligibly present in

the southern part of the river basin, while during 2017 (*Fig. 8d*), they are present throughout the river basin area, with dominant spatial outlines in the valley of the main stream of the Sana River.

Values of spatially represented indices (ranging from -1 to 1) were reclassified according to the recommendation of *Kogan* (1995a) into the following categories: extreme drought, severe drought, moderate drought, mild drought, and areas without drought (*Fig. 8e-h*). During 2016, according to the *TCI* results (*Fig. 8e*), mild and moderate droughts were identified in the river basin area, with these types of drought present in the southern, eastern, and central parts of the basin. Similar results during the same year were observed with the *VCI* indicator (*Fig. 8g*). "Small signs" of drought with negligible consequences are visible in the southern and southwestern parts of the basin. During 2017, according to the *TCI* results (*Fig. 8f*), a dominant spread of severe and extreme droughts was identified throughout the river basin area. These results were confirmed by the *VCI* results (*Fig. 8h*), based on which the occurrence of severe and extreme drought in the river basin area was identified. The lack of precipitation, low *SPI* values, and a decrease in the water level of the main stream (from May to August) are the main causes of the occurrence of extreme vegetation stress, manifested by the deterioration of vegetation "health" throughout the basin, especially in the northeastern, western, and southeastern parts of the basin. The occurrence of extreme drought is dominant in the valley of the main stream of the Sana River.

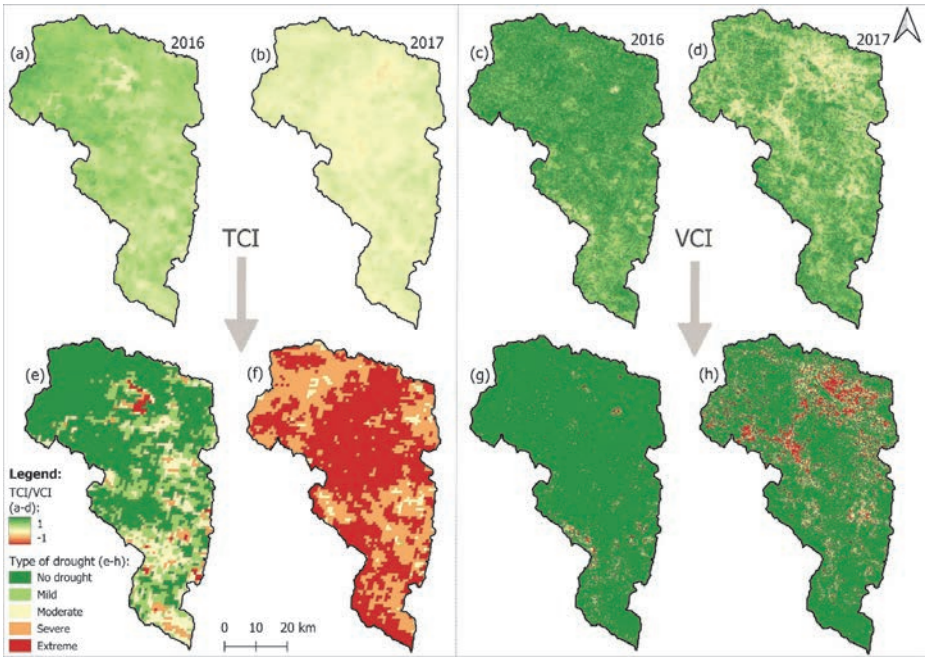

Fig. 8. Mapped and reclassified results of *TCI* and *VCI* for the year 2016 and 2017.

The overall "picture" of the negative impact of agricultural drought at the river basin level was obtained by calculating the *VHI* and creating a map of different drought types based on the results of this index (*Fig. 9*). The initial results of *VHI*, like other indices, range numerically from -1 to 1, where negative values indicate poor vegetation conditions, and positive values indicate good vegetation conditions. During 2016 (*Fig. 9a*), negative values were noticeable in a negligible spatial extent in the southern part of the river basin. In contrast, during 2017 (*Fig. 9c*), negative values were noticeable throughout the entire river basin area. Like *TCI* and *VCI*, the *VHI* index was reclassified into different drought categories according to the recommendation of *Kogan* (1995a) (*Fig. 9b,d*). According to the results from 2016 (*Fig. 9b*), the category representing areas without drought dominates the entire river basin area. The presence of mild and moderate agricultural drought categories is observed in the southern part. On the other hand, according to the results from 2017 (*Fig. 9d*), a significant drought occurrence is visible. Almost the entire river basin area is affected by some category of drought (mild, moderate, severe, or extreme). Severe and extreme droughts predominate in the area of the main stream of the Sana River.

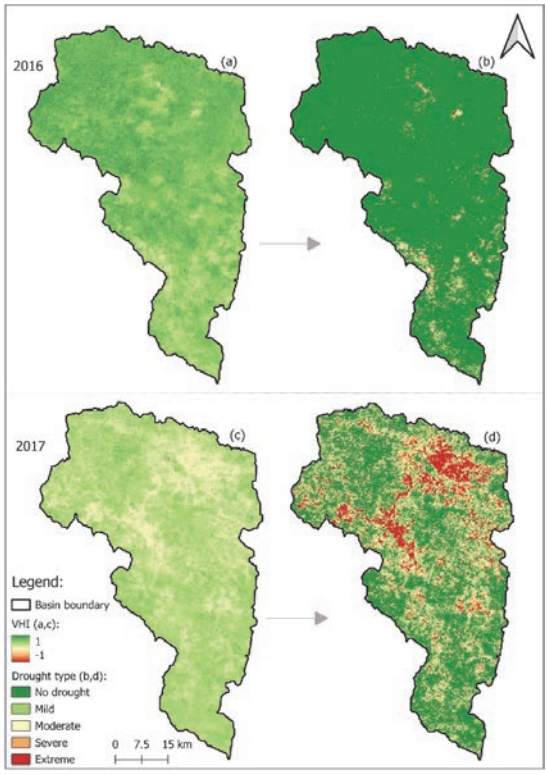

Fig. 9. Comparison of *VHI* indicator results (2016 and 2017)

Seiler et al. (1998) confirm in their research results that the *VHI* (by combining *TCI* and *VCI*) closely aligns with precipitation patterns in the studied areas, and it is of crucial importance in characterizing the spatial extent and severity of agricultural droughts. Additionally, *Tsiros et al.* (2004) and *Parviz* (2016) have confirmed in their research results that *VCI* and *TCI* in combination yield satisfactory outcomes at the global level when used for drought identification, assessing the impact of weather on droughts, and evaluating vegetation conditions. According to *Gidey et al.* (2018), previous studies have shown that low values of *VCI* and *TCI*, or warm weather, largely indicate stressful conditions for vegetation and eventually the occurrence of agricultural droughts. Similarly to the results of the mentioned authors, through the results of this research at the level of the Sana River basin, a high degree of mutual alignment of *TCI*, *VCI*, and *VHI* has been demonstrated, as well as alignment with precipitation patterns and water level. The calculation of *SPI* successfully identified the occurrence of meteorological drought, and the consequent occurrence of hydrological drought. These droughts acted as triggers for the occurrence of agricultural drought, which was successfully identified by calculating *TCI*, *VCI*, and *VHI*. *Marufah et al*. (2017) have shown through their research results that it is possible to establish the duration, spatial distribution, severity, and category of agricultural drought using VHI. Similarly, during 2016 and 2017, the spatial extent of agricultural drought was identified in the Sana River basin. Moderate drought was observed in 2016 to a negligible extent, while severe and extreme drought were observed dominantly in the Sana River valley in 2017.

During 2017, agricultural drought resulted in the manifestation of socio-economic drought. According to the report of the Ministry of Foreign Trade and Economic Relations in Bosnia and Herzegovina (MOFTER, 2017), there was a decrease in yields and total production of crops, vegetables, fruits, and grapes at the national level. The most significant negative impact of the drought was observed in the corn crop, with a yield of 3.7 t/ha, which was 39% lower than the yield achieved in the previous year. The reduced corn yield per hectare also led to a 40% decrease in the total corn production. The yield of wheat was lower by 6%, with a yield of 4.1 t/ha, while the yield of potatoes was lower by 21%, with a yield of 9.6 t/ha, during 2017 compared to 2016. Additionally, according to the aforementioned report, significant crops with a decline in yields included: soybeans (-36.95%), carrots (-35.92%), green corn (-33.35%), peas (-29.51%), grass-clover mixtures (-29.40%), cabbage (-26.15%), tobacco (-23.97%), white onion (-23.40%), black onion (-21.45%), alfalfa (-21.21%), tomatoes (-19.10%), clover (-18.56%), peas (-13.27%), green lettuce (-11.07%), peppers (-10.85%), cucumbers (-10.79%), strawberries (-4.19%), and watermelons (-2.13%).

Monitoring of socio-economic drought at the level of the Sana River basin was conducted by comparing agricultural yields at the study area level for the period of 2016 and 2017 (*Fig. 10*). Yield data were aggregated at the municipal

level and included the yields of the following crops: wheat, corn, barley, potatoes, apples, pears, and plums. During 2017 compared to 2016, a decrease in potato yield by 26.39% (18707 – 13770 t), corn by 41.36% (92803 – 54416 t), barley by 1.13% (6885 – 6807 t), potatoes by 20.76% (61692 – 48882 t), pears by 19.57% (4507 – 3625 t), and plums by 63.07% (25650 – 9472 t) was identified. A negligible increase in apple yield was observed during the observed period, specifically by 2.02% (9134 – 9287 t).

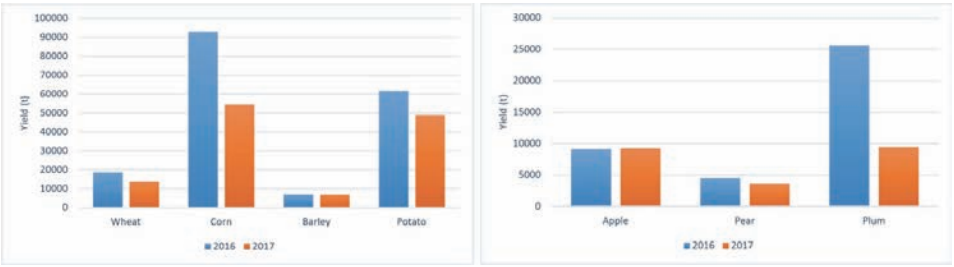

Fig. 10. Comparison of agricultural production yields for selected crops

The presented data clearly indicate that the occurrence of agricultural drought had serious consequences for agricultural yields in 2017, and that it also contributed to the manifestation of socio-economic drought. The sensitivity of the agricultural sector to drought is largely reflected in its dependence on land and water resources affected directly or indirectly by drought. Additionally, according to *Zurovec et al*. (2015), significant challenges for the agricultural sector in B&H stem from the complex governance structure, whereby all levels of authority (from local to national) have jurisdiction over planning and management in agriculture. For these reasons, it is necessary to invest additional efforts in activities, measures, processes, and plans aimed at mitigating drought. Some examples of good practices and implemented activities include establishing methods for calculating drought indices, processing time series data, analyses and mapping (using GIS), as well as using software for irrigation planning during crisis situations. By enhancing the capacity for drought preparedness and management, including the formulation of comprehensive manifestation plans at the local and national levels, B&H could further develop comprehensive vulnerability assessment approaches that incorporate remote sensing methods and techniques for drought monitoring and management. This would entail the implementation of effective mitigation strategies, as well as the creation and improvement of policies for planning and responding to crisis situations.

5. Conclusion

Modern technologies and data collection methods, such as GIS and remote sensing, offer the possibility of advanced monitoring of natural disasters like droughts. Using these technologies, it is possible to identify and track negative occurrences in space, conduct assessments of their harmful impact, and assist in the development of projects to rehabilitate degraded areas. So far, there is a limited number of drought studies in the territory of B&H, while integrated research based on remote sensing about droughts, their causes, and consequences is almost non-existent for now.

Spatio-temporal monitoring at the study area level for a defined time period (2016 and 2017), through satellite data processing, identified the onset of drought. CHIRPS satellite precipitation data, available from 1981 to nearly real-time, enabled efficient monitoring of precipitation changes over a wide time range (1981–2023). Based on the mentioned data, a precipitation deficit was identified for the observed time period (2016 and 2017), the standardized precipitation index, SPI, was calculated, and the occurrence of meteorological drought was established. The lack of precipitation led to a decrease in the average mid-level water level of the Sana River, and consequently, the the occurrence of hydrological drought. These events directly impacted the manifestation of agricultural drought during the period of intensive agricultural activities (planting and harvesting). Processing MOD13Q1 and MOD11A2 satellite data calculated various temperature and vegetation indices, and the occurrence of agricultural drought was identified and mapped. It should be noted that higher spatial resolution of satellite data for mapping agricultural drought would contribute to more precise results of spatial drought identification compared to those presented in this study. The identified agricultural drought affected agricultural production, through reduced yields, and consequently led to the onset of socio-economic drought. By analyzing statistical yield data, socio-economic drought was identified in the study area, with a deficit in yields of wheat, maize, barley, potatoes, pears, and plums.

The results of the research can be valuable to relevant institutions for drought monitoring, timely warning of its occurrence, and for the development of studies for drought adaptation and mitigation in river basin areas. Further advancement in research based on the presented results would involve the application of supervised classification processes of land use with elements of precision agriculture. This process would entail detailed classification of various agricultural crops in the study area. Integrating this type of classification into the presented research would contribute to a clearer spatial identification and reflection of agricultural drought on individual agricultural crops in the study area.

Acknowledgment: The authors would like to thank the Ministry of Agriculture, Forestry, and Water Management of the Republic of Srpska, as well as the Republic Hydrometeorological Institute of the Republic of Srpska, for providing meteorological data (No. 12/1.03-79-1/24). Furthermore, Tin Lukić

and Slobodan B. Marković express their gratitude to the Provincial Secretariat for Higher Education and Scientific Research of Vojvodina (Serbia), No. 000871816 2024 09418 003 000 000 001 04 002 (GLOMERO), under Program 0201 and Program Activity 1012. Part of the research was supported by the Program of Cooperation with the Serbian Scientific Diaspora – Joint Research Projects – DIASPORA 2023, from the Science Fund of the Republic of Serbia, under the project LAMINATION (The Loess Plateau Margins: Towards Innovative Sustainable Conservation), Project number: 17807. The authors are grateful to the anonymous reviewers whose comments and suggestions improved the manuscript.

References

Agency for Statistics of Bosnia and Herzegovina, 2016: Census of Population, Households and Dwellings in Bosnia and Herzegovina 2013 Final Results.

Alsilibe, F., Bene, K., Bilal, G., Alghafli, K., and *Shi, X.*, 2023: Accuracy Assessment and Validation of Multi-Source CHIRPS Precipitation Estimates for Water Resource Management in the Barada Basin, Syria. *Remote Sensing 15*(7), 1778. http://doi.org/10.3390/rs15071778

Anyamba, A., Tucker, C.J., and *Eastman, J.R.*, 2001: NDVI anomaly patterns over Africa during the 1997/98 ENSO warm event. *Int. J. Remote Sensing*, *22*(10), 1847–1860. https://doi.org/10.1080/01431160010029156

Bajić, D., Adžić, D., and *Sabljić, L.*, 2022: Winter Crops Classification using Combination of Multi-Temporal Optical Sentinel-2 and Radar Sentinel-1 Images. *Гласник/Herald 26*, 27–50. https://doi.org/10.7251/HER2226027B

Bento, V.A., Gouveia, C.M., DaCamara, C.C., and *Trigo, I.F.*, 2018: A climatological assessment of drought impact on vegetation health index. *Agricult. Forest Meteorol. 259*, 286–295. https://doi.org/10.1016/j.agrformet.2018.05.014

Bhuiyan, C., Singh, R.P., and *Kogan, F.N.*, 2006: Monitoring drought dynamics in the Aravalli region (India) using different indices based on ground and remote sensing data. *Int. J. Appl. Earth Observ. Geoinform 8*(4), 289–302. https://doi.org/10.1016/j.jag.2006.03.002

Briffa, K.R., van der Schrier, G., and *Jones, P.D.*, 2009: Wet and dry summers in Europe since 1750: evidence of increasing drought. *Int. J. Climatol.*, *29*, 1894–1905. https://doi.org/10.1002/joc.1836

Council, R., 1992: Grasslands and Grassland Sciences in Northern China. National Academies Press: Washington, DC, USA.

Čadro, S., Žurovec, J., and *Cherni-Čadro, S.*, 2017: Severity, Magnitude and Duration of Droughts in Bosnia and Herzegovina Using Standardized Precipitation Evapotranspiration Index (SPEI). *Agricult. Forestry 63*(3), 199–206. https://doi.org/10.17707/AgricultForest.63.3.20

Didan, K., 2021: MODIS/Terra Vegetation Indices 16-Day L3 Global 250m SIN Grid V061 [Data set]. NASA EOSDIS Land Processes Distributed Active Archive Centar. https://doi.org/10.5067/MODIS/MOD13Q1.061

Dong, Z., Liu, H., Baiyinbaoligao, H., Khan, A., Wen, J., Chen, L., and *Tian, F.*, 2022: Future Projection of Seasonal Drought Characteristics Using CMIP6 in the Lancang-Mekong River Basin. *J. Hydrol.* 610, 127815. https://doi.org/10.1016/j.jhydrol.2022.127815

Ducić, V., Burić, D., Trbić, G., and *Cupać, R.*, 2014: Analysis of precipitation and droughts on territory Bosnia and Herzegovina based upon standardized precipitation index (SPI). *Гласник/Herald, 18*, 53–70. https://doi.org/10.7251/HER1814053D

Điderlija, M., Kulo, N., Mulahusić, A., and *Topoljak, J.*, 2023: Correlation analysis of different optical remote sensing indices for drought monitoring: a case study of Canton Sarajevo, Bosnia and Herzegovina. *Environ. Monitor. Asses. 195*, 1338. https://doi.org/10.1007/s10661-023-11930-2

Ezzine, H., Bouziane, A., and *Ouazar, D.*, 2014: Seasonal comparisons of meteorological and agricultural drought indices in Morocco using open short time-series data. *Int. J. Appl. Earth Observ. Geoinform. 26*, 36–48. https://doi.org/10.1016/j.jag.2013.05.005

Feng, G., Chen, Y., Mansaray, L. R., Xu, H., Shi, A., and *Chen, Y.*, 2023: Propagation of Meteorological Drought to Agricultural and Hydrological Droughts in the Tropical Lancang–Mekong River Basin. *Remote Sensing 15*, 5678. https://doi.org/10.3390/rs15245678

Funk, C., Peterson, P., Landsfeld, M., Pedereros, D., Verdin, J., Shukla, S., Husak, G., Rowland, J., Harrison, L., Hoell, A., and *Michaelsen, J.*, 2015: The climate hazards infrared precipitation with stations—a new environmental record for monitoring extremes. *Scientific Data 2*, 150066. https://doi.org/10.1038/sdata.2015.66

Gabrić, O. and *Plavšić, J.*, 2019: Methodology for deriving synthetic meteorological droughts and its application for Budapest. *Időjárás, 123*, 501–519. https://doi.org/10.28974/idojaras.2019.4.6

Gao, F., Zhang, Y., Ren, X., Yao, Y., Hao, Z., and *Cai, W.*, 2018: Evaluation of CHIRPS and its application for drought monitoring over the Haihe River Basin, China. *Nat. Hazards 92*, 155–172. https://doi.org/10.1007/s11069-018-3196-0

Gidey, E., Dikinya, O., Sebego, R., Segosebe, E., and *Zenebe, A.*, 2018: Analysis of the long-term agricultural drought onset, cessation, duration, frequency, severity and spatial extent using Vegetation Health Index (VHI) in Raya and its environs, Northern Ethiopia. *Environ. Syst. Res. 7*, 13. https://doi.org/10.1186/s40068-018-0115-z

Gnjato, S., 2018: Analysis of the Water Discharge at the Sana River. *Гласник/Herald, 22*, 103–116. https://doi.org/10.7251/HER2218103G

Gudmundsson, L., and *Seneviratne, S. I.*, 2015: European drought trends. *Proc. IAHS 369*, 75–79. https://doi.org/10.5194/piahs-369-75-2015

Habitou, N., Morabbi, A., Ouazar, D., Bouziane, A., Hasnaoui, M. D., and *Sabri, H.*, 2020: CHIRPS precipitation open data for drought monitoring: application to the Tensift basin, Morocco. *J. Appl. Remote Sens 14(3)*, 034526. https://doi.org/10.1117/1.JRS.14.034526

Hao, Z., and *Singh, V. P.*, 2015: Drought Characterization from a Multivariate Perspective: A Review. *J.f Hydrol. 527*, 668–678. https://doi.org/10.1016/j.jhydrol.2015.05.031

Hashim, M., Reba, N.M., Nadzri, M.I., Pour, A.B., Mahmud, M.R., Mohd Yusoff, A.R., Ali, M.I., Jaw, S.W., and *Hossain, M.S.*, 2016: Satellite-based run-off model for monitoring drought in Peninsular Malaysia. *Remote Sensing, 8*, 633. https://doi.org/10.3390/rs8080633

Hoerling, M., Eischeid, J., Perlwitz, J., Quan, X., Zhang, T., and *Pegion, P.*, 2012: On the Increased Frequency of Mediterranean Drought. *J. Climate, 25*, 2146–2161. https://doi.org/10.1175/JCLI-D-11-00296.1

Hsu, J., Huang, W.-R., Liu, P.-Y., and *Li, X.*, 2021: Validation of CHIRPS Precipitation Estimates over Taiwan at Multiple Timescales. *Remote Sensing, 13(2)*, 254. http://doi.org/10.3390/rs13020254

Ji, L., and *Peters, A. J.*, 2003: Assessing vegetation response to drought in the northern Great Plains using vegetation and drought indices. *Remote Sens. Environ 87(1)*, 85–98. https://doi.org/10.1016/S0034-4257(03)00174-3

Karnieli, A., Bayasgalan, M., Bayarjargal, Y., Agam, N., Khudulmur, S., and *Tucker, C. J.*, 2006: Comments on the use of the vegetation health index over Mongolia. *Int. J. Remote Sens. 27*, 2017–2024. https://doi.org/10.1080/01431160500121727

Katsanos, D., Retalis, A., Tymvios, F., and *Michaelides, S.*, 2016: Analysis of precipitation extremes based on satellite (CHIRPS) and in situ data set over Cyprus. *Nat. Hazards 83*, 53–63. https://doi.org/10.1007/s11069-016-2335-8

Kogan, F.N., 1990: Remote sensing of weather impacts on vegetation in non-homogeneous areas. *Int. J. Remote Sens 11*, 1405–1419. https://doi.org/10.1080/01431169008955102

Kogan, F.N., 1995a: Application of vegetation index and brightness temperature for drought detection. *Adv. Space Res. 15*(11), 91–100. https://doi.org/10.1016/0273-1177(95)00079-T

Kogan, F.N., 1995b: Droughts of the late 1980s in the United States as derived from NOAA polar-orbiting satellite data. *Bull. Amer. Meteorol. Soc. 76*, 655–668. https://doi.org/10.1175/1520-0477(1995)076%3C0655:DOTLIT%3E2.0.CO;2

Kogan, F.N., 1997: Global Drought Watch from Space. *Bull. Amer. Meteorol. Soc., 78*, 621–636. https://doi.org/10.1175/1520-0477(1997)078<0621:GDWFS>2.0.CO;2

Kogan, F.N., Salazar, L., and *Roytman, L.*, 2012: Forecasting crop production using satellite-based vegetation health indices in Kansas, USA. *Int. J. Remote Sens. 33*, 2798–2814. https://doi.org/10.1080/01431161.2011.621464

Korjenić, A., 2012: Climate as Spatial Planning Factor of the Una Sana Canton, Bosnia and Herzegovina. *Geographica Pannonica, 16(4)*, 126–135. https://doi.org/10.5937/GeoPan1204126K

Kottek, M., Grieser, J., Beck, C., Rudolf, B., and *Rubel, F.*, 2006: World Map of the Köppen-Geiger climate classification updated. *Meteorol. Zeitsch. 15*, 259–263.

https://doi.org/10.1127/0941-2948/2006/0130
Kourtis, I. M., Vangelis, H., Tigkas, D., Mamara, A., Nalbantis, I., Tsakiris, G., and *Tsihrintzis, V. A.*, 2023: Drought Assessment in Greece Using SPI and ERA5 Climate Reanalysis Data. *Sustainability 15*, 159999. https://doi.org/10.3390/su152215999
Lee, J., Kim, Y., and *Wang, D.*, 2022: Assessing the characteristics of recent drought events in South Korea using WRF-Hydro. *J. Hydrol. 607*, 127459. https://doi.org/10.1016/j.jhydrol.2022.127459
Li, J., Wang, Z., and *Lai, C.*, 2020a: Severe drought events inducing large decrease of net primary productivity in mainland China during 1982–2015. *Sci. Total Environ. 703*, 135541. https://doi.org/10.1016/j.scitotenv.2019.135541
Li, Q., He, P., He, Y., Han, X., Zeng, T., Lu, G., and *Wang, H.*, 2020b: Investigation to the relation between meteorological drought and hydrological drought in the upper Shaying River Basin using wavelet analysis. *Atmosp. Res. 234*, 104743. https://doi.org/10.1016/j.atmosres.2019.104743
Liu, X., Zhu, X., Pan, Y., Li, S., Liu, Y., and *Ma, Y.*, 2016: Agricultural drought monitoring: Progress, challenges, and prospects. *J. Geograph. Sci. 26*, 750–767. https://doi.org/10.1007/s11442-016-1297-9
Liu, W., Ma, S., Feng, K., Gong, Y., Liang, L., and *Tsubo, M.*, 2023: The Suitability Assessment of Agricultural Drought Monitoring Indices: A Case Study in Inland River Basin. *Agronomy*, *13*(2), 469. http://doi.org/10.3390/agronomy13020469
Lukić, T., Micić Ponjiger, T., Basarin, B., Sakulski, D., Gavrilov, M., Marković, S., Zorn, M., Komac, B., Milanović, M., Pavić, D., Mesaroš, M., Marković, N., Durlević, U., Morar, C., and *Petrović, A.*, 2021: Application of Angot precipitation index in the assessment of rainfall erosivity: Vojvodina Region case study (North Serbia). *Acta Geographica Slovenica*, *61*(2), 123–153. https://doi.org/10.3986/AGS.8754
Marufah, U., Hidayat, R., and *Prasasti, I.*, 2017: Analysis of relationship between meteorological and agricultural drought using standardized precipitation index and vegetation health index. In: *IOP Conference Series: Earth Environ. Sci. 54*(1), 012008. https://doi.org/10.1088/1755-1315/54/1/012008
McKee, T. B., Doesken, N. J., and *Kleist, J.*, 1993: The Relationship of Drought Frequency and Duration to Time Scales. In: *Proceedings of the 8th Conference on Applied Climatology, 17*, 179–183. Anaheim, CA, USA.
MOFTER, 2018: Ministry of Foreign Trade and Economic relations of Bosnia and Herzegovina: Rural Development Strategy of Bosnia and Herzegovina for Period 2018–2021. Available online: http://www.mvteo.gov.ba/data/Home/Dokumenti/Poljoprivreda/BOS_SPRR_2018-2021-korekcija.pdf
Monteleone, B., Bonaccorso, B., and *Martina, M.*, 2020: A joint probabilistic index for objective drought identification: the case study of Haiti. *Natural Haz. Earth Syst. Sci. 20*, 471–487. https://doi.org/10.5194/nhess-20-471-2020
Nalbantis, I. and *Tsakiris, G.*, 2009: Assessment of Hydrological Drought Revisited. *Water Resour. Manage. 23*, 881–897. https://doi.org/10.1007/s11269-008-9305-1
Nicholson, S.E. and *Farrar, T.J.*, 1994: The influence of soil type on the relationships between NDVI, rainfall, and soil moisture in semiarid Botswana. I. NDVI response to rainfall. *Remote Sens. Environ. 50*(2), 107–120. https://doi.org/10.1016/0034-4257(94)90038-8
Orimoloye, I. R., 2022: Agricultural drought and its potential impacts: Enabling decision-support for food security in vulnerable regions. *Front. Sustain. Food Syst. 6*, 838824. https://doi.org/10.3389/fsufs.2022.838824
Oukaddour, K., La Page, M., and *Fakir, Y.*, 2024: Toward a Redefinition of Agricultural Drought Periods – A Case Study in a Mediterranean Semi-Arid Region. *Remote Sensing 16*, 83. https://doi.org/10.3390/rs16010083
Parviz, L., 2016: Determination of effective indices in the drought monitoring through analysis of satellite images. *Agricult. Forest 62*, 305. https://doi.org/10.17707/AgricultForest.62.1.34
Popov, T., Gnjato, S., Bajić, D., and *Trbić, G.*, 2019: Spatial Patterns of Precipitation in Bosnia and Herzegovina. *Journal of the Geographical Institute "Jovan Cvijić" SASA, 69*, 185–195. https://doi.org/10.2298/IJGI1903185P
Prasad, A. K., Chai, L., Singh, R. P., and *Kafatos, M.*, 2006: Crop yield estimation model for Iowa using remote sensing and surface parameters. *Int. J. Appl. Earth Observ. Geoinform. 8*, 26–33. https://doi.org/10.1016/j.jag.2005.06.002

Rivera, J.A., Marianetti, G., and *Hinrichs, S.*, 2018: Validation of CHIRPS precipitation dataset along the Central Andes of Argentina. *Atmos. Res. 213*, 437–449. https://doi.org/10.1016/j.atmosres.2018.06.023

Robock, A., Vinnikov, K. Y., Srinivasan, G., Entin, J. K., Hollinger, S. E., Speranskaya, N. A., Liu, S., and *Namkhai, A.*, 2000: The global soil moisture data bank. *Bull. Amer. Meteorol. Soc. 81*, 1281–1300. https://doi.org/10.1175/1520-0477(2000)081<1281:TGSMDB>2.3.CO;2

Rossi, G., 2000: Drought Mitigation Measures: A Comprehensive Framework. In: Vogt, J.V., Somma, F. (Eds) Drought and Drought Mitigation in Europe. *Adv. Nat. Technol. Haz. Res. 14*, Springer, Dordrecht. https://doi.org/10.1007/978-94-015-9472-1_18

Sabljić, L., Pavić, D., Savić, S., and *Bajić, D.*, 2023: Extreme Precipitations and their Influence on the River Flood Hazards – A Case Study of the Sana River Basin in Bosnia and Herzegovina. *Geographica Pannonica 27(3)*, 184–198. https://doi.org/10.5937/gp27-456

Seiler, R. A., Kogan, F., and *Sullivan, J.*, 1998: AVHRR-based vegetation and temperature condition indices for drought detection in Argentina. *Adv. Space Res 21*, 481–484. https://doi.org/10.1016/S0273-1177(97)00884-3

Seiler, R. A., Kogan, F., and *Wei, G.*, 2000: Monitoring weather impact and crop yield from NOAA AVHRR data in Argentina. *Adv. Space Res. 26*, 1177–1185. https://doi.org/10.1016/S0273-1177(99)01144-8

Spinoni, J., Lakatos, M., Szentimrey, T., Bihari, Z., Szalai, S., Vogt, J., and *Antofie, T.*, 2015a: Heat and cold waves trends in the Carpathian Region from 1961 to 2010. *Int. J. Climatol. 35*, 4197–4209. https://doi.org/10.1002/joc.4279

Spinoni, J., Naumann, G., and *Vogt, J.*, 2015b: Spatial patterns of European droughts under a moderate emission scenario. *Adv. Sci. Res. 12*, 179–186. https://doi.org/10.5194/asr-12-179-2015

Spinoni, J., Naumann, G., and *Vogt, J.*, 2017: Pan-European seasonal trends and recent changes of drought frequency and severity. *Glob. Planet. Change 148*, 113–130. https://doi.org/10.1016/j.gloplacha.2016.11.013

Spinoni, J., Vogt, J. V., Naumann, G., Barbosa, P., and *Dosio, A.*, 2018: Will drought events become more frequent and severe in Europe? International *J. Climatol 38*, 1718–1736. https://doi.org/10.1002/joc.5291

Tan, M. L., Tan, K. C., Chua, V. P., and *Chan, N. W.*, 2017: Evaluation of TRMM product for monitoring drought in the Kelantan River Basin, Malaysia. *Water 9*, 57. https://doi.org/10.3390/w9010057

Tang, J., Zeng, J., Zhang, L., Zhang, R., Li, J., Li, X., Zou, J., Zeng, Y., Xu, Z., Wang, Q., and *Zhang, Q.*, 2020: A modified flexible spatiotemporal data fusion model. *Front. Earth Sci. 14*, 601–614. https://doi.org/10.1007/s11707-019-0800-x

Tian, Y., Xu, Y. P., and *Wang, G.*, 2018: Agricultural drought prediction using climate indices based on Support Vector Regression in Xiangjiang River basin. *Sci. Total Environ. 622*, 710–720. https://doi.org/10.1016/j.scitotenv.2017.12.025

Tladi, T. M., Ndambuki, J. M., and *Salim, R. W.*, 2022: Meteorological drought monitoring in the Upper Olifants sub-basin, South Africa. *Phys. Chemistry Earth, Parts A/B/C, 128*, 103273. https://doi.org/10.1016/j.pce.2022.103273

Torres-Vázquez, M.A., Halifa-Marín, A., Pedro Montávez, J., and *Turco, M.*, 2023: High resolution monitoring and probabilistic prediction of meteorological drought in a Mediterranean environment. *Weather Climate Extr. 40*, 100558. https://doi.org/10.1016/j.wace.2023.100558

Trbic, G., Popov, T., Djurdjevic, V., Milunovic, I., Dejanovic, T., Gnjato, S., and *Ivanisevic, M.*, 2022: Climate Change in Bosnia and Herzegovina According to Climate Scenario RCP8.5 and Possible Impact on Fruit Production. *Atmosphere 13*, 1. https://doi.org/10.3390/atmos13010001

Trbić, G., Bajić, D., Popov, T., and *Oprašić, S.*, 2013: Problems of Drought in Bosnia and Herzegovina. *Гласник/Herald 17*, 103–120. https://doi.org/10.7251/HER1714103T

Trbić, G., Đurđević, V., Bajić, D., Cupać, R., Vukmir, G., and *Popov, T.*, 2014: Climate change and adaptation options in Bosnia and Herzegovina – Case study in agriculture. In: Proceedings of the International Conference "ADAPT to CLIMATE", Nicosia, Cyprus, 27–28 March.

Tsiros, E., Domenikiotis, C., Spiliotopoulos, M., and *Dalezios, N. R.*, 2004: Use of NOAA/AVHRR-based vegetation condition index (VCI) and temperature condition index (TCI) for drought monitoring in Thessaly, Greece. In: *EWRA* Symposium on water resources management: risks and challenges for the 21st century, 2–4, Izmir, Turkey.

Van Loon, A. F., 2015: Hydrological drought explained. *WIREs Water 2*, 359–392. https://doi.org/10.1002/wat2.1085

Vicente-Serrano, S. M., Lopez-Moreno, J. I., Beguería, S., Lorenzo-Lacruz, J., Sanchez-Lorenzo, A., García-Ruiz, J. M., Azorin-Molina, C., Morán-Tejeda, E., Revuelto, J., Trigo, R., Coelho, F., and *Espejo, F.*, 2014: Evidence of increasing drought severity caused by temperature rise in southern Europe. *Environ. Res. Lett. 9*, 044001. https://doi.org/10.1088/1748-9326/9/4/044001

Wan, Z., Hook, S., and *Hulley, G*, 2021: MODIS/Terra Land Surface Temperature/Emissivity 8-Day L3 Global 1km SIN Grid V061 [Data set]. NASA EOSDIS Land Processes Distributed Active Archive Center. https://doi.org/10.5067/MODIS/MOD11A2.061

Wang, J., Price, K. P., and *Rich, P. M.*, 2001: Spatial patterns of NDVI in response to precipitation and temperature in the central Great Plains. *Int. J. Remote Sens. 22*, 3827–3844. https://doi.org/10.1080/01431160010007033

Wilhite, D.A., and *Glantz, M.H.*, 1985: Understanding the Drought Phenomenon: The Role of Definitions. *Water Int. 10(3)*, 111–120. https://doi.org/10.1080/02508068508686328,198

Wilhite, D. A., 2000: Drought as a Natural Hazard: Concepts and Definitions (Chapter 1). In: (*D.A. Wilhite* Ed), Drought: A Global Assessment, *1* and *2*, Routledge Publishers, London.

Wilhite, D. A., Svoboda, D., and *Hayes, J.*, 2007: Understanding the complex impacts of drought: A key to enhancing drought mitigation and preparedness. *Water Resour. Manage. 21*, 763–774. https://doi.org/10.1007/S11269-006-9076-5

Xie, X., and *Li, A.* 2020a: Development of a topographic – Corrected temperature and greenness model (TG) for improving GPP estimation over mountainous areas. *Agricult. Forest Meteorol 295*, 108193. https://doi.org/10.1016/J.AGRFORMET.2020.108193

Xie, X., and *Li, A.*, 2020b: An adjusted two-leaf light use efficiency model for improving GPP simulations over mountainous areas. *J.Geophys. Res.: Atmos., 125*, e2019JD031702. https://doi.org/10.1029/2019JD031702

Yoon, D. H., Nam, W. H., Lee, H. J., Hong, E. M., Feng, S., Wardlow, B. D., Tadesse, T., Svoboda, M. D., Hayes, M. J., and *Kim, D-E.*, 2020: Agricultural drought assessment in East Asia using satellite-based indices. *Remote Sensing 12*(3), 444. https://doi.org/10.3390/rs12030444

Zeng, J., Zhang, R., Qu, Y., Bento, V. A., Zhou, T., Lin, Y., Wu, X., Qi, J., Shui, W., and *Wang, Q.*, 2022: Improving the drought monitoring capability of VHI at the global scale via ensemble indices for various vegetation types from 2001 to 2018. *Weather Climate Extr. 35*, 100412. https://doi.org/10.1016/j.wace.2022.100412

Zhang, X., Duan, J., Cherubini, F., and *Ma, Z.*, 2023: A global daily evapotranspiration deficit index dataset for quantifying drought severity from 1979 to 2022. *Scientific Data 10*, 824. https://doi.org/10.1038/s41597-023-02756-1

Zhu Q., Luo Y., Zhou D., Xu Y-P., Wang G., and *Gao H.*, 2019: Drought Monitoring Utility using Satellite-Based Precipitation Products over the Xiang River Basin in China. *Remote Sensing 11*, 1483. https://doi.org/10.3390/rs11121483

Zhu, Y., Wang, W., Singh, V. P., and *Liu, Y.*, 2016: Combined use of meteorological drought indices at multi-time scales for improving hydrological drought detection. *Sci. Total Environ. 571*, 1058–1068. https://doi.org/10.1016/j.scitotenv.2016.07.096

Zurovec, O., Vedeld, P. O., and *Sitaula, B. K.*, 2015: Agricultural Sector of Bosnia and Herzegovina and Climate Change – Challenges and Opportunities. *Agriculture 5*, 245–266. https://doi.org/10.3390/agriculture5020245

Žurovec J., Čadro, S., and *Murtić, S.*, 2011: Drought Analysis in Sarajevo Using Standardized Precipitation Index (SPI). *22nd International Scientific expert Conference in Agriculture and Food Industry*.

Žurovec, O., Čadro, S., and *Sitaula, B. K.*, 2017: Quantitative Assessment of Vulnerability to Climate Change in Rural Municipalities of Bosnia and Herzegovina. *Sustainability 9*, 1208. https://doi.org/10.3390/su9071208

DOI:10.28974/idojaras.2024.4.2

IDŐJÁRÁS

Quarterly Journal of the HungaroMet Hungarian Meteorological Service
Vol. 128, No. 4, October – December, 2024, pp. 425–438

Investigation of 15 knots tailwind triggering go-around maneuver of eight flights at the Soekarno-Hatta International Airport using the WRF-ARW model

Achmad F. Rais [1,*], **Heri Ismanto** [2], **Eko Widyantoro** [3], **Bayu Umbaran** [2], and **Rezky Yunita**[4]

[1]*Research and Innovation Agency of Indonesia (BRIN), Bogor*

[2]*Center for Aeronautical Meteorology (BMKG), Jakarta*

[3]*Meteorological Station of Soekarno Hatta International Airport (BMKG), Tangerang*

[4]*Center for Research and Development (BMKG), Jakarta*

**Corresponding Author E-mail: achm050@brin.go.id*

(Manuscript received in final form January 3, 2024)

Abstract— A numerical simulation of the 15 knots tailwind triggering the go-around maneuver of 8 flights at the Soekarno-Hatta International Airport was explored. The Advancer Weather Research an Forecasting (WRF-ARW) numerical weather prediction model was used to simulate the events. The results showed that WRF-ARW with temporal and spatial resolutions of 2 minutes and 1 km could simulate the tailwind events. The tailwind was triggered by the background wind from the Indian Ocean and by cloud initiation near the final approach path (FAP), then the tailwind speed was reduced by the wind gust south of the FAP at 11:00 UTC, on November 3, 2021. These findings cannot be resolved by analyzing in-situ, weather satellite, and radar data with limited coverage and sensing the wind out of the cloud. It suggests that high-resolution numerical simulation can be used in the operation of aviation weather investigation. Assimilating observation data to the model is essential to be investigated for further study to understand the tailwind mechanism more accurately.

Key-words: background wind, downburst, airplane trajectory, final approach path.

1. Introduction

Airplane accidents related to weather primarily stem from dynamic factors, with wind being a significant contributor (*Gultepe et al.*, 2019). Wind is defined as the movement of air in any direction (*Ahrens* and *Henson*, 2014; *Stull*, 2020), and its assessment necessitates the utilization of both on-site and remote sensing technologies to provide quantitative measurements at surface and upper air levels (*WMO*, 2021; *Arta Kusuma et al.*, 2022). Data from these sources enables meteorologists to evaluate wind conditions for aviation safety accurately. The wind generation is attributed to a combination of forces, including the pressure gradient force, gravity, Coriolis force, centrifugal force, and friction (*Oliver*, 2005).

A flight's approach and landing phases account for more than half of all fatal accidents (*Boeing*, 2021). To address this, the go-around maneuver is employed, which involves discontinuing the approach or landing, and instead, initiating another attempt or diverting to alternate airports. The implementation of this procedure has proven to be effective in preventing 54% of potential accidents. Additionally, permissible crosswind components, as the Federal Aviation Administration (FAA) and the International Civil Aviation Organization (ICAO) stipulated, range from 10 to 20 knots (19 to 37 kilometers per hour), depending on runway dimensions and the airport reference code (*Chang*, 2015). Tailwinds can lead to accidents when they exceed speeds of 10 knots (*Blajev*, 2017). Depending on the aircraft type, the minimum tailwind value for a go-around is generally set at 10 knots (*Es* and *Karwal*, 2001). A tailwind is a wind blowing in the same direction as an airplane's flight path. Tailwinds are calculated based on the projection of wind direction onto the direction of the runway in use (*Rais et al.*, 2020), providing additional thrust during the landing phase.

On November 3, 2021, the pilots executed a go-around maneuver for eight aircrafts in the process of approaching the runway at the Soekarno-Hatta International Airport. The pilots reported encountering a 15-knot tailwind near runways 07 right (07R) and 07 left (07L) within a brief timeframe from 09:58 to 10:12 UTC. The presence of this tailwind can have an impact on aircraft operations at the Soekarno-Hatta International Airport. Given the extensive volume of over two million domestic flights and aircraft movements in 2018, the potential risks associated with such winds should not be underestimated (*PUSTIKOM*, 2019).

Numerical weather prediction (NWP) has proven to be a valuable instrument in investigating aviation incidents, allowing researchers to probe meteorological factors in regions and altitudes devoid of direct observations. In a study by *Regmi et al*. (2020), 13 plane accidents in Nepal attributed to near-surface turbulence were researched utilizing NWP. *Verayanti* and *Kusuma* (2021) and *Andari et al.* (2022) used NWP simulations to identify turbulence in the vicinity of clouds, which contributed to the turbulent flight paths of aircraft ID6890 on October 24, 2017, and EY474 on May 4, 2016. *Chan* (2014) also focused on forecasting

tailwinds resulting from wind interaction with terrain via NWP simulations. *Tse et al.* (2014) showcased NWP's capability to predict tailwinds associated with thunderstorms. Meanwhile, *Sardjono et al.* (2021) simulated tailwinds with the weather research and forecasting (WRF) model that closely matched observations.

The analysis of tailwinds during the approach phase at various altitudes using NWP has been a relatively underexplored area of research. *Chan* (2014) and *Tse et al.* (2014) conducted some of these limited studies. Most of the existing research primarily relies on surface wind data (*Fadholi*, 2013; *Perdana* and *Putra*, 2017; *Nanda et al.*, 2020; *Sardjono et al.*, 2021), sometimes in combination with satellite imagery and 1000 feet (305 meters) wind data to investigate the atmospheric dynamics during tailwinds (*Rais et al.*, 2020). To further delve into this phenomenon, we intend to employ the Weather Research and Forecasting (WRF) model to comprehensively analyze the mechanisms that induce tailwinds and enhance our comprehension of the underlying atmospheric processes.

2. Materials and method

We analyzed go-around reports from four aircrafts over runway 07L, namely JT023, GA221, QG251, and QG331, and four aircrafts over runway 07R, namely JT291, ID6871, GA113, and JT335. These reports highlight go-around actions due to 15-knot tailwinds during approaches at the Soekarno-Hatta International Airport on November 3, 2021. These reports were sourced from the air navigation services provider AirNav Indonesia, and we cross-referenced them with aircraft trajectories obtained from flightradar24 for confirmation. The details of these go-around incidents are provided in *Table 1*.

Table 1. AirNav Reports of the Go-around

Aircraft	Go-around	Landing
JT023	09:58UTC RWY 07L	10:28 UTC RWY 25R
JT291	10:05UTC RWY 07R	10:30 UTC RWY 25L
GA221	10:06UTC RWY 07L	10:30 UTC RWY 25R
ID6871	10:07UTC RWY 07R	10:33 UTC RWY 25L
QG251	10:08UTC RWY 07L	10:40 UTC RWY 25R
GA113	10:09UTC RWY 07R	10:36 UTC RWY 25L
QG331	10:12UTC RWY 07L	10:35 UTC RWY 25R
JT355	10:11UTC RWY 07R	10:39 UTC RWY 25L

We employed the Advanced Research Weather Research and Forecasting (ARW-WRF) version 4.1 numerical weather prediction model (*Skamarock et al.*, 2019). The WRF-ARW model is widely used in aviation meteorological analysis. *Chan* (2014), *Tse et al*. (2014), *Regmi et al*.(2020), *Verayanti* and *Kusuma* (2021), *Sardjono et al*. (2021), and *Andari et al*. (2022) use the WRF-ARW in their research. For the initial conditions, we utilized data from the NCEP GDAS/FNL (Global Data Assimilation System/Final Analysis of the National Centers for Environmental Prediction, USA) with a horizontal grid resolution of 0.25° and a temporal resolution of 6 hours, covering the period from November 2, 2021, 18 UTC to November 3, 2021, 12 UTC. The WRF-ARW configuration is detailed in *Table 2*. To validate the cloud top temperature of the WRF-ARW model, we used satellite observation data of the Himawari 8 geostationary meteorological satellite operated by the Japan Meteorological Agency and computed the correlation coefficient between 09:50 and 11:00 UTC. Further information regarding the model configuration can be found in *Table 2*. *Fig. 1* presents the three models domains (D1, D2, and D3) used for simulations by the WRF-ARW model.

Table 2. WRF-ARW configuration for domain 1 (D1), domain 2 (D2), and domain 3 (D3)

	D1	**D2**	**D3**
Resolution	9 km	3 km	1 km
Temporal interval	3 hours	1 hour	2 minutes
Vertical Layer	34	34	34
Parameterization	Tropical	Tropical, Cu=0	Tropical, Cu=0
Topography	GMTED	GMTED	SRTM 1s

We employed tropical-specific physical parameterizations, which included the WRF single moment 6 class (WSM6) scheme for microphysics, the newer Tiedtke scheme for cumulus convection, the rapid radiation transfer model for global circulation models (RRTMG) scheme for shortwave and longwave radiations, and the Yonsei University scheme for the boundary layer. Notably, the WSM6 scheme encompasses graupel production within the microphysical processes (*Song-You Hong* and *Jeong-Ock Jade Lim*, 2006), a feature that distinguishes it from WSM5 *(Lim* and *Hong 2005)*. The newer Tiedtke scheme calculates mixing ratios for cloud and ice, momentum tendencies, and shallow convection (*Skamarock et al.*, 2019). This scheme has demonstrated the ability to capture the fundamental characteristics of the marine boundary layer structure and low clouds (*Zhang et al.*, 2011), as well as to offer improved diurnal precipitation simulation (*Sun and Bi*, 2019). Additionally, the RRTMG scheme delivers radiative forcing results that exhibit closer agreement with high-resolution calculations (*Iacono et al.*, 2008).

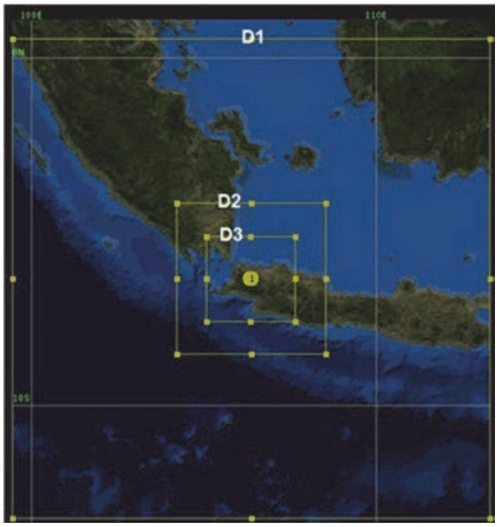

Fig. 1. WRF-ARW domain 1 (D1), domain 2 (D2), and domain 3 (D3).

The following equation was used to calculate the tailwind based on vector projection to the runway in use (*Belo-Pereira*, 2015; *Maruhashi et al.*, 2019; *Rais et al.*, 2020) :

$$Tw = -f\cos(d - r), \tag{1}$$

where *Tw* is the tailwind (kt), *f* is the wind speed (kt), *d* is the wind direction (°), and *r* is the direction of the runway in use (°).

3. Results and discussion

3.1. Track analysis

Fig. 2 shows that aircraft destined for runway 07L follow a relatively shorter final approach path (FAP), denoted as A-B compared to the trajectories leading to runway 07R, marked as C-D. A-B and C-D measure 9.15 nautical miles (approximately 16.94 kilometers) and 15 nautical miles (roughly 27.78 kilometers), respectively. It is worth noting that the maximum allowable FAP length, as per ICAO standards (*ICAO*, 2018), is 15 nautical miles. Aircraft flying over segment A transitioned from an altitude of 2175 feet to 2875 feet, while those over segment C experienced altitude changes from 4150 feet to 4225 feet. Moreover, runway 07 is more susceptible to tailwinds due to a higher incidence of wind blowing from the direction of runway 07 than runway 25, as indicated by windrose analysis (*Sardjono et al.*, 2021).

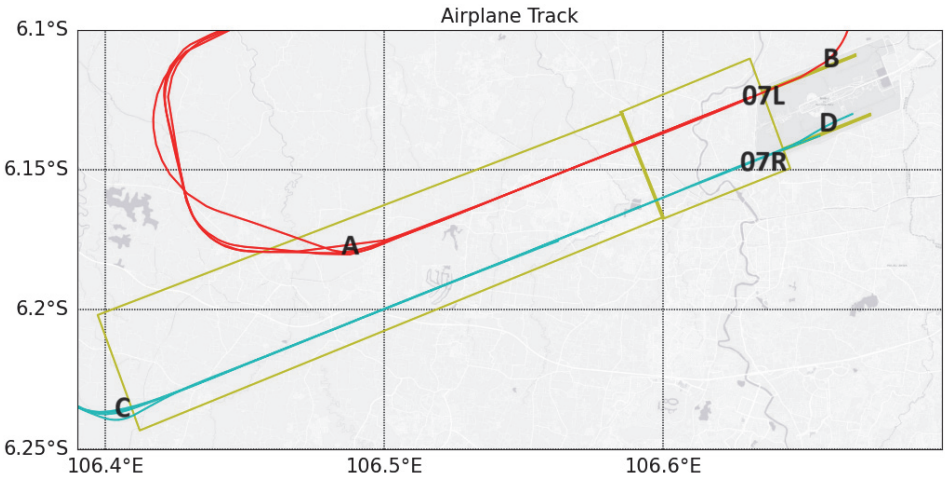

Fig. 2. Flights tracking to runway 07L (red line), runway 07R (cyan line), ARENA (small box), and FAP (small box + big box).

In sections A-B (*Fig. 3*), four flights, namely JT023, GA221, QG251, and Q331 traverse the A-B segment within specific time windows: 09:56 to 10:00, 10:04 to 10:08, 10:06 to 10:08, and 10:08 to 10:12, respectively. Among these aircraft JT023, GA221, and QG251 approach altitudes of 700 feet (213 meters), 500 feet (152 meters), and 450 feet (137 meters) above the surface, respectively, before executing a go-around maneuver and subsequently taking off again. These planes performed the go-around near the ARENA area, located at 3 nautical miles (5556 meters) from the runway, as indicated by *Chan* and *Hon* (2016).

Conversely, the QG331 aircraft maintains an approach altitude of only up to 1675 feet (510 meters). Notably, all aircraft experienced a consistent tailwind of approximately 15 knots (8 meters per second) at altitudes of up to 1500 feet (457 meters). This specific altitude represents the low-level wind shear region, where atmospheric dynamics significantly influence aircraft take-off and landing procedures, in accordance with ICAO guidelines (*ICAO*, 2005).

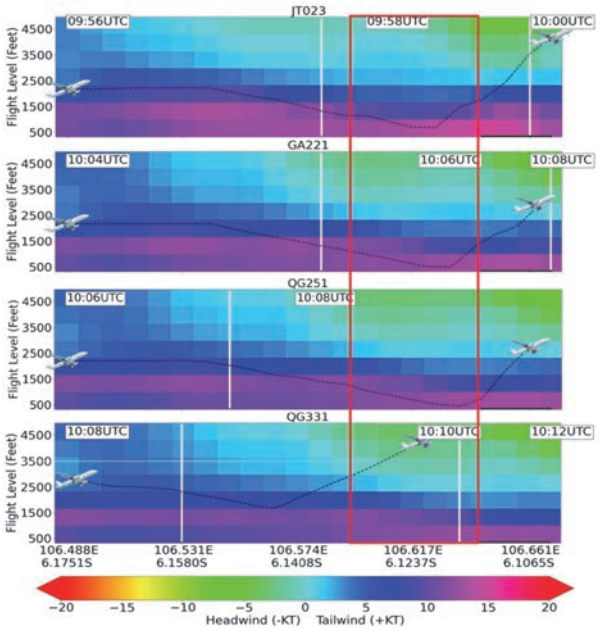

Fig. 3. Tailwind/Headwind (kt) in the A-B section overlayed by vertical flight track to runway 07L in every 2 minutes. The red box is ARENA, and the black line at the bottom right is the runway.

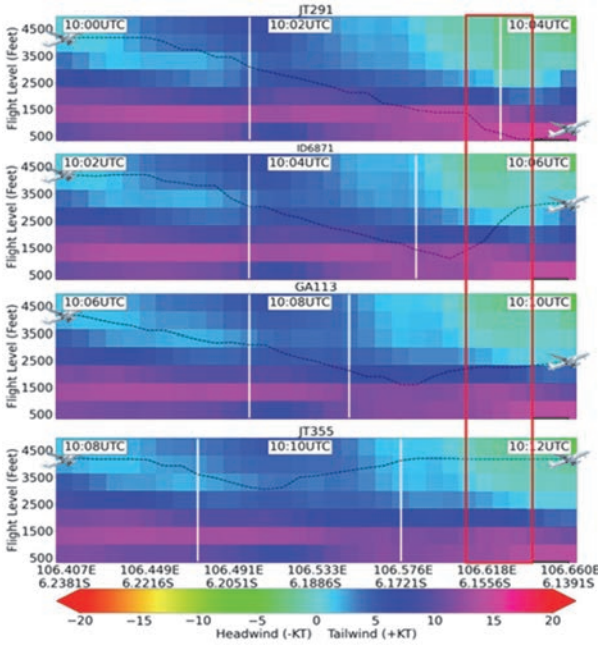

Fig. 4. Tailwind/Headwind (kt) in the C-D section overlayed by vertical flight track to runway 07L in every 2 minutes. The red box is ARENA, and the black line at the bottom right is the runway.

Within the C-D segment (*Fig. 4*), flights JT291, ID6871, GA113, and JT355 traverse the C-D portion during specific intervals: 10:00 to 10:04, 10:02 to 10:06, 10:06 to 10:10, and 10:08 to 10:12 UTC, respectively. The altitudes at which these aircrafts operate at the lowest points are 250 feet (76 meters) for JT291, 1100 feet (335 meters) for ID6871, 1600 feet (487 meters) for GA113, and 3050 feet (929 meters) for JT355. Of these, JT291 is in closest proximity to the runway.

As observed in the A-B sections, tailwinds persist at lower altitudes along the C-D route. These tailwinds, measured at 15 knots (8 m/s), surpass the minimum limit for B737 aircraft (10 knots or 5 m/s) and reach the tailwind limit for A320 aircraft, set at 15 knots or 8 m/s, as reported by *Es* and *Karwal* (2001). It is worth noting that the final approach path (FAP) to runway 07L experiences lower tailwind speeds than the FAP for runway 07R. Further exploration of this aspect will be undertaken in the Numerical Weather Prediction analysis section.

3.2. NWP analysis

This outcome validates the cloud top temperature of the WRF-ARW model, indicating a correlation coefficient of 0.6286 compared to the cloud top temperature of Himawari 8. This value closely resembles the correlation found in the study of *Chae* and *Sharewood* at an altitude of 14 km (*Chae* and *Sherwood*, 2010).

In *Fig. 5*, it is evident that a 15-knot (8 m/s) wind is present over the Indian Ocean, located to the south of Java, from 09:58 UTC to 10:12 UTC, at an altitude of 1500 feet (457 meters), and it shifts towards the final approach path (FAP). According to *Kurniawan et al*. (2011), wind speeds in this region, specifically the Indian Ocean, can reach up to 20 knots or 10 m/s during November. These strong winds result from the still-active Australian winter monsoon (*Alifdini*, 2021).

In area A, the wind entering the FAP is not obstructed by any terrain features, as indicated by the absence of white contours. As a result, the wind within the FAP region maintains a speed of 15 knots (8 m/s). Furthermore, the air mass located over the FAP is drawn into an area of wind convergence, denoted as area B. Wind convergence describes the phenomenon, where wind vectors converge towards a common point (*Stull*, 2020). This convergence of winds is closely associated with cloud formation, as *Banacos et al.* (2005) outlined.

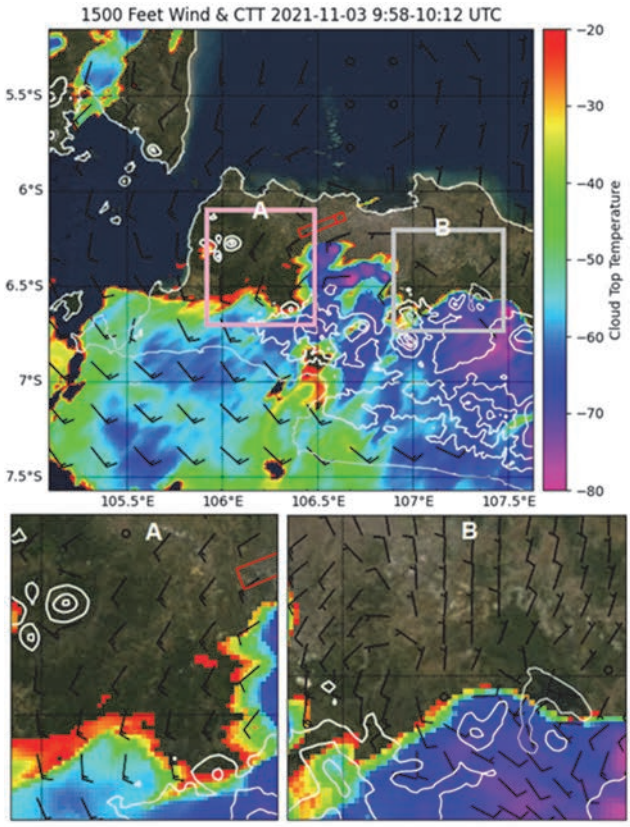

Fig. 5. Composite wind 1500 ft (457 m) over D3 from 09:58 to 10:12 UTC. The red box is the FAP. Box A and Box B are the areas of interest in the analysis.

The tailwind speed over the A-B segment is comparatively lower than the C-D segment (*Figs. 3* and *4*). This disparity is because the wind from the Indian Ocean initially reaches the C-D segment before progressing to A-B. As mentioned, C-D represents a longer trajectory than A-B, resulting in a broader wind coverage.

Fig. 6 shows a notable presence of vertical wind in area B, extending to an altitude of 20,000 meters (approximately 65,616 feet). This upward vertical movement of air masses at lower levels is significant. As *Shinozaki et al.* (2019) discussed, cloud analysis can be conducted based on cloud fraction. A higher cloud fraction indicates a greater cloud density. It is worth noting that at 09:59 UTC, convective clouds were still forming, reaching an altitude of 10,000 meters (around 32,808 feet). The convection in this area draws air masses from the Indian Ocean, causing a 15-knot wind to enter the FAP in a parallel direction.

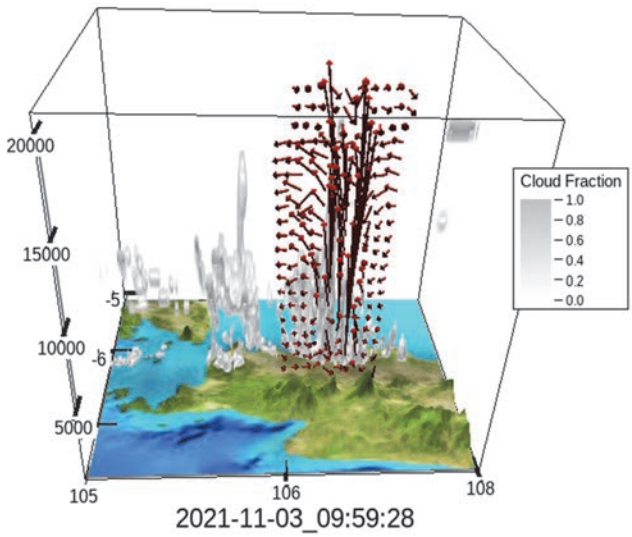

Fig. 6. A vertical section of wind in area B (*Fig. 5*) is overlayed with cloud fraction.

At 11 UTC (*Fig. 7*), a cloud with a cold top (around -80 °C), is observed south of the FAP. A cold top indicates a high cloud altitude. In area A, there is a presence of wind divergence. This divergence causes the wind, which previously flowed in the same direction as the FAP, to veer towards the north. This, in turn, influences the *d-r* component in Eq.(1), causing it to expand and reduce the cosine value. As a result, the tailwind magnitude becomes smaller.

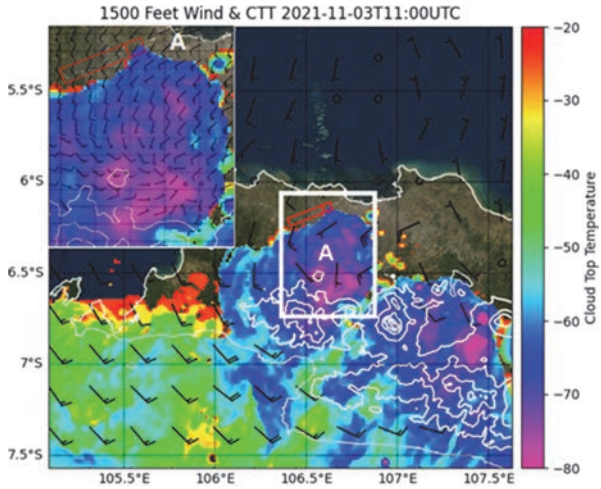

Fig. 7. Wind at 1500 ft (457 m) over D3 at 11:00 UTC. The red box is the FAP. Box A is the area of interest in the analysis.

Fig. 8 shows that high-altitude clouds with tops reaching 20,000 meters (65,616 feet) are present in area A. Concurrently, there is noticeable downdraft activity blown from this mature cloud at lower altitudes. This downdraft generates divergence at a height of 1500 feet, similar to the findings in Yoshino's study (*Yoshino,* 2019). It is worth noting that compared to the research conducted by *Auly et al.* (2018), the wind gust observed in this case is not a result of the downdraft itself. Instead, it is initiated by the background wind originating from the Indian Ocean, which experiences a reduction due to the downdraft's influence, particularly in a direction perpendicular to the wind gust.

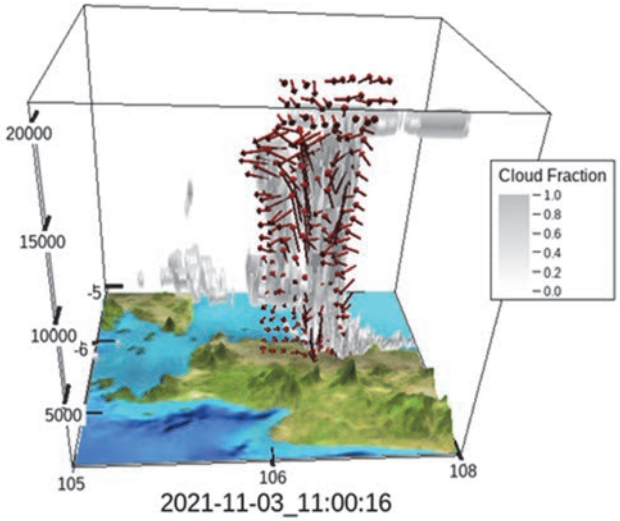

Fig. 8. A vertical section of wind over area A in *Fig. 7* is overlayed with cloud fraction.

4. Conclusions

We conducted weather simulations related to eight aircraft go-arounds to understand wind dynamics better. These simulations were performed using the WRF-ARW model with a spatial and temporal resolution of 1 km and 2 minutes, verified against Himawari 8 cloud top temperatures. Eight flights executed go-around maneuvers triggered by tailwinds, as depicted in *Figs. 3* and *4*, and these could be accurately simulated using WRF-ARW. In *Figs. 5* and *6*, we analyze that wind from the Indian Ocean, in conjunction with the cloud formation process, generated tailwinds over the FAP. Meanwhile, at 11:00 UTC, as evident in *Figs. 7* and *8*, we documented a reduction in wind speed due to gusts originating from downdrafts southward near the FAP.

This study has revealed the significant impact of background winds on tailwinds, a factor not explicitly addressed in previous researches. By expanding our analysis beyond the airport's observation points and utilizing the WRF-ARW model, this research provides valuable insights into how background winds can influence the occurrence of tailwinds. This knowledge holds the potential to enhance aviation safety and operational efficiency. Future research must assimilate observation data into the NWP for more precise investigations.

Funding: The research was performed without external funding.

References

Ahrens, C.D. and *Henson, R.*, 2014: Meteorology today: an introduction to weather, climate, and the environment. Cengage, 662 p.

Alifdini, I., 2021: Seasonal distribution and variability of surface winds in the Indonesian seas using scatterometer and reanalysis data 1–19. *Int. J. Climatol. 41*, 4825–4843. https://doi.org/10.1002/joc.7101

Andari, B.R.T., Trilaksono, N.J., and *Munandar, M.A.*, 2022: A Numerical Study of Near Cloud Turbulence Encounters over Bangka Island On 4 May 2016. *Jurnal Meteorlogi Klimatologi dan Geofisika*, 65–72. https://doi.org/10.31172/jmg.v23i3.912

Arta Kusuma, L.K.N., Pratiwi, I., Ismanto, H., and *Fitrianto, M.A.*, 2022: Utilization of Doppler Weather Surveillance Radar for Wind-Shear Detection in Airport, In: Proceedings - 2022 8th International Conference on Science and Technology, ICST 2022. Institute of Electrical and Electronics Engineers Inc. https://doi.org/10.1109/ICST56971.2022.10136300

Auly, A., Nugraha, A., and *Trilaksono, N.J.*, 2018: Simulation of Wind Gust – Producing Thunderstorm Outflow over Mahakam Block Using WRF 020051. *Jurnal Ilmu Fisika | Universitas Aandalas 15(2)*,175–187. https://doi.org/10.1063/1.5047336

Banacos, P.C., Oceanic, N., and *Schultz, D.M.*, 2005: The Use of Moisture Flux Convergence in Forecasting Convective Initiation: Historical and Operational Perspectives. *Semantic Scholar* ID: 2927533. https://doi.org/10.1175/WAF858.1

Belo-Pereira, M., 2015: Comparison of in-flight aircraft icing algorithms based on ECMWF forecasts. *Meteorol. Appl. 22*, 705–715. https://doi.org/10.1002/met.1505

Blajev, T., 2017: Go-Around Decision-Making and Execution Project. Flight Safety Foundation. https://flightsafety.org/wp-content/uploads/2017/03/Go-around-study_final.pdf

Boeing, 2021: Statistical Summary of Commercial Jet Airplane Accidents.

Chae, J.H. and *Sherwood, S.C.*, 2010: Insights into Cloud-top height and Dynamics from the Seasonal cycle of cloud-top heights observed by MISR in the west Pacific region. *J. Atmos.Scie. 67*, 248–261. https://doi.org/10.1175/2009JAS3099.1

Chan, P.W., 2014: A tail strike event of an aircraft due to terrain-induced wind shear at the Hong Kong international airport. *Meteorol. Appl. 21*, 504–511. https://doi.org/10.1002/met.1303

Chan, P.W. and *Hon, K.K.*, 2016: Observation and Numerical Simulation of Terrain-Induced Windshear at the Hong Kong International Airport in a Planetary Boundary Layer without Temperature Inversions. *Adv. Meteorol. 1016*. https://doi.org/10.1155/2016/1454513

Chang, S.W., 2015: Crosswind-based optimization of multiple runway orientations. *J. Adv. Transport. 49*, 1–9. https://doi.org/10.1002/atr.1247

Es, G.V. and *Karwal, A.K.*, 2001: Safety aspects of tailwind operations Safety aspects of tailwind operations. NLR-TP-2001-003. https://skybrary.aero/sites/default/files/bookshelf/1148.pdf

Fadholi, A., 2013: Analisis Komponen Angin Landas Pacu (Runway) Bandara Depati Amir Pangkalpinang. *Statistika 13*, 45–53.

Gultepe, I., Sharman, R., Williams, P.D., Zhou, B., Ellrod, G., Minnis, P., Trier, S., Griffin, S., Yum, S.S., Gharabaghi, B., Feltz, W., Temimi, M., Pu, Z., Storer, L.N., Kneringer, P., Weston, M.J., Chuang, H. ya, Thobois, L., Dimri, A.P., Dietz, S.J., França, G.B., Almeida, M. V., and *Neto, F.L.A.*, 2019: A Review of High Impact Weather for Aviation Meteorology. *Pure Appl. Geophys. 176*, 1869–1921. https://doi.org/10.1007/s00024-019-02168-6

Iacono, M.J., Delamere, J.S., Mlawer, E.J., Shephard, M.W., Clough, S.A., and *Collins, W.D.*, 2008: Radiative forcing by long-lived greenhouse gases: Calculations with the AER radiative transfer models. *J. Geophys. Res. Atmos. 113*. https://doi.org/10.1029/2008JD009944

ICAO, 2005: Manual on Low-level Wind Shear. ICAO.

ICAO, 2018: Annex 10 to the Convention on International Civil Aviation : Aeronautical Telecommunications. ICAO.

Kurniawan, R., Habibie, M.N., and *Suratno, S.*, 2011: Variasi Bulanan Gelombang Laut Di Indonesia. *Jurnal Meteorologi dan Geofisika, 12*, 221–232. https://doi.org/10.31172/jmg.v12i3.104

Lim J.O.J and *Hong S.Y.* 2005 : Effects of bulk ice microphysics on the simulated monsoonal precipitation over east Asia. *J Geophys Res Atmos. 110(24):1–16.* https://doi.org/10.1029/2005JD006166.

Maruhashi, J., Serrano, P., and *Bello Pereira, M.*, 2019: Analysis of Mountain Wave Effects on a Hard Landing Incident in Pico Aerodrome Using the AROME Model and Airborne Observations. *Atmosphere 10*(7), 350; https://doi.org/10.3390/atmos10070350

Nanda, R.F., Sobirin, and *Saraswati, R.*, 2020: Place exposure pattern toward landslide disaster due to heavy rainfall in Probolinggo District, East Java, In: IOP Conference Series: Earth and Environmental Science. Institute of Physics Publishing. https://doi.org/10.1088/1755-1315/481/1/012058

Oliver, J.E., 2005: Encyclopedia of world Climatology. Springer, Dordrecht, 874 p. https://doi.org/10.1007/1-4020-3266-8

Perdana, Y.H. and *Putra, I.D.G.A.*, 2017: Kejadian Crosswind di Landasan Pacu Bandara Supadio Pontianak Tahun 2016, In: Seminar Nasional Iptek Penerbangan Dan Antariksa XXI-2017. 0–5.

PUSTIKOM, 2019: Statistik Perhubungan Buku I 2018. Kementrian Perhubungan, 224 p.

Rais, A.F., Wijayanto, B., and *Meinovelia, E.*, 2020: Analisis Tailwind Penyebab Go-Around pada 38 Bandara di Indonesia dalam Periode Januari-Februari 2020. *Warta Penelitian Perhubungan*, *32*, 77–82. https://doi.org/10.25104/warlit.v32i2.1546

Regmi, G., Shrestha, S., Maharjan, S., Khadka, A.K., Regmi, R.P., and Kaphle, G.C., 2020: The Weather Hazards Associated with the US-Bangla Aircraft Accident at the Tribhuvan International Airport Nepal. *Weather Forecast. 35*, 1891–1912. https://doi.org/10.1175/WAF-D-19-0183.1

Sardjono, W., Zulkarnain, Kusnoputranto, H., Soesilo, T.E.B., Utama, D.N., and *Sudirwan, J.*, 2021: Study of runway crosswind and tailwind potential for airport sustainability: A study of Soekarno Hatta airport, Cengkareng, Indonesia, In: IOP Conference Series: Earth and Environmental Science. IOP Publishing Ltd. https://doi.org/10.1088/1755-1315/729/1/012012

Shinozaki, K., Monte, S., Ferrarese, S., Manfrin, M., Bertaina, M.E., Anzalone, A., Bisconti, F., Bruno, A., and *Diaz, A.*, 2019: Cloud distribution evaluated by the WRF model during the EUSO-SPB1 flight 05006, 1–6. https://doi.org/10.1051/epjconf/201921005006

Skamarock, W.C., Klemp, J.B., Dudhia, J., Gill, D.O., Liu, Z., Berner, J., Wang, W., Powers, J.G., Duda, M.G., Barker, D.M., and *Huang, X.-Y.*, 2019: A Description of the Advanced Research WRF Model Version 4. Boulder. doi:10.5065/1dfh-6p97

Song-You Hong, and *Jeong-Ock Jade Lim*, 2006: The WRF Single-Moment 6-Class Microphysics Scheme (WSM6). *J Korean Meteorl. Soc. 42*(2) 129–151.

Stull, R., 2020: Practical Meteorology: An Algebra-based Survey of Atmospheric Science Roland. The University of British Columbia, 944 p.

Sun, B.Y., and *Bi, X.Q.*, 2019: Validation for a tropical belt version of WRF: sensitivity tests on radiation and cumulus convection parameterizations. *Atmos. Ocean. Sci. Lett. 12*, 192–200. https://doi.org/10.1080/16742834.2019.1590118

Tse, S.M., Chan, P.W., and *Wong, W.K.*, 2014: A case study of missed approach of aircraft due to tailwind associated with thunderstorms. *Meteorol. App. 21*, 50–61. https://doi.org/10.1002/met.1296

Verayanti, N P.T and *Kusuma, I.K.N.A.*, 2021: Simulasi Numerik Mekanisme Turbulensi Dekat Awan Konvektif. *Jurnal Sains and Teknologi Modifikasi CuacaModifikasi Cuaca 22*, 25–33. https://doi.org/10.29122/jstmc.v22i1.4560

WMO, 2021: Guide to Instruments and Methods of Observation Volume I-Measurement of Meteorological Variables, 2021st ed. WMO, Geneva.

Yoshino, K., 2019: Low-level wind shear induced by horizontal roll vortices at Narita international airport, Japan. *J. Meteorol. Soc. Japan 97*, 403–421. https://doi.org/10.2151/jmsj.2019-023

Zhang, C., Wang, Y., and Hamilton, K., 2011: Improved representation of boundary layer clouds over the southeast pacific in ARW-WRF using a modified tiedtke cumulus parameterization scheme. *Month. Weather Rev. 139*, 3489–3513. https://doi.org/10.1175/MWR-D-10-05091.1

DOI:10.28974/idojaras.2024.4.3

IDŐJÁRÁS

Quarterly Journal of the HungaroMet Hungarian Meteorological Service
Vol. 128, No. 4, October – December, 2024, pp. 439–450

The connection between time of concentration and rainfall intensity based on rainfall-runoff modeling

Klaudia Négyesi* and **Eszter Dóra Nagy**

Department of Hydraulic and Water Resources Engineering
Faculty of Civil Engineering
Budapest University of Technology and Economics
Műegyetem rkp. 3., H-1111 Budapest, Hungary.

**Corresponding Author E-mail: negyesiklaudia@edu.bme.hu*

(Manuscript received in final form November 10, 2023)

Abstract— The study aims to examine the relation between rainfall intensities and times of concentration based on rainfall-runoff modeling using the recently developed features of the Hydrologic Engeneering Center – Hydrologic Modeling System (HEC-HMS) modeling software. The time of concentration is generally considered a constant characteristic of a catchment. However, various publications have shown that response time is a dynamic property and a function of rainfall intensity. Model simulations were performed to gain more insight into the relationship mentioned. The applicability of the dynamic time of concentration was examined with the help of a recent version of the HEC-HMS software that can interpret the dynamic relationship between time of concentration and rainfall intensity. The models were built for characteristic and dynamic cases. In the characteristic case, the time of concentration values of the catchments were calculated using the commonly applied Wisnovszky empirical equation, while in the dynamic case, the applicability of the rainfall intensity, i.e., the time of concentration function, was examined. The applicability of the new HEC-HMS feature was reviewed, and the relationship between the time of concentration and rainfall intensity was confirmed. The dynamic approach improved the models' performance, especially where the Wisnovszky equation yields an inadequate estimation of the time of concentration based on the results.

Key-words: rainfall, rainfall-runoff, modeling, event-based, lumped, time of concentration, rainfall intensity, HEC-HMS

1. Introduction

Numerical modeling became one of the most important tools in hydrological sciences. The rapid development of informatics has allowed us to use different software to build various models for countless purposes, even simulating highly complex phenomena. Several hydrological programs enable us to build accurate and efficient models. A precise hydrological model depends critically on available data (*Beven*, 2012). If our input data is unreliable, it can lead to numerous uncertain parameters and an inaccurate or falsely accurate model. Therefore, the thorough analysis of different data types and the approaches of inserting input data in a model can help the users select the most appropriate sources and tools for their tasks.

One of the most significant parts of hydrological modeling is rainfall-runoff modeling. In the case of such models, the unit hydrograph theory became the most commonly used hydrograph modeling technique. The unit hydrograph represents a discrete transfer function for effective rainfall to reach the basin outlet, lumped to the catchment scale (*Beven*, 2012). Response time parameters are essential when using unit hydrograph theory in modeling. These parameters can be the lag time, the time to peak, the time to equilibrium, or the time of concentration (τ or T_C). The most commonly applied parameter is the time of concentration, which can also be defined in many ways (*Nagy* and *Szilágyi*, 2020). In this study, time of concentration is reviewed as the period of time required for storm runoff to flow to the outlet from the point of a drainage basin having the longest travel time (*WMO*, 1974). In both Hungarian and international engineering practice, it is usually considered a constant characteristic of a catchment; however, this simplification results in unreliable model simulations in the case of extreme precipitation events. Many publications have shown that the response time is a dynamic property, as it decreases exponentially with increasing rainfall intensity (*Szilágyi*, 2007; *Reed et al.*, 1975; *Saghafian et al.*, 2002; *Zhang et al.*, 2007; *Mathias et al.*, 2016; *Cuevas et al.*, 2019). Unfortunately, the intensity of current rainfall events varies noticeably due to climate change (*Mattányi et al.*, 2015). Higher intensity leads to a shorter response time, which has a significant effect on the hydrograph shape. It results in a steeper rising limb and a higher flood peak; the latter is a crucial value in the case of any designing parameter. This aspect also justifies the need to better understand response time and its relationship with rainfall intensity.

The problem of time of concentration estimation is also widely discussed worldwide. In international publications, several different empirical equations can be found. Due to the many definitions and methods found to determine the time of concentration, the estimation is one of the most uncertain elements of modern hydrology and is also generally reviewed as a paradox (*Grimaldi et al.*, 2012; *Michailidi et al.*, 2018). This research applies the Clark Unit Hydrograph method, a modified version of the UH theory. Short-term water storage

throughout a watershed – in the soil, on the surface, and in the channel – plays an important role in transforming precipitation excess into runoff. The linear reservoir model is a common representation of the effect of this storage. (*Feldman*, 2000)

The Hydrologic Engineering Center – Hydrologic Modeling System (HEC-HMS) modeling software was applied to analyze the characteristic and dynamic approaches of time of concentration estimation. HEC-HMS is a US-developed software, and its application is widespread both abroad and in Hungary. The program is freely available and can be easily downloaded and installed from the Hydrologic Engineering Center's website. The software's recent versions include the so-called "variable parameter" method in the Clark Unit Hydrograph method, which means applying a dynamic time of concentration. This latest option can help us produce more realistic and precise models in the future. The following chapters examine the characteristic and dynamic approaches of time of concentration with the help of literature review and simulation runs using the recent modules of HEC-HMS. Thereby, the performance of the rainfall-runoff models is analyzed, and the rainfall intensity-time of concentration relationship is further confirmed.

2. Study area and materials

Two different river catchments (Zala and Kiskomárom) were examined in western Hungary (*Fig. 1*) The catchment of Zala with the outlet point of Zalalövő has an area of 188 km^2. In contrast, Kiskomárom has an area of 99 km^2. According to the Köppen climate classification, the catchments' climate is predominantly warm-summer humid continental (*Peel et al.*, 2007). The region has high precipitation rates; the long-term mean annual precipitation is above 800 mm at Zala and around 660 mm at Kiskomárom. In both cases, the maximum precipitation values occur in June and July, while January has the least precipitation. Precipitation occurs 100–110 days per year and can exceed 10 mm on 20 days annually. The region's maximum precipitation values were 80–120 mm/day (*NYUDUVIZIG*, 2016).

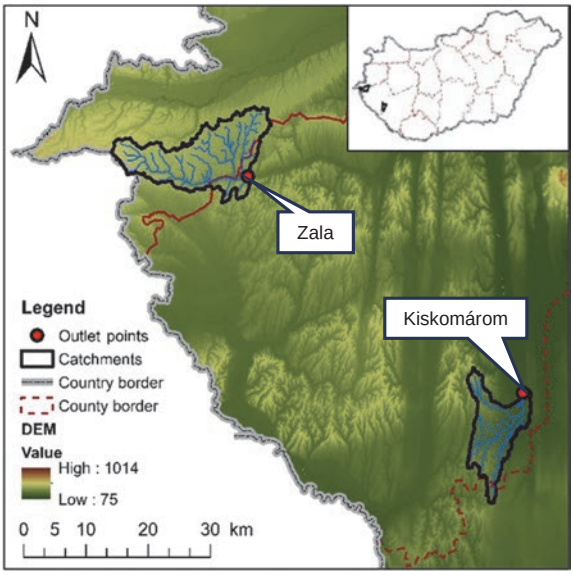

Fig. 1. Study catchments in Hungary.

A watershed's land use and soil characteristics are significant during rainfall-runoff modeling. Based on the CORINE Land Cover maps, the ratio of artificial surfaces is very similar between the two catchments; at Kiskomárom it is 4%, while at Zala this value is 5%. Agricultural areas are more significant at Kiskomárom (61%), while this rate is significantly lower at Zala (36%). Consequently, the rate of forests and semi-natural areas is notably higher at Zala (60%) than at Kiskomárom (34%) (*CORINE*, 2018). Regarding the soil texture of the study area, Kiskomárom is covered mostly with loam, but a smaller area of sand, and clay loam can also be found. Zala is almost completely covered with loam or clay loam. A negligible area of coarse fragments is present at the eastern part of the catchment (*AGROTOPO*, 2016).

In a previous study by *Nagy* (2018), an exponential relationship between rainfall intensity and time of concentration was detected. This study included the analysis of rainfall-runoff events at six Hungarian catchments, out of which two were selected for the present study. The precipitation and discharge time series, the suitable events for modeling, and the geometric models of the catchments were already available from this previous study. The local water directorates from staff gauges of Zalakomár and Zalalövő provided discharge time series (*Nagy*, 2018). Precipitation data were collected from the European Centre for Medium-Range Weather Forecasts (ECMWF) ERA5-Land re-analysis database (*Muñoz Sabater*, 2019), which is the database of an independent organization, supported by plenty of European countries, providing grid-based precipitation data with a spatial resolution of 0.1° (~ 9 km). All data was used with an hourly time resolution.

Seven events were selected for model calibration for both catchments, while six were chosen to validate the model. The events were selected from the snow-free (or summer) season between 2006 and 2014 to avoid the complex process of snowmelt modeling. This way, the number of free parameters is reduced, which can lead to more reliable results regarding the research of time of concentration and its relationship to rainfall intensity. During the selection of the events, it was essential to avoid possible measurement errors seen from the analysis of runoff rates and the shapes of the hyeto- and hydrographs. Runoff rates can be calculated as the observed runoff volume divided by the precipitation volume. If a runoff rate is above one, the precipitation and/or runoff data is insufficient, while values within 0.01 and 0.2 are typical for summer events (*Kovács*, 1979). The events selected in this study showed reasonable values regarding the runoff rates ranging from 0.05 to 0.24.

3. Methods

The HEC-HMS software was applied in this study, including the Clark Unit Hydrograph transform method. This method can be used to perform simulations with a characteristic value of time of concentration (*standard method*) or with a dynamic approach (*variable parameter method*). The standard method was applied for the characteristic case, in which the time of concentration and storage coefficient are the input parameters. The Wisnovszky equation estimated the characteristic value of time of concentration, while the storage coefficient was calibrated by trial and error. For the dynamic approach, the *variable parameter* method was selected. In this case, the curves of time of concentration – rainfall intensity and storage coefficient – rainfall intensity were calibrated.

3.1. Characteristic case

The time of concentration can be determined through measurements or by semi-empirical or empirical methods. The most common method for calculating the time of concentration in Hungary is the empirical equation introduced by *Wisnovszky* in 1958, which was derived from the Chézy equation and based on the observations regarding the geometry of Hungarian catchments:

$$\tau = \frac{L^2}{\sqrt{A * I}} \; [min], \tag{1}$$

where L is the length of the longest flow path [km], I is the slope of the longest flow path [-], A is the catchment area [km ^{2}].

In this study, Eq.(1) was applied in the characteristic case as it is the most commonly applied form of the Wisnovszky formula. However, Eq.(1) is only a simplified version of the formula introduced by Wisnovszky. The original equation had a multiplier dependent on the catchment size. Based on the publication, the complete equation is applicable for catchments with areas between 500 and 2000 km^2. Wisnovszky stated that it cannot be proved that his equation gives a better result than the other former equations he presented in his publication (*Wisnovszky*, 1958). The uncertainty of the time of concentration calculated by the Wisnovszky equation was proved in 2016 by *Nagy et al*. Based on their results, the equation does need revision and it can also be stated that we cannot expect to find a universal formula for all Hungarian watersheds (*Nagy et al.*, 2016). In 2021, *Nagy* and *Szilágyi* further confirmed the need for revision of the Wisnovszky equation and found that error in the estimation of time of concentration can be more than halved using the appropriate morphological parameters (*Nagy* and *Szilágyi*, 2021a). Despite the described problems, the current study analyzes the applicability of the Wisnovszky equation in the characteristic case, since the Hungarian engineering practice generally still uses this formula. In HEC-HMS, the characteristic value of time of concentration can be applied within the Clark Unit Hydrograph standard method.

3.2. Dynamic case

The reason for the dynamic property of the response time is related to the dynamic property of the aquifer: the subsurface soil saturates faster during high-intensity rainfall events, resulting in surface runoff sooner. This dynamic behavior of the aquifer and its effect on runoff generation is often overlooked (*Szilágyi*, 2007). The dynamic property of the response time of a catchment is acknowledged in many international studies. In general, it is most often associated with the characteristics of rainfall in the formulas and methods which have been published in recent decades (*Izzard* and *Hicks*, 1946; *Henderson* and *Wooding*, 1964; *Morgali* and *Linsley*, 1965; *Aron et al*., 1991; *Corps of Engineers*, 1954; *Askew*, 1970; *Kadoya* and *Fukushima*, 1977; *Papadakis* and *Kazan*, 1987; *Loukas* and *Quick*, 1996; *Schmidt* and *Schulze*, 1984*; McCuen et al*. 1984; *Nagy et al.*, 2022). It should also be noted that these formulas could not be applied in Hungary without analyzing their applicability. To the authors' best knowledge, no formula has been developed in Hungary that considers rainfall intensity when calculating the time of concentration.

Starting from HEC-HMS version 4.3 (*Scharffenberg et al.*, 2018), the so-called variable parameter method is available within the Clark Unit Hydrograph (UH) method, which deals with dynamic response characteristics. In this study, HEC-HMS version 4.7. was applied. UH theory assumes a linear relationship between precipitation and the runoff response. This assumption can lead to errors in timing and peak magnitude when simulating events that result

from extremely large excess precipitation rates. When using the Clark Unit Hydrograph, tables relating the time of concentration and storage coefficient to the excess precipitation can be used to vary the runoff response throughout the simulation. The *Index Excess* is an excess precipitation rate that is used to relate the time of concentration and storage coefficient defined in the editor against the variable parameter relationships. Typically, this rate is 1 mm/hour, indicating the intensity of rainfall. The variable parameter relationships must be defined as monotonically increasing percentage curves. The x-axis of the percentage curves defines the excess precipitation rate relative to the index excess. The y-axis of the percentage curves defines either the time of concentration or storage coefficient for each percent excess precipitation rate (again, relative to the index excess). (*Scharffenberg et al.*, 2020) The starting values of the variable parameter method can be determined easily. However, the calibration of the curves can be difficult as the whole range of rainfall intensities has to be considered for an accurate model for all events with different rainfall characteristics.

The approach of dynamic calculation can provide a method for using UHs for a range of flood events. The variable Clark Unit Hydrograph method could be the most useful for modeling extreme events since it can apply the dynamic relationship. The linearity assumption with UHs often leads modelers to arbitrarily adjust the UH parameters when using models for simulating extreme floods.

3.3. Applied model

The rainfall-runoff model applied in this study is deterministic, event-based, and lumped. *Fig. 2* is a flowchart of the calculation steps in HEC-HMS, including the selected methods. The effect of s*urface*, *routing*, and *loss/gain* methods were taken into consideration within the loss method. The parameters for the *canopy*, *loss*, and *baseflow* method were calibrated. The *transform* method is the key component of the study. It performs the actual surface runoff calculations contained within the subbasin. Out of the nine available transform methods, the Clark Unit Hydrograph method was applied. With the Clak method, the user is not required to develop a unit hydrograph through the analysis of past observed hydrographs; instead, a time versus area curve (time-area curve) is used to develop the translation hydrograph resulting from a burst of precipitation. The resulting translation hydrograph is routed through a linear reservoir to account for storage attenuation effects across the subbasin (*Scharffenberg*, 2020). In practice, this method can be used to perform simulations with a characteristic value of time of concentration (*standard method*) or with a dynamic approach (*variable parameter method*).

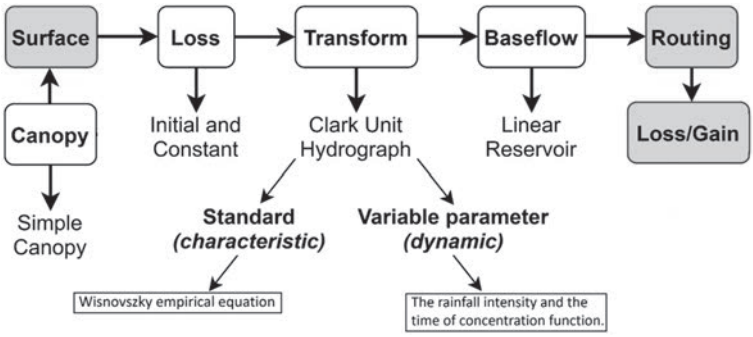

Fig. 2. Scheme of the rainfall-runoff model created in HEC-HMS.

The model performance was evaluated by two metrics: the Nash-Sutcliffe efficiency coefficient (*NSE*) and the differences between measured and observed peak times. The *NSE* values were reviewed for each simulation calculated according to the following formula:

$$NSE = 1 - \frac{\sum_{t=1}^{T}\left(Q_m^t - Q_0^t\right)^2}{\sum_{t=1}^{T}\left(Q_0^t - \bar{Q}_0\right)^2}, \quad T = 1,2,\dots,n. \ , \tag{2}$$

where $\bar{Q}_0$ is the mean of observed discharges, Q_m is the modeled discharge, Q_0^t is the observed discharge at time *t*, *n* the number of the observed discharges (*Nash* and *Sutcliffe*, 1970).

The value of *NSE* can vary between –∞ and 1.0. If *NSE* < 0, calculation with the average of the observed time series gives a better approximation than the model, which means that the model performance is unsatisfactory. If the value is between 0 and 0.5, the results are satisfactory, while between 0.5 and 0.8, the model simulation results are good. Above 0.8, the model performance is excellent. The perfect fit occurs when *NSE* = 1; therefore, the higher the value of *NSE*, the better the model. (*Nash* and *Sutcliffe*, 1970) The results were also categorized by noting the differences between observed and modeled time of peak discharges (Δt [hr]). When Δt is close to zero, it is considered excellent. The model is categorized as good if the difference is smaller than three hours. Values between three and five hours were labeled satisfactory, while differences above five hours were categorized as unsatisfactory.

4. Results and discussion

The results of the simulations can be seen in *Fig. 3/a*, where the lighter the color, the better the model performance is. The ID-s of the events of Zala start with Z, while the events of Kiskomárom have an ID starting with K. In *Fig. 3/b*, the results are summarized according to the previously described categories of

unsatisfactory, satisfactory, good, and excellent. The dynamic case's *NSE* values are improved both at Zala and Kiskomárom, which is also shown in the categories, where more events shifted towards the excellent category. The differences between peak times in the case of the calibration events also improved based on the categories. However, it is visible that in the case of events K26 and K28, the dynamic case yielded significantly worse results. The greatest improvements due to applying the dynamic approach can be seen during the calibration at the Zala catchment.

During validation, the events of the Zala catchment have worse or only slightly improved values of *NSE* in most cases. However, the events of Kiskomárom have enhanced *NSE* values after applying the dynamic approach since the categories of the events are moving more towards the direction of excellent. Reviewing the differences in peak time can show similar but less significant tendencies.

Overall, it is visible that applying the dynamic approach results in better *NSE* and Δt values in most of the cases, as the increasing number of simulated events falling into the excellent or good category clearly shows.

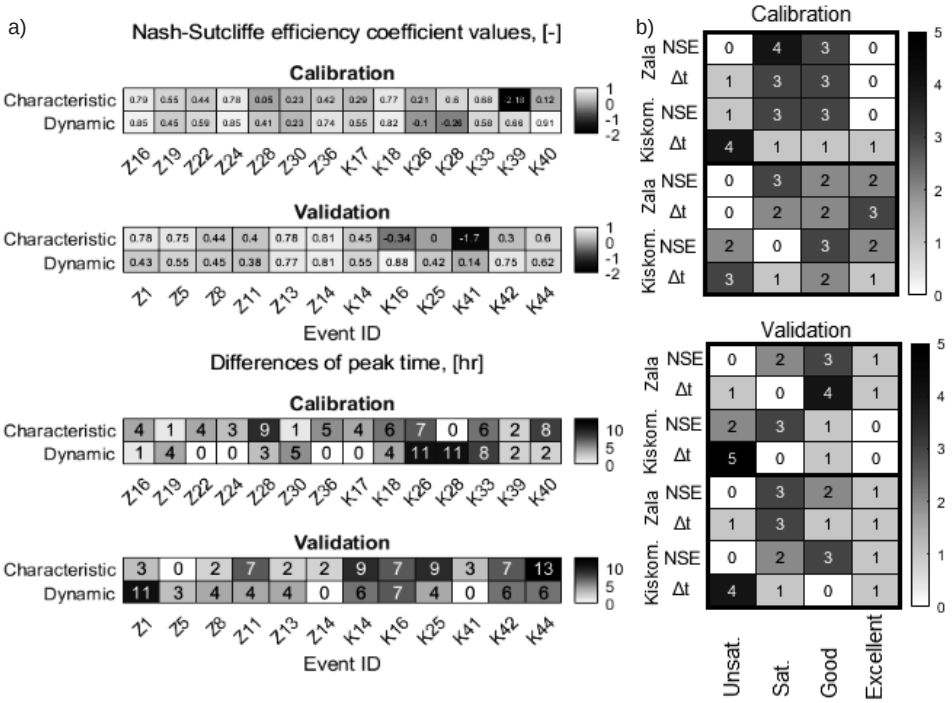

Fig.3. a) Results of simulations (*NSE* and Δt). b) Categorization of results.

To summarize the results, the model performance according to the NSE and the differences in the time of peak discharges can be improved using the dynamic approach of the time of concentration, especially when the Wisnovszky equation yields an inadequate estimation. The calibration is more difficult to perform than in the characteristic case as a whole range of rainfall characteristics has to be taken into consideration. However, if the proper curves are applied, the simulations can give significantly better results. *Fig. 4* shows the calibrated percentage curves for the time of concentration and storage coefficient. It is notable that the curves of the two catchments are different as the catchments have different characteristics.

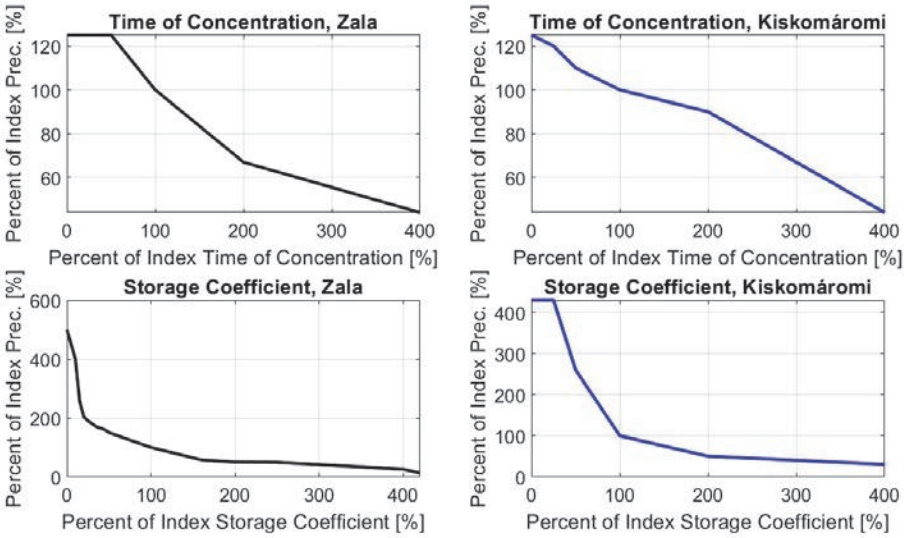

Fig.4. The calibrated percentage curves of the time of concentration and the storage coefficient.

In the current study, the dynamic approach did not improve the results in a few cases. The reason could be that the curves were not calibrated suitably for the rainfall characteristics of the given events. To avoid the mentioned errors, reviewing the possibility of applying measured data for the input curves to improve the model performance in a future study would be practical. Another interesting aspect for the extension of the study is the analysis of rainfall data. In the ECMWF rainfall database, the high-intensity rainfall events can be underestimated if a local rainfall event has a smaller spatial scale than the grid size of the ECMWF data (*Nagy* and *Szilágyi*, 2021b). In a following study, it would be interesting to see the calibration process and the simulation results using rainfall gauge data, which could further confirm the current paper's outcome.

The variable parameter, a recent feature of HEC-HMS, proved to be applicable, while the need to revise the commonly applied Wisnovszky equation is further emphasized. In addition, the results verify the dynamic relation between the time of concentration and the rainfall intensity. Since the Wisnovszky equation proved to give inaccurate estimations in general, and the value of time of concentration is confirmed to vary with rainfall intensity, using the dynamic approach is highly recommended in the Hungarian modeling practice, despite the complexity of the calibration.

***Acknowledgments*:** The work presented was supported by the Doctoral Excellence Fellowship Programme (DCEP) which is funded by the National Research Development and Innovation Fund of the Ministry of Culture and Innovation and the Budapest University of Technology and Economics, under a grant agreement with the National Research, Development and Innovation Office.

References

Aron, G., Ball, J.E., and *Smith, T.A.,* 1991: Fractal concept used in time-of-concentration estimates. *J. Irrigat. Drainage Engin 117*(5), 635–641. https://doi.org/10.1061/(ASCE)0733-9437(1991)117:5(635)

Askew, A.J., 1970: Derivation of formulae for variable lag time. *J. Hydrol. 10,* 225–242. https://doi.org/10.1016/0022-1694(70)90251-9

AGROPOPO, 2016*: Attachments of AGROTOPO Database* – data from MTA ATK TAKI. http://www.elkh-taki.hu/hu/osztalyok/kornyezetinformatikai-osztaly/agrotopo

Beven, K., 2012: Rainfall-Runoff Modelling, The Primer. Second Edition. John Wiley & Sons, Ltd., 51. https://doi.org/10.1002/9781119951001

CORINE, 2018: Land Cover – Copernicus: CLC 2018, Accessed: 2021.09.01. https://land.copernicus.eu/pan-european/corine-land-cover

Corps of Engineers, 1954: Airfield drainage investigation. Washington, DC: U.S. Army, Los Angeles District for the Office of the Chief of Engineers, Airfield Branch Engineering Division, Military Construction, Data Report.

Cuevas, J. G., Arumí, J. L., and *Dörner, J.,* 2019: Assessing methods for the estimation of response times of stream discharge: The role of rainfall duration. *J. Hydrol. Hydromech. 67*(2), 143–153. https://doi.org/10.2478/johh-2018-0043

Feldman, A.D., 2000: Hydrologic Modeling System HEC-HMS Technical Reference Manual. Washington.

Grimaldi, S., Petroselli, A., Tauro, F., and *Porfiri, M.,* 2012: Time of concentration: a paradox in modern hydrology. *Hydrol. Sci. J. 57,* 217–228. https://doi.org/10.1080/02626667.2011.644244

Henderson, F.M. and *Wooding, R.A.,* 1964: Overland flow and groundwater flow from a steady rainfall of finite duration. *J. Geophys. Res. 69,* 1531–1540. https://doi.org/10.1029/JZ069i008p01531

Izzard, C.F. and *Hicks, W.I.,* 1946: Hydraulics of runoff from developed surfaces. In: 26th Annual Meetings of the Highway Research Board, 5–8 December, Washington, DC, 129–150.

Kadoya, M. and *Fukushima, A.,* 1977: Concentration time of flood runoff in smaller river basins. *In:* (eds. *H.J. Morel-Seytoux, et al.*) Proceedings of the 3rd International Hydrology Symposium on Theoretical and Applied Hydrology, 27–29 July, Fort Collins, CO. Fort Collins: Water Resources Publication, Colorado State University, 75–88.

Kovács, Gy., 1979: A hófelhalmozódás, a hóolvadás és a hóból származó lefolyás tér- és időbeli változékonysága Magyarországon. VITUKI Közlemény, Budapest. (In Hungarian)

Loukas, A. and *Quick, M.C.,* 1996: Physically-based estimation of lag time for forested mountainous watersheds. *Hydrol. Sci. J. 41,* 1–19. https://doi.org/10.1080/02626669609491475

Mathias, S.A., McIntyre, N., and *Oughton, R.H.,* 2016: A study of non-linearity in rainfall-runoff response using 120 UK catchments. *J. Hydrol. 540,* 423–436. https://doi.org/10.1016/j.jhydrol.2016.06.039

Mattányi, Z., Homolya, E., and *Turczi, G.,* 2015: A klímaváltozás hatása a villámárvíz kockázatra, D4.10 kutatási jelentés. (In Hungarain)

McCuen, R.H., Wong, S.L., and *Rawls, W.J.,* 1984: Estimating urban time of concentration. *J.Hydraulic Engin. 110,* 887–904. https://doi.org/10.1061/(ASCE)0733-9429(1984)110:7(887)

Michailidi, E.M., Efstratiadis, A., and *Koukouvinos A.,* 2018: Timing the time of concentration: shedding light on a paradox. *Hydrol. Sci. J. 63,*721–740. https://doi.org/10.1080/02626667.2018.1450985

Morgali, J.R. and *Linsley, R.K.,* 1965: Computer simulation of overland flow. *J. Hydraul. Division ASCE, 91* (HY3), 81–100. https://doi.org/10.1061/JYCEAJ.0001269

Muñoz Sabater, J., 2019: ERA5-Land hourly data from 1950 to present. Copernicus Climate Change Service (C3S) Climate Data Store (CDS*).* Accessed on 30-09-2021. DOI: 10.24381/cds.e2161bac

Nagy, E.D. and *Szilágyi, J.,* 2020: Comparative analysis of catchment response times and their definitions using measured and reanalysis rainfall data. HydroCarpath International Conference: Processes, Patterns and Regimes in the Hydrology of the Carpathians: Coupling Experiments, Remote Sensing, Citizen Science, 9. https://doi.org/10.13140/RG.2.2.29763.02089

Nagy, E.D. and *Szilágyi, J.,* 2021a: A Wisnovszky-féle összefüggés felülvizsgálata hazai vízgyűjtőkön mért összegyülekezési idők és számos morfológiai jellemző vizsgálatával. *Hidrológiai Közlöny 101*(1). 19–32. (In Hungarian)

Nagy, E.D. and *Szilágyi, J.,* 2021b: Az ECMWF reanalízis idősorok hidrológiai alkalmazhatóságának vizsgálata az OMSZ homogenizált idősorainak függvényében, hazai közepes méretű vízgyűjtőkön. Hidrológiai Közlöny *101*(4), 45–51. (In Hungarian)

Nagy, E.D., Szilágyi, J., and *Torma, P.,* 2022: Estimation of catchment response time using a new automated event-based approach. *J. Hydrol. 613,* 128355. https://doi.org/10.1016/j.jhydrol.2022.128355

Nagy, E.D., Torma, P., and *Bene, K.,* 2016: Comparing Methods for Computing the Time of Concentration in a Medium-sized Hungarian Catchment. *Slovak J. Civil Engin. 24,* 8–14. https://doi.org/10.1515/sjce-2016-0017

Nagy, E.D., 2018: Towards an improved estimation of the time of concentration in medium-sized Hungarian catchments. HydroCarpath International Conference: Catchment processes in regional hydrology: field experiments and modelling in Carpathian Basins.

Nash, J.E. and *Sutcliffe, J. V.,* 1970: River flow forecasting through conceptual models part I – A discussion of principles, *J. Hydrol. 10,* 282–290. https://doi.org/10.1016/0022-1694(70)90255-6

NYUDUVIZIG, 2016:Nyugat-dunántúli Vízügyi Igazgatóság, 2016: *VGT, 4*-1 Zala alegység.

Papadakis, K.N. and *Kazan, M.N.,* 1987: Time of concentration in small rural watersheds. In: Proceedings of the ASCE Engineering Hydrology Symposium. Williamsburg, VA: ASCE, 633–638.

Peel, M. C., Finlayson, B. L., and *Mcmahon, T. A.,* 2007: Updated world map of the KöppenGeiger climate classification. *Hydrol. Earth Syst. Sci. 11,* 1633–1644. https://doi.org/10.5194/hess-11-1633-2007

Reed, D. W., Johnson, P., and *Firth, J. M.,* 1975: A non-linear rainfall-runoff model, providing for variable lag time. *J. Hydrol 25,* 295–305. https://doi.org/10.1016/0022-1694(75)90027-X

Saghafian, B., Julien, P. Y., and *Rajaie, H.,* 2002: Runoff hydrograph simulation based on time variable isochrone technique. *J. Hydrol. 261,* 193–203. https://doi.org/10.1016/S0022-1694(02)00007-0

Scharffenberg, B., Bartles M., Brauer T., Fleming M., and *Karlovits G.,* 2020: Hydrologic Modeling System HEC-HMS User's Manual, Version 4.7. Washington.

Scharffenberg, B., Bartles M., Brauer T., Fleming M., and *Karlovits G.,* 2018: Hydrologic Modeling System HEC-HMS User's Manual, Version 4.3. Washington.

Schmidt, E.J. and *Schulze, R.E.,* 1984: Improved estimation of peak flow rates using modified SCS lag equations. Pietermaritzburg: Department of Agricultural Engineering, University of Natal, ACRU Report No. 17.

Szilágyi, J., 2007: Analysis of the nonlinearity in the hillslope runoff response to precipitation through numerical modeling. *J. Hydrol 337,* 391–401. https://doi.org/10.1016/j.jhydrol.2007.02.005

Wisnovszky, I., 1958: Az összegyülekezési idő számítása, *Hidrológiai Közlöny 3.* 195. (In Hungarian)

WMO, 1974: International Glossary of Hydrology. WMO Report No. 385: Geneva.

Zhang, S., Liu, C., Yao, Z., and *Guo, L.,* 2007: Experimental study on lag time for a small watershed. *Hydrol. Process. 21,* 1045–1054. https://doi.org/10.1002/hyp.6285

DOI:10.28974/idojaras.2024.4.4

IDŐJÁRÁS

Quarterly Journal of the HungaroMet Hungarian Meteorological Service
Vol. 128, No. 4, October – December, 2024, pp. 451–472

Determination of changes in the total amount of precipitation using the Mann-Kendall trend test in Central Serbia for the period from 1949 to 2018

Nikola R. Bačević [1,*], **Aleksandar Valjarević**[2], **Milena Nikolić** [1], **Vladica Stevanović**[1], **Jovan Dragojlović**[1], **Milica G. Radaković**[3], **Dušan Kićović**[4], **Rastko S. Marković**[5], **Slobodan B. Marković**[3], and **Tin Lukić**[3]

[1]*University of Pristina, Faculty of Sciences and Mathematics, Department of Geography, 38220 Kosovska Mitrovica, Serbia*

[2]*University of Belgrade, Faculty of Geography, Department of Geospatial and Environmental Science, Studentski Trg 3/III, 11000 Belgrade, Serbia*

[3]*University of Novi Sad, Faculty of Sciences, Department of Geography, Tourism and Hotel Management, Trg Dositeja Obradovića 3, 21000 Novi Sad, Serbia*

[4]*Academy for applied studies Belgrade, The College of Tourism, 11000 Belgrade, Serbia*

[5]*Department of Geography and Tourism, Natural Sciences and Mathematics, University of Niš, Višegradska 11, 18000 Niš, Serbia*

**Corresponding author e-mail: nikola.bacevic@pr.ac.rs*

(Manuscript received in final form November 24, 2023)

Abstract— This study presents the trend analysis for a specific category of variables, namely the average annual precipitation. The geospatial distribution of the obtained results in Central Serbia is visualized using Geographic Information System (GIS) numerical analysis. The primary objective of this study is to identify potential changes in the trends of average annual precipitation within the observed area. Methodologically, the Mann-Kendall trend test, trend equation, and trend magnitude were employed for trend analysis. The data used for the analysis were sourced from the Meteorological Yearbooks of the Republic Hydrometeorological Service of Serbia, encompassing a total of 24 meteorological stations and spanning the period from 1949 to 2018. Based on the obtained results, statistically significant positive trends were observed in 17 time series, favoring the

alternative hypothesis. Conversely, a decline in precipitation was noted in the remaining 7 time series. Among the time series, the largest increases in the total amount of precipitation over the past 69 years were recorded ont he area of the Dinaric Mountains. Conversely, the lowest increase in average precipitation was observed in the central part od the country.Furthermore, the time series with the greatest decrease in average annual precipitation was recorded ont he southeastern part of the country. In order to effectively address water-related challenges associated with precipitation fluctuations, it is essential to gain a comprehensive understanding of the shifting trends in precipitation over the region of Central Serbia.

Key–words: climate change, precipitation variability, Central Serbia, average annual precipitation trends, Mann-Kendall trend test, GIS

1. Introduction

We are witnessing increasingly frequent modern climate changes, which, in the opinion of many world scientists, are faster, more dynamic, and more intense in the last three decades than those from some past eras. The basic property of precipitation is its spatial and temporal variability. Each climate element is variable, to a greater or lesser extent, while the spatial and temporal variability of precipitation is particularly pronounced (*Jones*, 1999). Variations in precipitation patterns have direct implications for the sustainable development of the environment, agriculture, energy production, and the planning and management of water resources. These variations can also impact the realization of sustainable development goals related to water (*Amiri* and *Gocic*, 2021a). Consequently, there has been a concerted effort over the past few decades to analyze trends in precipitation time series on different spatiotemporal scales. Different statistical methods have been employed, often with assumptions about the normality, independence, and temporal consistency of the time series, to actively explore these trends (*Amiri* and *Gocic*, 2021b).

The variability of the total amount of precipitation was among the first to be investigated by the scientist *Biel* (1929), who covered the space of the entire Earth. He came to the conclusion that the variability of the total amount of annual precipitation increases in areas with a small amount of precipitation, and vice versa, it decreases in areas with a bigger amount of precipitation.

According to *Biel* (1929), Europe has the smallest range of variability compared to other continents. On the territory of Europe and North America, in the subpolar and polar zones, the variability of precipitation is lower than the average values. On the other hand, the areas above the oceans and their coasts of the abovementioned continents, which are under the influence of cold sea currents, have high values of variability of the total amount of precipitation in relation to the average (*Conrad*, 1941). At the global level, observing the influence of the general air mass circulation in the atmosphere on the variability of the total annual amount of precipitation, led

to the conclusion, that the variability is bigger in the tropical and subtropical zones than in the temperate zone (*Morales*, 1977).

Similar claims as stated above are confirmed by the results obtained from the following modern scientific studies by the group of authors (*Trenberth et al.*, 2003; *Tebaldi et al.*, 2006; *Pall et al.*, 2007; *Lenderink* and *Van Meijgaard*, 2008; *Hardwick Jones et al.*, 2010; *Lenderink et al.*, 2011, 2017; *Utsumi et al.*, 2011; *Mishra et al.*, 2012; *Berg et al.*, 2013; *Collins et al.*, 2013; *Kharin et al.*, 2013; *Westra et al.*, 2014; *Roderick et al.*, 2019, 2020; *Ali et al.*, 2021; *Visser et al.*, 2021).

Previous research in the area of the Balkan Peninsula and surrounding countries dealt with the problem of analyzing trends in the total amount of precipitation and their variability (*Maradin*, 2011; *Radevski et al.*, 2013; *Ivanova* and*Radeva*, 2016; *Popov et al.*, 2018; *Alsafadi et al.*, 2020; *Ćulafić et al.*, 2020; *Porja* and *Nunaj*, 2020; *Spiridonov* and *Balabanova*, 2021; *Barbulescu* and *Postolache*, 2023; *Lukić et al.*, 2019). The obtained research results in the Balkans (*Valcheva* and *Spiridonov*, 2023) are very similar to the results of scientific studies for the analyzed area of Central Serbia, which in most cases indicate a slight increase in the total annual amount of precipitation and a positive trend, which is characteristic for almost the entire area of Southeastern Europe (*Leščešen et al.*, 2023).

The existing or similar studies for the observed and analyzed area of Central Serbia are rare and scarce, but there is a lot of research that refer to the entire territory of Serbia. The analysis of precipitation trends in the last few decades as a part of climate change is the subject of research of many researchers in Serbia (*Ducić* and *Luković*, 2005; *Đorđević*, 2008; *Ducić et al.*, 2009, 2010; *Stanojević*, 2012; *Luković et al.*, 2014; *Gavrilov et al.*, 2015; *Živanović et al.*, 2020; *Erić et al.*, 2021; *Popov* and *Svetozarević*, 2021; *Velimirović et al.*, 2021; *Amiri* and *Gocić*, 2021a,b, 2023). The results obtained in the previously mentioned research indicate a slight increase in the total annual amount of precipitation for the observed area, and that climate variability is not expressed sufficiently. They also indicate a higher total annual amount of precipitation in the western part of Central Serbia compared to its eastern parts. Furthermore, they indicate the influence of the Atlantic Ocean, the Mediterranean, and the orography of the terrain, which relate to the total annual amount of precipitation for the observed territory.

In the previous decade, the trend in the research of climate elements was taken over by climate models. Due to the area of the researched territory, regional climate models performed the best, and their results can be useful for agriculture as well (*Ruml et al.*, 2012). Precipitation predictions until the end of this century, based on climate models, indicate that the frequency of extreme precipitation will increase, and that their spatial distribution will shift to the south of Serbia (*Erić et al.*, 2021). However, there is no single best climate model; therefore, the results from multiple climate models for a specific region are always considered. Due to their unreliability, measured data will be utilized in this paper.

Knowledge of precipitation regimes has great scientific and practical importance in almost all domains of modern society, and they are of particular importance in water supply, ecology, and flood protection. This study tries to answer the following questions: (1) if the total annual precipitation in Central Serbia changed in the period 1949–2018, (2) whether the precipitation trends are decreasing or increasing, (3) if the obtained trends are statistically significant, and finally, (4) what is the regional context of precipitation changes in Serbia.

The answers to the given questions are provided by the analysis of the annual amount of precipitation at 24 meteorological stations located in the observed area. The main goal of this study is to perform the necessary analysis of the variability of the change in the total average annual precipitation in Central Serbia for the time period 1949–2018, using the Mann Kendall (MK) trend test, trend equation and trend magnitude analysis. Also, the geospatial distribution of the obtained results over the investigated territory were shown with the help of GIS numerical analysis.

2. Data and methods

2.1. Research area

Central Serbia is located in the central part of the Balkan Peninsula and is a toponym referring to the territory of Serbia without the Autonomous Provinces (*Fig. 1*). The total area of the observed territory is 55.947 km². The natural borders of Central Serbia towards neighboring countries are represented by the following natural entities: 1) to the west, there is the Drina River, which forms a natural border with Bosnia and Herzegovina; 2) to the north, it extends to the rivers Sava and Danube, which separate the observed territory from Vojvodina in the north and from Romania in the northeast; 3) to the east, the Balkan and Rhodope Mountains represent the border with Bulgaria; 4) and to the south and southwest, the state border is determined by the administrative line with the Republic of North Macedonia, as well as the provincial border with the Autonomous Province of Kosovo and Metohija, which continues to the state border with Montenegro (*Radaković, et al.,* 2018).

The morphological structure of this territory is complex and consists of three main mountain areas: the Dinaric Mountains stretching to the west, the Carpathian-Balkan Mountains to the northeast and the Rhodope Mountains to the east and southeast (*Bačević, et al.,* 2021). The hypsometric differences of the terrain are distinguished: the highest point of the terrain is the mountain peak Midzor, 2168 m above sea level (Stara planina), and the lowest point is the confluence of the Timok river with the Danube (28 m above sea level) (*Marković,* 1966). The total difference in altitude between these two points is 2140 m. The following orographic units have a great influence on the climate and transformation of air masses in Central Serbia: the Pannonian Basin and two

mountain ranges – the Dinarides and the Carpatho-Balkanides. Arctic continental air masses arrive in the observed area over the Pannonian Basin in the colder half of the year, while the Dinarides and Carpatho-Balkanides represent an orographic barrier which weakens the flow of air masses (*Ducić* and *Radovanović*, 2005).

As a consequence of this atmospheric circulation, three main climate types prevail in Central Serbia: continental, moderate-continental, and modified Mediterranean climates (*Bajat, et al.*, 2015). According to the Köppen's classification, Central Serbia falls under two climate categories: 1) Cfa climate (average temperature above 20 °C during warmer months and above -3 °C during colder months), 2) Dfa climate on high mountains (above 1500 m) (average temperature below 20 °C during warmer months and below -3 °C during colder months) (*Radinović*, 1981). The average annual air temperature for the time interval from 1949 to 2018 in Central Serbia is 10.7 °C, and the average amount of precipitation is 685.3 mm.

Fig. 1. The location of the meteorological stations in the studied area.

2.2. Materials

During the research, testing and analysis of trends was performed for one category of parameters, that is, for the total average annual precipitation as a climate variable for the area that includes Central Serbia. It is a time series of a total of 69 years (1949–2018). The data necessary for this type of research were taken from the Meteorological Yearbooks of the Republic Hydrometeorological Service of Serbia (RHMZ) (http://www.hidmet.gov.rs/) covering two 30-year cycles, which is in accordance with the World Meteorological Organization (WMO) standards. For the purposes of this study, precipitation data from 24 meteorological stations were used. The altitude of meteorological stations in Central Serbia varies: a) up to 200 m: Negotin, Veliko Gradište, Jagodina, Loznica, Smederevska Palanka, Belgrade, Ćuprija, Zaječar, Kruševac, Valjevo, and Kragujevac, b) from 200 to 500 m: Niš, Kraljevo, Leskovac, Knjaževac, Požega, Pirot, Kuršumlija, Bujanovac, Vranje, and Dimitrovgrad, c) from 500 to 1000 m: Novi Pazar, and d) over 1000 m: Zlatibor and Sjenica (*Bačević, et al.*, 2021).

Station names, geographic coordinates, and elevation belts are shown in *Fig. 1* and *Table 1*. The homogeneity of the annual precipitation series was examined according to *Alexandersson* (1986). The homogeneity test showed that the precipitation time series for 24 stations used in this study are homogeneous.

2.3. Methods

Three statistical approaches were used in the analysis of trends in the total average annual precipitation. The first approach is the linear trend equation (*Bačević et al*., 2020; *Mudelsee*, 2014), which is determined for each time series individually. Completely independent of the first step, all trends were tested using the non-parametric MK trend test (*Milentijević et al.*, 2018; *Zeleňáková et al.*, 2018). The third step consists of determining the trend magnitude obtained on the basis of the trend equation (*Bačević et al.*, 2022; *Gavrilov et al.*, 2016). The Exel program from the Microsoft Office software package was used to determine trends in the total average annual precipitation. The XLSTAT software was used for calculating the confidence level *p*, as well as for testing of the hypotheses (https://www.xlstat.com/en).

Table 1. List of meteorological stations located in Central Serbia, names of time series, geographic coordinates, and altitudes.

No.	Meteorological station	Name of time series	φ (°N)	λ (°E)	*h* (m)
1.	Belgrade	BG-P	44º48´	20º28´	132
2.	Bujanovac	BU-P	42º27´	21º46´	399
3.	Ćuprija	ĆU-P	43º56´	21º23´	123
4.	Dimitrovgrad	DI-P	43º01´	22º45´	450
5.	Jagodina	JA-P	43º59´	21º23´	115
6.	Knjaževac	KŽ-P	43º34´	22º15´	263
7.	Kragujevac	KG-P	44º02´	20º56´	181
8.	Kraljevo	KV-P	43º43´	20º42´	215
9.	Kruševac	KŠ-P	43º37´	21º15´	166
10.	Kuršumlija	KU-P	43º08´	21º16´	384
11.	Leskovac	LE-P	42º59´	21º57´	231
12.	Loznica	LO-P	44º32´	19º14´	121
13.	Negotin	NG-P	44º14´	22º32´	42
14.	Niš	NI-P	43º20´	21º54´	202
15.	Novi Pazar	NP-P	43º08´	20º31´	545
16.	Pirot	PI-P	43º09´	22º35´	373
17.	Požega	PŽ-P	43º51´	20º02´	311
18.	Sjenica	SJ-P	43º16´	20º00´	1038
19.	Smederevska Palanka	SP-P	44º22´	20º57´	121
20.	Valjevo	VA-P	44º17´	19º55´	174
21.	Veliko Gradište	VG-P	44º45´	21º30´	80
22.	Vranje	VR-P	42º33´	21º55´	433
23.	Zaječar	ZA-P	43º53´	22º17´	144
24.	Zlatibor	ZL-P	43º44´	19º43´	1029

2.3.1. The linear regression and the trend equation

The linear trend method is a technique of extreme importance for the analysis, evaluation, and distribution of short-term and long-term changes in the total average annual precipitation (*Bacevic et al.*, 2018; *Mudelsee*, 2019). Its general form is:

$$y = ax + b, \tag{1}$$

where y represents the total average annual precipitation expressed in mm, a is the magnitude of the slope, x is the time series, while b represents the total annual

precipitation at the beginning of the period. The value of the precipitation trend is a function of the magnitude of the slope. There are three possible cases: a) the magnitude of the slope is greater than zero – the trend is positive (growing); b) when it is less than zero – the trend is negative (declining); c) when it is equal to zero – there is no trend (no changes).

2.3.2. The trend magnitude

The trend magnitude is determined from the linear trend equation (*Gavrilov et al.*, 2016):

$$\Delta y = y(Pb) - y(Pe), \quad (2)$$

where Δy represents the trend magnitude expressed in mm, y (1949) in the trend equation represents the total annual amount of precipitation at the beginning of the period, and y (2018) represents the total annual amount of precipitation at the end of the period. Speaking of the trend magnitude, there are three possible cases: a) when it is greater than zero - the trend is negative (decreasing); b) when Δy is less than zero – the trend is positive (growing); c) when it is equal to zero – there is no trend (no changes).

2.3.3. The Mann-Kendall non-parametric test

In addition to the regression analysis, the non-parametric MK trend test (*Mann*, 1945; *Kendall*, 1975) was used for additional assessment of the existence or absence of a trend. Using the MK test, two hypotheses were tested: the null hypothesis (H_o), which indicates the absence of a trend in the time series; and the alternative hypothesis (H_a), where there is a statistically significant trend in the time series for the set significance level (α). The p value plays a central role in the MK test (*Karmeshu*, 2012). The p value determines the confidence level of the hypothesis. If the p value is lower than the chosen significance level α (typically α=0.05 or 5%), the hypothesis H_o should be rejected and the hypothesis H_a accepted. On the contrary, if the p value is greater than the significance level α, then the null hypothesis is accepted (*Razavi et al.*, 2016).

2.3.4. QGIS analysis

All digital cartographic analyzes were approved using three open-source software programs, namely the Quantum Geographical Information System (QGIS 3.12), System for Automated Geoscientific Analyzes (SAGA 8.2.0), and Google EarthEngine. Satellite data were downloaded from the National Aeronautics and Space Administration's two databases EarthData (NASA), (https://ladsweb.modaps.eosdis.nasa.gov/search/imageViewer/1), at 30 m resolution.

The digital elevation model (DEM) was downloaded from the official United States Geological Survey (USGS) website at 30 m resolution. These data were recorded in AsterDem (*Valjarević et al.*, 2022). After the accurate determination of geographic coordinates (longitude, latitude, altitude), the next step was to determine the kriging belt of monthly and annual average precipitation data for the meteorological stations. For this purpose, SAGA 8.2.0 and QGIS 3.12 were used.

In the last step, superpixel classification was used with the Google Earth Engine software to better analyze the spatial distribution of meteorological stations (*Valjarević et al.*, 2018). These methods are also useful for analyzing climate characteristics within an area (see *Fig. 1*). Following the remote sensing and GIS analyzes, the kriging and interpolation belts are analyzed to better represent the precipitation distribution and characteristics in the analyzed periods (*Valjarević et al*., 2023; *Alexakis et al.*, 2013).

3. Results

3.1. Trend parameters

In this paper, the main results are presented in *Table 2* and *Figs. 2* and *3*. Furthermore, the paper presents the analysis for a total of 24 meteorological stations which are located in the area of Central Serbia and for the same number of time series. The obtained results for the average annual precipitation, the results of the trend equation, linear trend equation, and trend magnitude are presented visually in *Fig. 2* and *Table 2*. The *p* value, results of trend testing using the MK trend test, and evaluation of hypotheses for accepting or rejecting the trend are shown in *Fig. 2*, for each meteorological station in the territory of Central Serbia.

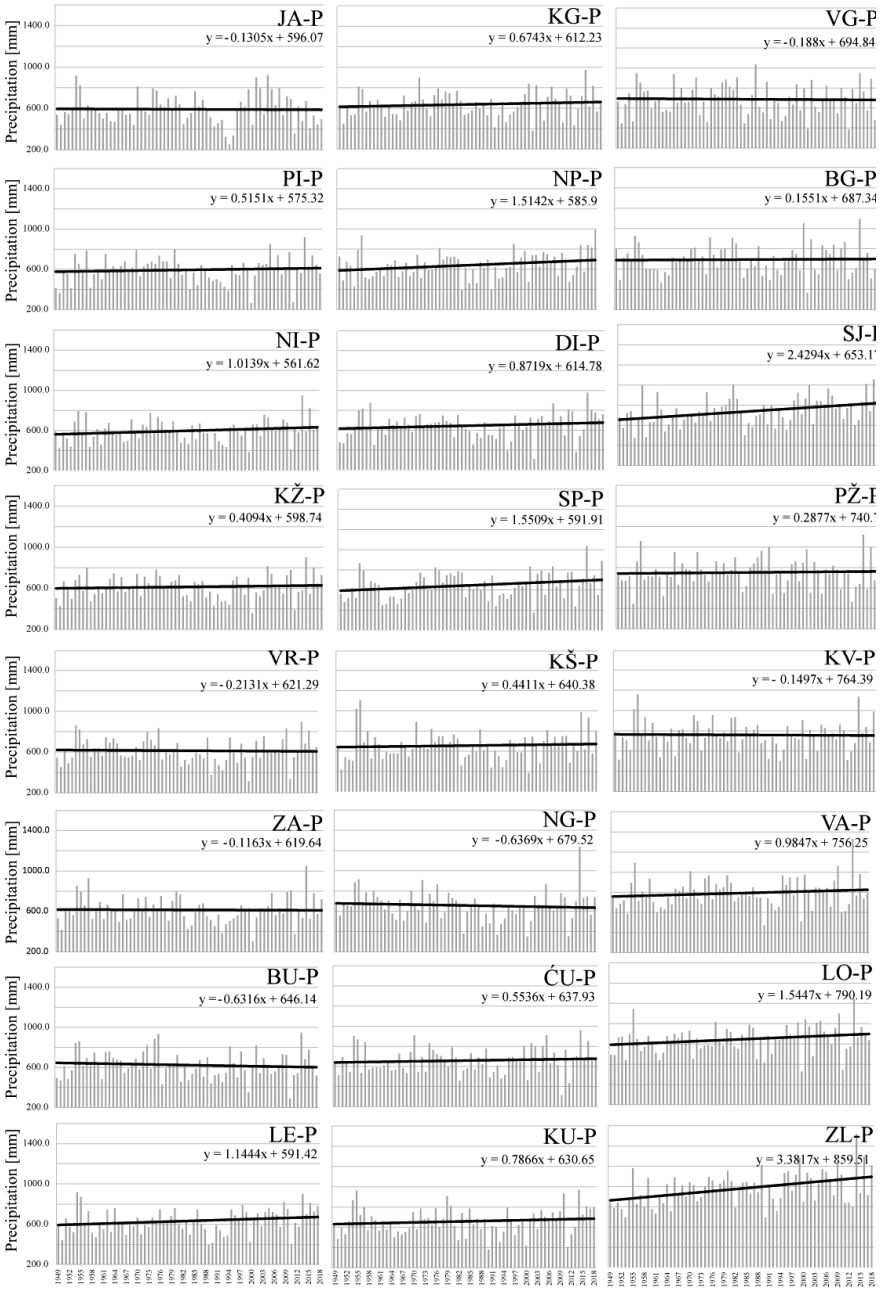

Fig. 2. Visual representation of average annual precipitation, trend equation, and linear trend for selected meteorological stations, arranged from the station with the lowest to the station with the highest average annual precipitation in Central Serbia for the observed time period from 1949 to 2018.

Table 2. Time series names, trend equation, trend magnitude Δy, and the average amount of precipitation, for 24 time series.

Time series	Trend equation	Δy (mm)	Average amount of precipitation (mm)
BG-P	y = 0.1551x + 687.34	10.7	692.8
BU-P	y = -0.6316x + 646.14	-43.6	623.7
ĆU-P	y = 0.5536x + 637.93	38.2	658.1
DI-P	y = 0.8719x + 614.78	60.2	644.4
JA-P	y = -0.1305x + 596.07	-9.0	591.4
KŽ-P	y = 0.4094x + 598.74	28.2	613.3
KG-P	y = 0.6743x + 612.23	47.0	635.4
KV-P	y = -0.1497x + 764.39	-10.3	757.8
KŠ-P	y = 0.4411x + 640.38	30.4	656.0
KU-P	y = 0.7866x + 630.65	54.3	658.6
LE-P	y = 1.1444x + 591.42	79.0	633.2
LO-P	y = 1.5447x + 790.19	106.6	845.0
NG-P	y = -0.6369x + 679.52	-43.9	656.9
NI-P	y = 1.0139x + 561.62	70.0	597.6
NP-P	y = 1.5142x + 585.90	105.0	639.7
PI-P	y = 0.5151x + 575.32	35.0	593.6
PŽ-P	y = 0.2877x + 740.70	19.9	750.9
SJ-P	y = 2.4294x + 653.17	167.6	739.4
SP-P	y = 1.5509x + 591.91	107.0	647.0
VA-P	y = 0.9847x + 756.25	67.9	791.0
VG-P	y = -0.1880x + 694.84	-13.0	688.2
VR-P	y = -0.2131x + 621.29	-14.7	613.7
ZA-P	y = -0.1163x + 619.64	-8.0	615.5
ZL-P	y = 3.3817x + 859.51	233.3	973.9

The results obtained from the above mentioned parameters, which are shown in *Fig. 2* and *Table 2*, indicate a slight increase in the average total annual precipitation in the territory of Central Serbia, which coincides with the results from the reports of other similar studies, which were carried out in countries from the region. Out of a total of 24 time series, a slight increase in the average total annual precipitation was recorded in 17 time series, while a decreasing amount of precipitation was recorded in the remaining 7 time series.

The biggest increase in the average total annual precipitation of 233.3 mm in the past 69 years was recorded in the Zl-P time series, followed by the SJ-P and SP-P time series, where the increase of 167.6 mm, and 107.0 mm was recorded

respectively. The smallest increase in the average total annual precipitation of 10.7 mm was recorded in the BG-P time series, followed by the KZ-P and KS-P time series with the increase of 28.2 mm and 30.4 mm, respectively.

The biggest decrease in the total average annual precipitation of -43.9 mm was recorded in the NG-P time series. It is followed by the BU-P time series with the decrease of -43.6 mm and the VR-P time series with the decrease of -14.7 mm. Based on the obtained results, the total average annual precipitation in Central Serbia amounts to 679.9 mm.

3.2. Trend assessment

The results obtained from the analysis of the MK trend test and the evaluation of hypotheses (*p* values, type of hypothesis, risk of rejecting the hypothesis) are described in *Fig. 3*. From a total of 24 time series, a significant statistically positive trend was recorded in 5 time series, where the H_a hypothesis prevails and the *p* value is lower than the significance level α, whose value is 0.05, while in 19 time series there is no trend, and in these cases hypothesis H_o prevails, where the *p* value is greater than the significance level α.

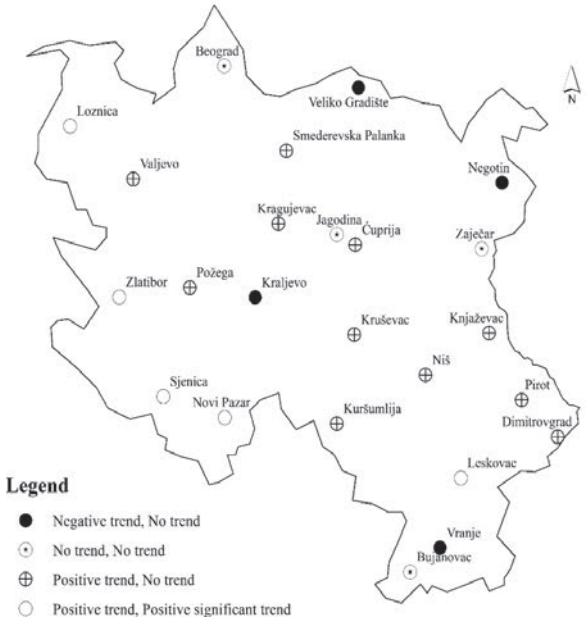

Fig. 3. Cartographic presentation of the obtained results of the linear equation and the Mann-Kendall trend test, respectively, for the total annual amount of precipitation in Central Serbia for the time period from 1949 to 2018.

From a total of 5 time series, where a significantly positive statistical trend prevails, hypothesis H_a prevails, with a very small percentage of risk ranging between 0.08% and 4.55% to reject the given hypothesis. From a total of 19 time series, where there is no trend and hypothesis H_o prevails in most cases, the risk of rejecting this hypothesis is very high. The risk values for rejecting this hypothesis range from 5.15% to 97.93%. A risk whose value is between 5.00% and 10.00% is recorded in one time series, which tells us that there is no trend. Values between 10.00% and 50.00% were recorded in nine time series, indicating that the trend is in stagnation. Furthermore, in the last nine time series the risk value ranges between 70.15% and 95.46%, where in the perspective the trend is likely to change to a positive one.

These results indicate that the total annual amount of precipitation in Central Serbia is stagnant, which coincides with the results of other researchers. In the majority of analyzed cases, the results of the trend equation deviate from the results of the MK trend test, more precisely in 15 time series. In the remaining 9 time series, the results coincide. In 11 cases (CU-P, DI-P, KZ-P, KG-P, KS-P, KU-P, NI-P, PI-P, PZ-P, SP-P, and VA-P) the MK trend test did not recognize a positive trend, while the trend equation indicates an increase in average annual precipitation, and in four cases (KV-P, NG-P, VG-P, and VR-P) the MK trend test indicates that there is no trend, while the trend equation indicates that the trend is negative. Time series in which the results coincide are: BG-P, BU-P, JA-P, LE-P, LO-P, NP-P, SJ-P, ZA-P , and ZL-P (*Fig. 3*).

3.3. GIS numerical analysis

The spatial distribution of the total annual amount of precipitation for the time period from 1949 to 2018 in Central Serbia is shown in more detail in *Fig. 4*.

Fig. 4 shows the geospatial distribution of average annual precipitation in the analyzed territory of Central Serbia. Interregional differences in the average annual amount of precipitation are caused by several reasons, among which the following could stand out: the influence of the influx of air masses from the Atlantic Ocean, the influence of the Mediterranean, presence of temporary atmospheric instabilities (on a season scale) that produce heavy showers, and the influence of the terrain morphology. Therefore, in the western and northwestern parts of the observed area, a higher average annual amount of precipitation was recorded, while in the central, southern, and southeastern parts, the average annual amount of precipitation was lower.

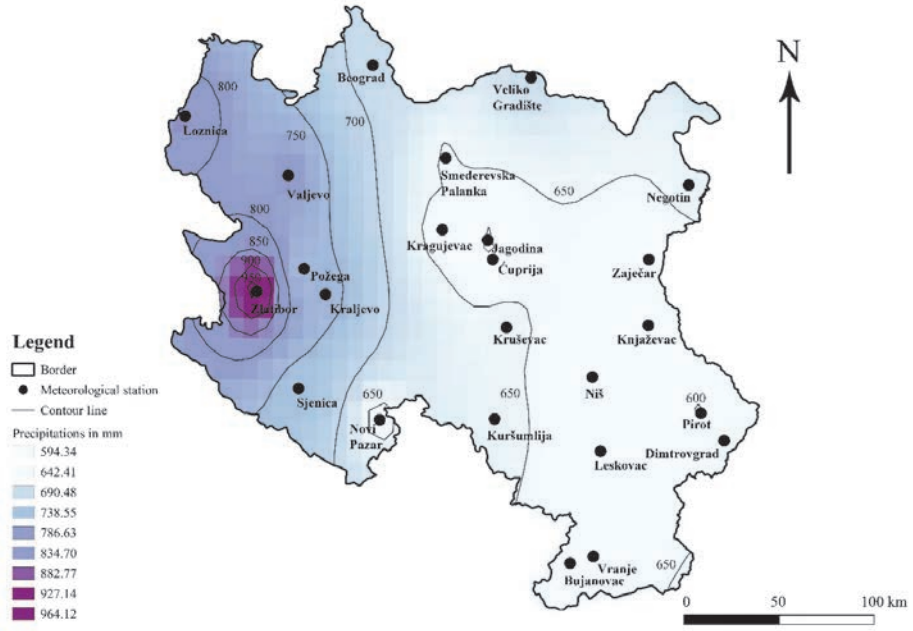

Fig. 4. Spatial distribution of the average amount of precipitation for the time period from 1949 to 2018 in Central Serbia.

The values for the total annual amount of precipitation in Central Serbia for the time period from 1949 to 2018 are 679.9 mm ranging between 591.4 and 973.9 mm. The lowest value of average annual precipitation (591.4 mm) was recorded in Jagodina, and the highest value (973.9 mm) was recorded in Zlatibor. Other values for the average annual amount of precipitation are shown chronologically from the lowest to the highest, and they are as follows: Pirot (593.6 mm), Niš (597.6 mm), Knjaževac (613.3 mm), Vranje (613.7 mm), Zaječar (615.5 mm), Bujanovac (623.7 mm), Leskovac (633.2 mm), Kragujevac (635.4 mm), Novi Pazar (639.7 mm), Dimitrovgrad (644.4 mm), Smederevska Palanka (647 mm), Kruševac (656 mm), Negotin (656.9 mm), Ćuprija (658.1 mm), Kuršumlija (658.6 mm), Veliko Gradište (688.2 mm), Belgrade (692.8 mm), Sjenica (739.4 mm), Požega (750.9 mm), Kraljevo (757.8 mm), Valjevo (791 mm), and Loznica (845 mm).

4. Discussion

Based on the analyzed climate variable, the following can be stated: in this paper, a total of 24 time series were analyzed using trend equations, trend magnitude

indicating an average increase or decrease in the total annual precipitation, MK trend test, and GIS numerical analysis. According to the trend equation and trend magnitude, seventeen time series recorded an increase in the total annual amount of precipitation in the following cases, which are arranged chronologically from the smallest to the biggest increase: BG-YP, PZ-YP, KZ-YP, KS-YP, PI-YP, KG-YP, KU-YP, DI-YP, VA-YP, NI-YP, LE-YP, NP-YP, LO-YP, SP-YP, and ZL-YP.

The biggest average increase in the average annual precipitation of 233.3 mm was recorded in the case of ZL-YP. The smallest increase in total annual precipitation of 10.7 mm was recorded in the case of BG-YT. A decrease in the total annual amount of precipitation was recorded in seven time series related to the average annual amount of precipitation, which are arranged chronologically from the smallest to the biggest decrease: ZA-YP, JA-YP, KV-YP, VG-YP, VR-YP, BU-YP, and NG-YP.

The smallest decrease in total annual precipitation of -8.0 mm was recorded in the case of ZA-YP, while the biggest increase of -49.9 mm was recorded in the case of NG-YP. Speaking of the MK test, the obtained results indicate that a statistically significant positive trend was recorded in the analyzed parameters in 5 time series. On the other hand, there are no changes (no trend) in 19 time series. The spatial distribution of the average annual amount of precipitation in Central Serbia is 679.9 mm. It ranges between 591.4 and 973.9 mm.

In the paper of *Gocić* and *Trajković* (2013), the average annual and seasonal trends for seven meteorological variables, including the average annual amount of precipitation for twelve meteorological stations in Serbia were analyzed. The time period covered in this paper is from 1980 to 2010. As in this study, the non-parametric Mann-Kandell trend test was used to determine whether there is a positive or negative trend in the time series for the observed variable. Speaking of precipitation, no significant trends were observed in the given study, except in the case of one meteorological station, Sombor, which can be seen in *Table 3*.

In general, the results of this study are very similar to the research conducted by *Gocić* and *Trajković* (2013). In most cases, there is no trend in both papers when applying the MK test. In the research of *Gocić* and *Trajković*, a positive trend was noted only for one meteorological station, i.e. Sombor, and in this work, a positive trend was recorded for five meteorological stations, namely: Novi Pazar, Leskovac, Loznica, Sjenica, and Zlatibor. From these results, it is evident that there is no correlation between the findings from the two studies for the meteorological stations Loznica and Zlatibor. However, the results align for other investigated stations. In the work of *Gocić* and *Trajković* (2013), the trend for these two meteorological stations is negative, and in this study, the trend for them is positive, which can be seen in *Table 3* and *Fig. 3*. Such discrepancies presumably result from the difference in the observed time period of 39 years. Special attention should be given to the period of the last nine years, specifically from 2010 to 2018, due to the increasingly pronounced climate changes observed

over the last two decades. This study can pave the way for new research, shedding light on the differences between these two studies, and contributing to fresh insights in the field.

Changes in the total annual amount of precipitation in the region differ depending on the country in which the research was conducted (e.g. *Lukić et al.*, 2019; *Micić Ponjiger et al.*, 2023). A slightly positive trend was recorded in the eastern part of Croatia, for the period from 1961 to 2010 (*Gajić-Čapka et al.*, 2014). The same is observed for the western parts of Romania, where an increase in total annual precipitation was also registered (*Croitoru et al.*, 2016). Also, the northern parts of Montenegro record an increase in the amount of precipitation for the time period from 1951 to 2010 (*Burić et al.*, 2015). These results coincide with this study.

In Hungary, no change was recorded in the total annual amount of precipitation (*Klapwijk et al.*, 2013), which, for example, is not in accordance with the results of this paper. The reason for the discrepancy between the results of these two studies is probably the influence of different orography, primarily the altitude at which the meteorological stations of the observed territories are located.

A slight decrease in the amount of precipitation, without statistical significance, was recorded in the paper written by *Bocheva et al.*, (2009) for the territory of Bulgaria. These results match the findings of this study for seven meteorological stations (Bujanovac, Jagodina, Kraljevo, Negotin, Veliko Gradište, Vranje, and Zaječar). Most of these meteorological stations are located in the eastern, southeastern, and southern regions of Central Serbia, i.e., in relative proximity to the border between Bulgaria and Serbia, which may indicate the similarities in the results of these two studies. Furthermore, these results align with other findings related to the European continent, where slight changes in precipitation were also observed (*Conrad*, 1941; *Klein Tank* and *Können*, 2003).

Table 3. Results of the statistical tests for seasonal and annual precipitation amounts over the period 1980–2010 (*Gocić* and *Trajković*, 2013)

Station	Test	Trends				
		Spring	**Summer**	**Autumn**	**Winter**	**Annual**
Belgrade	Z_s	-1.343	-0.476	1.003	0.136	-0.085
	Q_{med}	-2.333	-2.256	2.317	0.609	-0.333
Dimitrovgrad	Z_s	-0.573	-0.612	1.806	1.274	1.292
	Q_{med}	-1.050	-3.817	3.050	4.683	3.442
Kragujevac	Z_s	-1.173	-0.762	1.407	0.272	-0.051
	Q_{med}	-2.983	-2.600	2.367	0.875	-0.350
Kraljevo	Z_s	0.306	0.238	0.816	0.408	0.068
	Q_{med}	1.026	1.350	3.633	2.833	0.010
Loznica	Z_s	-0.001	0.646	1.241	1.802	1.870
	Q_{med}	-0.050	4.950	3.217	6.633	5.017
Negotin	Z_s	1.972*	0.136	0.935	1.122	0.340
	Q_{med}	2.550*	1.000	2.750	1.867	1.117
Niš	Z_s	0.357	-0.538	0.816	1.714	0.544
	Q_{med}	1.733	-2.433	3.133	3.367	1.055
Novi Sad	Z_s	0.612	0.417	2.532*	0.612	1.802
	Q_{med}	3.257	3.917	2.550*	2.583	4.579
Palić	Z_s	1.054	0.748	1.513	0.527	1.802
	Q_{med}	4.917	4.833	4.467	1.617	4.421
Sombor	Z_s	0.578	1.615	1.172	0.868	1.989*
	Q_{med}	2.070	3.700	3.800	3.300	4.183*
Vranje	Z_s	0.357	-0.382	1.394	0.544	1.309
	Q_{med}	1.850	-2.683	2.376	1.550	3.383
Zlatibor	Z_s	0.578	0.068	1.479	0.731	1.207
	Q_{med}	2.933	0.300	3.450	2.633	3.363**

Z_s: Mann – Kendall test, Q_{med}: Sen's slope estimator.
* Statistically significant trends at the 5% significance level.
** Statistically significant trends at the 1% significance level.

5. Conclusion

This study presents the analyzed trends and geospatial distribution of the obtained results for the average annual amount of precipitation (one category of variables) in the region of Central Serbia. The observed time period is from 1949 to 2018, which is a period of 69 years. The data used for this research were taken from the Meteorological Yearbooks of the Republic Hydrometeorological Service of

Serbia, with a total of 24 meteorological stations. The Mann-Kendall trend test was used for data processing and trend analysis. Additionally, trend equations and magnitudes were calculated using suitable formulas, and the results were presented visually through GIS numerical analysis.

By analyzing the obtained results of this study, it can be noticed that the total annual amount of precipitation in the territory of Central Serbia is slightly increasing. Based on the trend magnitude, an increase in the average annual amount of precipitation was recorded in seventeen cities of Central Serbia, while a decrease in the average annual amount of precipitation was recorded in seven cities of Central Serbia (*Table 2*). Observing the geospatial distribution of the obtained results, it can be concluded that the total average annual amount of precipitation for the observed period in Central Serbia is 679.9 mm. It ranges from 591.4 to 973.9 mm. The values are higher in the western parts compared to the eastern parts.

The biggest increase in the total amount of precipitation of 233.3 mm in the past 69 years was recorded in the time series Zl-P, followed by the time series SJ-P and SP-P, where the increase of 167.6 mm and 107.0 mm was recorded, respectively. The smallest increase in the average amount of precipitation of 10.7 mm was recorded in the time series BG-P, followed by the time series KZ-P and KS-P with the increase of 28.3 mm and 30.4 mm, respectively.

The bigest decrease in the average annual precipitation was recorded in the time series NG-P -43.9 mm, followed by time series BU-P with a decrease of -43.6 and VR-P with a decrease of -14.7 mm. The general conclusion of the results obtained in this way, indicating interregional differences in the average annual amount of precipitation, is that they are presumably preconditioned by several reasons, among which the followings stand out: the influence of the influx of air masses from the Atlantic Ocean, the influence of the Mediterranean, presence of temporary atmospheric instabilities (on a season scale) that produce heavy showers, and the influence of terrain morphology, i.e., orography. The results of this study can be used to effectively address water-related challenges associated with precipitation fluctuations, and therefore, they are crucial for gaining a thorough understanding of the changing trends in precipitation across Central Serbia induced by climate change.

References

Alexandersson, H. 1986: A homogeneity test applied to precipitation data. *J. Climatol. 6*, 661–675. https://doi.org/10.1002/joc.3370060607

Ali, H., Peleg, N., and *Fowler, H.J.,* 2021: Global scaling of rainfall with dewpoint temperature reveals considerable ocean-land difference. *Geophys. Res. Lett.* 48(15), e2021GL093798. https://doi.org/10.1029/2021GL093798

Alexakis, D.D., Hadjimitsis, D.G., and *Agapiou, A.,* 2013: Integrated use of remote sensing, GIS and precipitation data for the assessment of soil erosion rate in the catchment area of "Yialias" in Cyprus. *Atmosph. Res. 131,* 108–124. https://doi.org/10.1016/j.atmosres.2013.02.013

Alsafadi, K., Mohammed, S.A., Ayugi, B., Sharaf, M. and *Harsányi, E.*, 2020: Spatial–Temporal Evolution of Drought Characteristics Over Hungary Between 1961 and 2010. Pure Appl. *Geophys 177*, 3961–3978. https://doi.org/10.1007/s00024-020-02449-5

Amiri, M.A. and *Gocić, M.*, 2023: Analysis of temporal and spatial variations of drought over Serbia by investigating the applicability of precipitation-based drought indices. *Theor Appl Climatol 154*, 261–274. https://doi.org/10.1007/s00704-023-04554-6

Amiri, M.A. and *Gocić, M.*, 2021a: Innovative trend analysis of annual precipitation in Serbia during 1946–2019. *Environ. Earth Sci. 80*, 777. https://doi.org/10.1007/s12665-021-10095-w

Amiri, M.A. and *Gocić, M.*, 2021b: Analyzing the applicability of some precipitation concentration indices over Serbia. *Theor. Appl. Climatol. 146*, 645–656. https://doi.org/10.1007/s12665-021-10095-w

Bajat, B., Blagojević, D., Kilibarda, M., Luković, J. and *Tošić, I.* 2015. Spatial Analysis of the Temperature Trends in Serbia during the Period 1961–2010. *Theor. Appl. Climatol. 121*(1), 289–301. https://doi.org/10.1007/s00704-014-1243-7

Bačević, R. N., Pavlović, M., and *Rašljanin, I.* 2018. Trend Assessing Using Mann-Kendall's Test for Pristina Meteorological Station Temperature and Precipitation Data, Kosovo and Metohija, Serbia. *Univ. Thought – Publ. Nat.Sci. 8*(2), 39–43. https://doi.org/10.5937/univtho8-19513

Bačević, N.R., Valjarević, A., Milentijević, N., Kićović, D., Ivanović M. and *Mujević, M. 2020:* Analysis of air temperature trends: City of Podgorica (Montenegro). *Univ. Thought – Publ. Nat.Sci. 10*(1), 31–36. https://doi.org/10.5937/univtho10-24790

Bačević, R.N., Milentijević, M.N., Valjarević, A., Gicić, A., Kićović, D., Radaković, M., Nikolić, M. and *Pantelić, M. 2021:* Spatio-temporal variability of air temperatures in Central Serbia from 1949 to 2018. *Időjárás 125*, 229–253. https://doi.org/10.28974/idojaras.2021.2.4

Bačević, R.N., Milentijević, N., Valjarević, A., Nikolić, M., Stevanović, V., Kićović, D., Radaković, G.M., Papić, D. and *Marković, B.S.* 2022: The analysis of annual and seasonal surface air temperature trends of southern and southeastern Bosnia and Herzegovina from 1961 to 2017. *Időjárás 126*, 355–374. https://doi.org/10.28974/idojaras.2022.3.5

Bărbulescu, A. and *Postolache, F. 2023:* Are the Regional Precipitation and Temperature Series Correlated? Case Study from Dobrogea, Romania. *Hydrology 10*(5), 109. https://doi.org/10.3390/hydrology10050109

Berg, P., Moseley, C., and *Haerter, J. O.* 2013: Strong increase in convective precipitation in response to higher temperatures. *Na. Geosci. 6*(3), 181–185. https://doi.org/10.1038/ngeo1731

Biel, E. 1929: Die Verändelichkeit der Jahressumme des Niederschlages auf der Erde. Geogr. Jb. Aus Österreich, XIV und XV, Wien, 151–180.*Bocheva, L., Marinova, T., Simeonov, P.* and *Gospodinov, I.* 2009: Variability and trends of extreme precipitation events over Bulgaria (1961–2005). *Atmos. Res. 93*(1), 490–497. https://doi.org/10.1016/j.atmosres.2008.10.025

Burić, D., Luković, J., Bajat, B., Kilibarda, M. and *Živković, N*, 2015: Recent trends in daily rainfall extremes over Montenegro (1951–2010). *Nat. Hazards Earth Syst. Sci. 15*, 2069–2077. https://doi.org/10.5194/nhess-15-2069-2015

Croitoru, A.E., Piticar, A. and *Burada, D.C.* 2016: Changes in precipitation extremes in Romania. *Quat. Int. 415*, 325–335. https://doi.org/10.1016/j.quaint.2015.07.028

Collins, M., Knutti, R., Arblaster, J., Dufresne, J., Fichefet, T., Friedlingstein, P., et al. 2013: Long-term climate change: Projections, commit-ments and irreversibility. In Climate change 2013*:* The physical science. Climate change 2013 the physical science basis: Working group I contribution to the fifth assessment report of the intergovernmental panel on climate change.

Conrad, V. 1941: The variability of precipitation. *Month. Weather Rev. 69*, 5–11. https://doi.org/10.1175/1520-0493(1941)069<0005:TVOP>2.0.CO;2

Ćulafić, G., Popov, T., Gnjato, S., Bajić, D., Trbić, G., and *Mitrović, L.* 2020: Spatial and temporal patterns of precipitation in Montenegro. *Időjárás 124*, 499–519. https://doi.org/10.28974/idojaras.2020.4.5

Đorđević, V.S. 2008: Temperature and precipitation trends in Belgrade and indicators of changing extremes for Serbia. *Geographica Pannonica 12*(2), 62–68. https://doi.org/10.5937/GeoPan0802062D

Ducić, V. and *Luković, J.* 2005: Moguće veze izmedju El Ninjo južne oscilacije (ENSO) i promena količine padavina u Srbiji. *Zbornik radova* – Geografski fakultet Univerziteta u Beogradu 53, 13–22. (In Serbian)

Ducić, V. and *Radovanović, M.* 2005. Klima Srbije. *ZUNS*, Beograd. ISBN: 86-17-12290-0. (In Slovak)
Ducić, V., Luković J. and *Milovanović, B.* 2009: Promene temperature i padavina u Srbiji u drugoj polovini XX veka u sklopu globalnih klimatskih promena. *Zaštita prirode*, 60(1–2), 641–652. (In Serbian) http://www.hidmet.gov.rs/ciril/meteorologija/klimatologija_godisnjaci.php (accessed 20 May 2022)
Ducić, V., Luković, J. and *Stanojević, G.* 2010: Cirkulacija atmosfere i kolebanje padavina u Srbiji u periodu 1949-2004. *Glasnik Srpskog geografskog društva 90*(2), 85–107. (In Serbian) https://doi.org/10.2298/GSGD1002085D
Erić, R., Kadović, R., Đurdjević, V. and *Đukić, V. 2021:* Future changes in extreme precipitation in central Serbia. *J. Hydrol. Hydromech. 69*(2), 196–208. https://doi.org/10.2478/johh-2021-0006
Gajić-Čapka, M., Cindric, K. and *Pasarić, Z.* 2014: Trends in precipitation indices in Croatia, 1961–2010. *Theor. Appl. Climatol. 117*, 3–4. https://doi.org/10.1007/s00704-014-1217-9
Gavrilov, MB., Tošić, I., Marković, SB., Unkašević, M. and *Petrović, P.* 2016: The analysis of annual and seasonal temperature trends using theMann-Kendall test in Vojvodina, Serbia. *Időjárás, 120*, 183–198.
Gavrilov, M.B., Marković, S.B., Mlađan, D., Subošić, D., Zarić, M., Pešić, A., Janc, N., Nikolić, M., Valjarević, A., Bačević, N. and *Marković, S.J.* 2015: Extreme Floods In Serbia Occurring Simultaneously With The High Water Levels And Heavy Rains - Case Study, International Scientific Conference "Archibald Reiss Days, 3-4 March 2015, Academy Of Criminalistic And Police Studies, Proceedings Of International Significance, 25-36, Belgrade, Serbia. https://doi.org/10.1007/s00024-021-02688-0
Gocić, M. and *Trajković, S.*, 2013: Analysis of changes in meteorological variables using Mann-Kendall and Sen's slope estimator statistical tests in Serbia. *Glob. Planet. Change 100*, 172–182. https://doi.org/10.1016/j.gloplacha.2012.10.014
Hardwick Jones, R., Westra, S., and *Sharma, A.* 2010: Observed relationships between extreme sub-daily precipitation, surface temperature, and relative humidity. *Geophys. Res. Lett. 37*(22), L22805. https://doi.org/10.1029/2010GL045081
Ivanova, V. and *Radeva, S.* 2016: Precipitation extremes trends in east and south Bulgaria from 1961 to 2010. 16th International Multidisciplinary Scientific GeoConference. SGEM, 507–514, Curran Associates, Inc.
Jones, P. 1999: The Instrumental Data Record: Its Accuracy and Use in Attempts to Identify the "CO2 Signal", u: Analysis of Climate Variability (ur. *Von Storch, H., Navarra, A.*), Springer, Heidelberg, 53–76. https://doi.org/10.1007/978-3-662-03744-7_4
Karmeshu, N. 2012: Trend Detection in Annual Temperature and Precipitation using the Mann Kendall Test - A Case Study to Assess Climate Change on Select States in the Northeastern United States. Master's thesis, University of Pennsylvania.
Kendall, M.G. 1975: Rank correlation methods. Charles Griffin, London.
Kharin, V. V., Zwiers, F. W., Zhang, X., and *Wehner, M.* 2013: Changes in temperature and recipitation extremes in the CMIP5 ensemble. *Climatic Change 119*(2), 345–357. https://doi.org/10.1007/s10584-013-0705-8
Klapwijk, M., Csóka, G., Hirka, A. and *Björkman, C.* 2013: Forest insects and climate change: long-term trends in herbivore damage. *Ecol. Evol. 3*, 4183–4196. https://doi.org/10.1002/ece3.717
Klein Tank, A.M.G. and *Können, G.P.* 2003: Trends in indices of daily temperature and precipitation extremes in Europe, 1946-99. *J. Climate 16*, 3665–3680. https://doi.org/10.1175/1520-0442(2003)016<3665:TIIODT>2.0.CO;2
Lenderink, G., and *van Meijgaard, E.* 2008: Increase in hourly precipitation extremes beyond expectations from temperature changes. *Nat. Geosci. 1*(8), 511–514. https://doi.org/10.1038/ngeo262
Lenderink, G., Mok, H. Y., Lee, T. C., and *van Oldenborgh, G.J.* 2011: Scaling and trends of hourly precipitation extremes in two different climate zones – Hong Kong and the Netherlands. *Hydrol. Earth Syst. Sci. 15*, 3033–3041. https://doi.org/10.5194/hess-15-3033-2011
Lenderink, G., Barbero, R., Loriaux, J. M. and *Fowler, H. J.* 2017: Super-clausius–clapeyron scaling of extreme hourly convective precipitation and its relation to large-scale atmospheric conditions. *J. Climate 30*, 6037–6052. https://doi.org/10.1175/JCLI-D-16-0808.1

Leščešen, I., Basarin, B., Podraščanin, Z. and *Mesaroš, M.* 2023: Changes in Annual and Seasonal Extreme Precipitation over Southeastern Europe. *Environ. Sci. Proc. 26*(1), 48. https://doi.org/10.3390/environsciproc2023026048

Lukić, T., Lukić, A., Basarin, B., Micić Ponjiger, T., Blagojević, D., Mesaroš, M., Milanović, M., Gavrilov, M.B., Pavić, D., Zorn, M., Komac, B., Miljković, Đ., Sakulski, D., Babić-Kekez, S., Morar, C. and *Janićević, S.* 2019: Rainfall erosivity and extreme precipitation in the Pannonian basin. *pen Geosci. 11*, 664–681. https://doi.org/10.1515/geo-2019-0053

Luković, J., Bajat, B., Blagojević, D. and *Kilibarda, M.* 2014: Spatial pattern of recent rainfall trends in Serbia (1961–2009). *Reg. Environ. Change 14*, 1789–1799. https://doi.org/10.1007/s10113-013-0459-x

Mann, H.B. 1945: Nonparametric tests against trend. *Econometrica 13*, 245–259. https://doi.org/10.2307/1907187

Maradin, M. 2011: Geografski aspekt razlika u varijabilnosti padavina kontinentskog i maritimnog pluviometrijskog rezima u Republici Hrvatskoj, doktorski rad, Prirodoslovno-matematicki fakultet, Zagreb, 126. (In Serbian)

Marković, Đ.J. 1966: Geografske oblasti Socijalističke Federativne Republike Jugoslavije, *Beograd: ZUNS.*

Micić Ponjiger, T., Lukić, T., Wilby, R.L., Marković, S.B., Valjarević, A., Dragićević, S., Gavrilov, M.B., Ponjiger, I., Durlević, U., Milanović, M.M., Basarin, B., Mlađan, D., Mitrović, N., Grama, V. and *Morar, C.* 2023: Evaluation of Rainfall Erosivity in the Western Balkans by Mapping and Clustering ERA5 Reanalysis Data. *Atmosphere 14*, 104. https://doi.org/10.3390/atmos14010104

Milentijević, N., Bačević, R. N., Ristić, D., Valjarević, A., Pantelić, M. and *Kićović, D.* 2018: Application of Mann-Kendal (mk) test in trend analysis of air temperature and precipitation: case of Mačva district (Serbia). *The University Thought - Publication in Natural Sciences 10*(1), 37–43. https://doi.org/10.5937/univtho10-24774

Mishra, V., Wallace, J. M., and *Lettenmaier, D. P. 2012*: Relationship between hourly extreme precipitation and local air temperature in the United States. *Geophys. Res. Lett. 39*(16), L16403. https://doi.org/10.1029/2012GL052790

Morales, C. 1977: Rainfall Variability – A Natural Phenomenon. *Ambio 6*(1), 30–33.

Mudelsee, M. 2014. Climate Time Series Analysis: Classical Statistical and Bootstrap Methods, 2nd edition. Cham, Switzerland: Springer. https://doi.org/10.1007/978-3-319-04450-7

Mudelsee, M. 2019. Trend analysis of climate time series: A review of methods. *Earth-Sci. Rev.190*, 310–322. https://doi.org/10.1016/j.earscirev.2018.12.005

Pall, P., Allen, M. R., and *Stone, D. A.* 2007: Testing the Clausius–Clapeyron constraint on changes in extreme precipitation under CO2 warming. *Climate Dynam. 28*(4), 351–363. https://doi.org/10.1007/s00382-006-0180-2

Popov, T., Gnjato, S., and *Trbić, G.* 2018a: Anal-ysis of Extreme Precipitation over the Peri-pannonian Region of Bosnia and Hercegovina. *Időjárás 122*, 433–452. https://doi.org/10.28974/idojaras.2018.4.5

Popov, H. and *Svetozarević, J.* 2021. Changes and contemporary trends in the annual amounts of precipitation in Serbia. *J. Bulgarian Geograph. Soc. 44*, 73–79. https://doi.org/10.3897/jbgs.e77102

Proja, T and *Nunaj L.*, 2020. Three decades of heat waves and extremeprecipitation in Tirana. 11th International Conference of the Balkan Physical Union (BPU11), 28 August - 1 September 2022, Belgrade, Serbia. https://doi.org/10.22323/1.427.0195

Radaković, G.M., Tošić, A.I., Bačević, R.N., Mlađan, D., Marković S.B. and *Gavrilov M.B.* 2018: The analysis of aridity in Central Serbia from 1949-2015. *Theor. Appl. Climatol. 133*, 887–898. https://doi.org/10.1007/s00704-017-2220-8

Radinović, Đ. 1981: Vreme i klima Jugoslavije. Beograd: IRO "Gradjevinska knjiga". (In Serbian)

Radevski, I., Gorin, S., Markoski, B., Dimitrovska, O. and *Todorovska, S.* 2013: Spatial Precipitation Distribution In Prespa Basin (Republic Of Macedonia). Hilly-Mountain-Areas Problems and Perspectives, Ohrid, 12-15 IX 2013.

Roderick, T. P., Wasko, C., and *Sharma, A.* 2019: Atmospheric moisture measurements explain increases in tropical rainfall extremes. *Geophys. Res. Lett. 46*, 1375–1382. https://doi.org/10.1029/2018GL080833

Roderick, T.P., Wasko, C. and *Sharma, A.* 2020: An improved covariate for projecting future rainfall extremes? *Water Resour. Res. 56*(8), 1-11. https://doi.org/10.1029/2019WR026924

Razavi, T., Switzman, H., Arain, A. and *Coulibaly, P.* 2016. Regional climate change trends and uncertainty analysis using extreme indices: A case study of Hamilton, Canada. *Climate Risk Manage. 13*, 43–63. https://doi.org/10.1016/j.crm.2016.06.002

Ruml, M., Vukovic, A., Vujadinovic, M., Djurdjevic, V., Rankovic-Vasic, Z., Atanackovic, Z., Sivčev, B., Marković, N., Matijašević, S. and *Petrovic, N.* 2012: On the use of regional climate models: Implications of climate change for viticulture in Serbia. *Agricult. Forest Meteorol. 158*, 53–62. https://doi.org/10.1016/j.agrformet.2012.02.004

Spiridonov, V., and *Balabanova, S.* 2021: The impact of climate change on intensive precipitation and flood types in Bulgaria. *In (Ed. M.-M. Nistor*) Climate and Land Use Impacts on Natural and Artificial, 153–169. https://doi.org/10.1016/B978-0-12-822184-6.00001-6

Stanojević, G. 2012. Analiza godišnjih padavinskih suma na prostoru Srbije, Geografski institut „Jovan Cvijić", SANU, Beograd. UDC: 911.2:551.58(497.11). https://doi.org/10.2298/IJGI1202001S

Tebaldi, C., Hayhoe, K., Arblaster, J.M., and *Meehl, G.A. 2006: Going to the extremes. Climatic Change*, 79(3), 185–211. https://doi.org/10.1007/s10584-006-9051-4 (In Serbian)

Trenberth, K.E., Dai, A., Rasmussen, R. M., and *Parsons, D.B.* 2003: The changing character of precipitation. *Bull. Amer. Meteorol. Soc. 84*, 1205–1217. https://doi.org/10.1175/BAMS-84-9-1205

Utsumi, N., Seto, S., Kanae, S., Maeda, E.E., and *Oki, T.*, 2011: Does higher surface temperature intensify extreme precipitation? *Geophys. Res. Lett. 38*(16), L16708. https://doi.org/10.1029/2011GL048426

Valcheva, R. and *Spiridonov, V.* 2023: Regional climate projections of heavy precipitation over the Balkan Peninsula. *Időjárás 127*, 77–106. https://doi.org/10.28974/idojaras.2023.1.5

Valjarević, A., Popovici, C., Štilic, A., and *Radojković, M.* 2022: Cloudiness and water from cloud seeding in connection with plants distribution in the Republic of Moldova. *Appl. Water Sci. 12*, 262. https://doi.org/10.1007/s13201-022-01784-3

Valjarević, A., Đjekic, T., Stevanović, V., Ivanović, R., and *Jandzikoviċ, B.*, 2018: GIS numerical and remote sensing analyses of forest changes in the Toplica region for the period of 1953–2013. *Appl. Geogr. 92*, 131–139. https://doi.org/10.1016/j.apgeog.2018.01.016

Valjarević, A., Algarni, S., Grama, V., Stupariu, M., Tiba, A., and *Lukić, T.*, 2023: The coastal fog and ecological balance for plants in the Jizan region, Saudi Arabia. *Saudi J. Biol. Sci 30*, 103494. https://doi.org/10.1016/j.sjbs.2022.103494

Velimirović, L., Stanković, S.M., Gocić, M., and *Trajković, S.* 2021. Determining the best fitting distribution of annual precipitation data in Serbia using L-moments method. *Earth Sci. Inform. 14*, 633–644. https://doi.org/10.1007/s12145-020-00543-9

Visser, J. B., Wasko, C., Sharma, A., and *Nathan, R.* 2021: Eliminating the "Hook" in precipitation–temperature scaling. *J. Climate 34*, 9535–9549. https://doi.org/10.1175/JCLI-D-21-0292.1

Zeleňáková, M., Purcz, P., Blisťan, P., Vranayová, Z., Hlavatá, H., Diaconu, D.C., and *Portela, M.M.* 2018: Trends in Precipitation and Temperatures in Eastern Slovakia (1962-2014). *Water 10*(6), 727. https://doi.org/10.3390/w10060727

Westra, S., Fowler, H.J., Evans, J.P., Alexander, L.V., Berg, P., Johnson, F., Kendon, E.J., Lenderink, G., and *Roberts, N.M.* 2014: Future changes to the intensity and frequency of short-duration extreme rainfall. *Rev. Geophys 52*(3), 522–555. https://doi.org/10.1002/2014RG000464

Živanović, S., Ivanović, R., Nikolić, M., Đokić, M., and *Tošić, I.* 2020: Influence of air temperature and precipitation on the risk of forest fires in Serbia. *Meteorol. Atmosp. Phys. 132*, 869–883. https://doi.org/10.1016/j.spasta.2017.11.006

DOI:10.28974/idojaras.2024.4.5

IDŐJÁRÁS

Quarterly Journal of the HungaroMet Hungarian Meteorological Service
Vol. 128, No. 4, October – December, 2024, pp. 473–496

Observed changes in the characteristics of heat waves in hot and dry regions of Iran

Atefeh Ansari, Peyman Mahmoudi*, and **Hamid Nazaripour**

Department of physical geography
Faculty of Geography and Environmental Planning
University of Sistan and Baluchestan, Zahedan, Iran

** Correspondening Author E-mail: p_mahmoudi@gep.usb.ac.ir*

(Manuscript received in final form October 24, 2023)

Abstract— Research on heat waves is greatly important not only due to their effect on social, economic, and ecological systems, but also due to the complexity of the processes that create them. Therefore, this research mainly investigated the trend of long-term changes in various characteristics of heat waves in hot and dry regions of Iran. For this purpose, the daily maximum temperature data of 15 meteorological stations in the central and southeastern parts of Iran were used from 1985 to 2018. Using the excess heat factor (*EHF*) index, five different features of heat waves including the number of heat waves (HWN), heat waves duration (HWD), heat waves frequency (HWF), heat waves mean (HWM), and heat waves magnitude (HWA) were extracted for all the studied stations. Then, their trend of long-term changes was analyzed using the Sen's slope estimator nonparametric method. The results showed that on a regional scale, all five characteristics of heat waves have an increasing trend at a significance level of 95%, so an increase of 0.5 events per decade has been observed for the HWN. The trend of long-term changes in the HWD has also indicated an increase of 0.91 days per decade. The HWF has shown more drastic changes than other characteristics of heat waves, so in every decade 2.61 days have been added to the frequency of days contributing to the occurrence of heat waves. The regional intensity of HWM and HWA also show an increase of 0.1 and 0.4 °C in each decade, respectively. These findings show the importance of choosing a suitable index for monitoring different characteristics of heat waves. The *EHF* index is a suitable index, which can be one of the efficient indices in this regard.

Key-words: climate change, trend, Sen's slope estimator, heat waves, Iran

1. Introduction

It is important to research extreme climate events due to their effect on social, economic, and ecological systems and the complexity of the processes that create them. Investigating extreme climate events always requires considering different spatial and temporal scales, different modes of variability, and thermodynamic processes that create them (*Stocker et al.*, 2013). Researches show that scientific knowledge about some atmospheric processes has made substantial progress and has provided a platform for designing climate models and forecasting numerical weather models (*Tavosi et al.*, 2010).

According to the Special Report of Extreme Events (SREX) prepared by Working Groups I (WGI) and II (WGII) of the Intergovernmental Panel on Climate Change (IPCC), weather and climate extremes are rare events that occur in a certain period by passing a certain threshold value. The threshold value can vary from place to place (*Field*, 2012). In this definition, the two terms of weather and climate extremes are mentioned. Extreme weather events are events that occur in a short period, for example, from a few hours to several weeks, while extreme climate events are a set of events that occur in a longer period, for example, during a season (*Stocker et al.*, 2013).

The American Meteorological Society defines a heat wave simply as "a period of abnormally and uncomfortably hot and usually humid weather" (AMS, 2000). Many efforts have been made to add more details to this definition. Unfortunately, due to the lack of a common set of parameters, it has become more complicated (*Choi* and *Meentemeyer*, 2002; *Robinson*, 2001). The excess heat factor (*EHF*) (*Nairn et al.*, 2009) is one of the important indicators for studying the effects of heat waves on human health, especially in mid-latitude climates (*Scalley et al.*, 2015; *Hatvani-Kovacs et al*., 2016; *Jegasothy et al.*, 2017; *Nairn et al.*, 2018; *Oliveira et al.*, 2022). *Nairn* and *Fawcett* (2013) have introduced this index as a simpler and more efficient index compared to other bioclimatic indices such as universal thermal climate index (UTCI) (*Zare et al*., 2018) and physiological equivalent temperature (PET) (*Höppe*, 1999). The Expert Team of Sector-Specific Climatic Indicators (ET-SCI) affiliated with the World Meteorological Organization (WMO) has introduced 64 precipitation and temperature extreme indices to improve decision-making for planning, organization, risk management, and adaptation to climatic variability and change. Out of these 64 precipitation and temperature extreme indices, about 47 of them were related to temperature extreme indices. The *EHF* index is one of the main indicators of detecting heat waves that have been used by this team. Based on this index, five different characteristics of heat waves such as the number of heat waves (HWN), heat waves duration (HWD), heat waves frequency (HWF), heat waves mean (HWM), and heat waves magnitude (HWA) can be extracted (*Perkins* and *Alexander*, 2013).

According to the report of the Intergovernmental Panel on Climate Change (IPCC) in 2013, "it is very likely that the number of cold days and nights will decrease and the number of warm days and nights will increase on a global scale". In addition, “the heat waves frequency is likely to increase in large parts of Europe, Asia, and Australia" (IPCC, 2013). Various studies have also confirmed increasing trends in indicators related to heat waves in different parts of the world (*Li et al*., 2022; *Perkins-Kirkpatrick* and *Lewis*, 2020; *Rousi et al.*, 2022; *Yin et al.*, 2022). In Iran, many studies have focused on the changes in average minimum and maximum monthly, seasonal, and annual temperatures in different spatial scales (*Alijani et al.*, 2015; *Halabian et al.*, 2017; *Jahanbaksh et al*., 2018; *Khoshakhlagh et al*., 2011; *Montazeri*, 2014). The total results of these studies show that the changes in the average minimum temperatures were almost twice the changes in the average maximum temperatures (*Alijani et al*., 2012a). In this regard, in the average national scale of Iran, an increase of 0.2 °C per decade for the average annual maximum temperature and an increase of 0.4 °C per decade for the average annual minimum temperature have been reported (*Mahmoudi et al*., 2019). In addition, the results of regional scale studies in Iran are also increasing the annual average minimum temperature in a decade for Tehran to 0.68 °C (*Bidokhti* and *Ranjbar*, 2003), confirming the increase of 2 °C in Iran's day and night temperature in a hundred years (*Masoudian*, 2004) and predicting an increase of 2.75 °C for Northeast Iran (*Alizadeh* and *Kamali*, 2002).

This increase in average maximum and minimum temperatures can naturally intensify heat waves in Iran. *Darand* (2014) revealed three indices based on the 90th, 95th, and 99th percentiles of maximum temperatures and the intensity, duration, and frequency of Iran's heat waves to identify heat waves and analyze their trends in Iran. Then, the significance of the trends of these three indices was analyzed using the Mann-Kendall nonparametric test and their trend slope using linear regression. The findings of this research showed that the frequency, duration, and intensity of heat waves are increasing on low and flat lands such as Dasht-e Lut (northeast of Kerman province), plain lands of northeast Hormozgan province, Dasht-e Kavir and Khuzestan province and are decreasing on the heights of the Zagros and Alborz mountain ranges and other scattered heights. *Namroodi et al.* (2021) also reported an increasing trend in the number of heat wave in Iran. In that study, they showed that about 85% of the studied stations in Iran had an increasing trend in the heat wave number. *Esmailnejad et al.* (2014) also confirmed the same increasing trend in the heat wave number in Iran.

The central and southeastern parts of Iran are one of the most vulnerable areas of Iran to climate change due to their dry climate (*Alijani et al.*, 2015; *Mahmoudi et al.*, 2011). The increasing trend of temperature (*Sari Sarraf et al*., 2018) and the decreasing trend of precipitation (*Mahmoudi* and *Rigi Chahi*, 2019) in the last few decades have aggravated this vulnerability. Intensifying the various characteristics of heat waves is one of the climate hazards that can harm the fragile economic, social, environmental, health, and even political structure of this part

of Iran. As mentioned above, various research have studied the changes in the characteristics of heat waves in Ira,n but there are still many study gaps for the central and southeastern parts of Iran. In these studies, the central and southeastern parts of Iran have not been considered independent geographical units. The heat wave indices used in these studies are mostly based on percentile thresholds and mostly focused on the heat waves frequency. Therefore, this study mainly aims to fill these study gaps for this part of Iran. Therefore, the *EHF* will be used for the first time to extract five different characteristics of heat waves in Iran. The trend of long-term changes in these five different characteristics of heat waves will also be analyzed for the cental and southeastern parts of Iran.

2. The study area

The area studied in this research includes the five provinces of Sistan and Baluchestan, Kerman, South Khorasan, Yazd, and Hormozgan, which cover an area of about 659,378 square kilometers, equal to 40% of Iran's area, in the center, south, and east of it (*Fig. 1a*). According to the 2016 census, these five provinces had a population of 9,623,578 people, equal to 12% of the total population of Iran (Statistical Center of Iran, 2016).

According to De Martonne's climate classification (*De Martonne*, 1909), the entire studied area has a dry climate (*Table 1*). The average annual rainfall in this area is nearly 109 mm, and its spatial distribution is very different in different parts, so the average annual rainfall in Bandar Abbas station is 171.1 mm, and in Zabol station is 52.6 mm (*Fig. 1b*). The average annual temperature of this area is 22.2 degrees Celsius. The lowest average annual temperature belongs to Birjand station at 16.5 °C and the highest one at 27.8 °C belongs to Bandar-e Lengeh station (*Fig. 1c*).

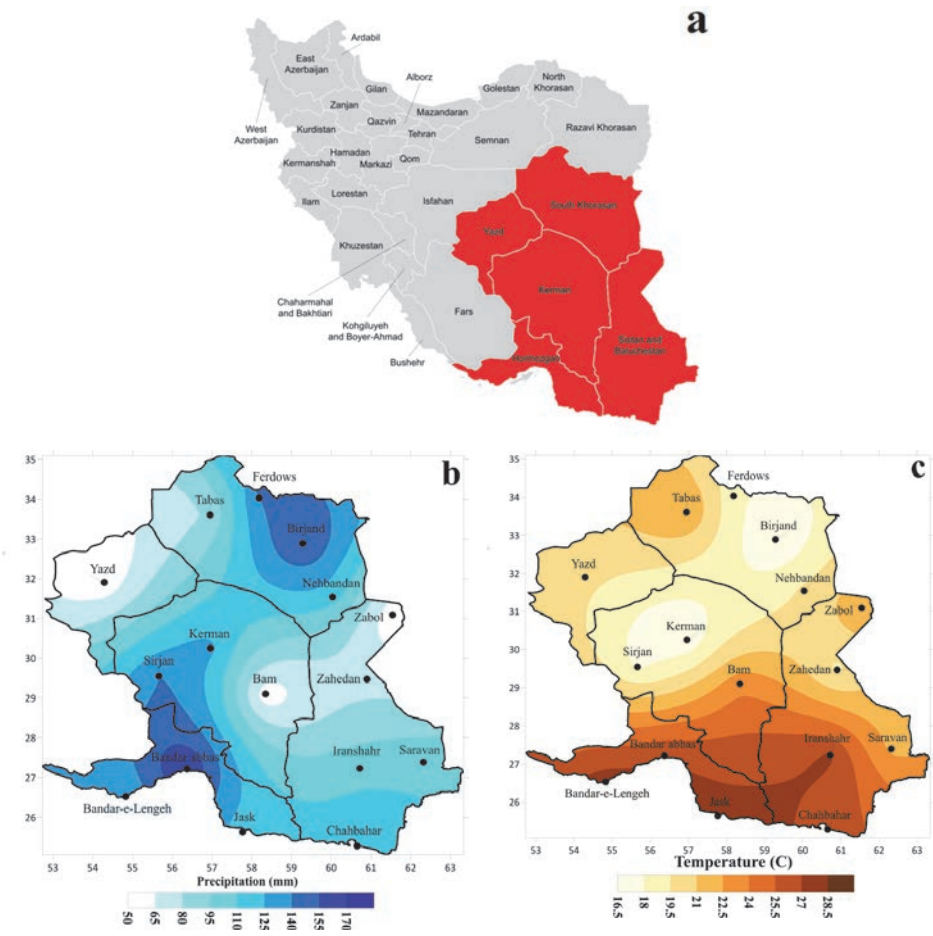

Fig. 1. (a) Geographical location of the cental and southeastern parts of Iran and its administrative divisions. (b) Spatial distribution of the long-term average annual precipitation in the cental and southeastern parts of Iran (1985–2018). (c) Spatial distribution of the long-term average annual temperature in the center and south Eastern Iran (1985–2018).

3. Data

In this research, the trend of long-term changes in the *EHF* was used as an index proposed by the World Meteorological Organization (WMO) to extract different characteristics of heat waves in the cental and southeastern parts of Iran. The daily maximum temperature data of 15 Iranian meteorological stations for a period of 34 years (1985–2018) were received from the Iran Meteorological Organization.

The geographic location of the studied stations is shown in *Fig. 2* and their geographic characteristics are given in *Table 1*. These stations have the most complete and reliable data in the cental and southeastern parts of Iran. The few statistical gaps in this station were reconstructed using the Pearson's correlation coefficient and the linear regression method. Quality control of data and their homogeneity tests were carried out using the runs test method and the homogeneity of all data was confirmed at a probability level of 95%.

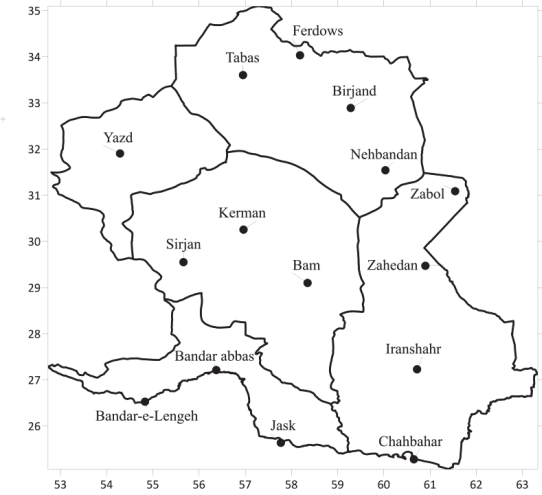

Fig. 2. The name and geographical location of the studied stations in the cental and southeastern parts Iran

Table 1. Geographical characteristics of the studied stations in the cental and southeastern parts of Iran

Station	longitude	latitude	altitude (m)	climate
Zahedan	60° 53´	29° 28´	1370	dry
Bam	58° 21´	29° 06´	1067	dry
Bandar abbas	56° 22´	27° 13´	10	dry
Bandar-e-Lengeh	54° 50´	26° 35´	14	dry
Birjand	59° 12´	32° 52´	1491	dry
Chabahar	60° 37´	25° 17´	8	dry
Ferdows	58° 10´	34° 01´	1293	dry
Iranshar	60° 42´	27° 12´	591	dry
Jask	57° 46´	25° 38´	5.2	dry
Kerman	56° 58´	35° 15´	1754	dry
Minab	57° 05´	27° 06´	30	dry
Sirjan	55° 41´	29° 28´	1739	dry
Tabas	56° 55´	33° 36´	711	dry
Yazd	54° 17´	31° 54´	1237	dry
Zabol	61° 29´	31° 02´	489	dry

4. Methodology

4.1. Excess heat index (EHF)

The calculation of *EHF* is the result of multiplying two sub-indexes of excess heat: (1) the significance excess heat index (EHF_{sig}), which measures the difference between the average maximum temperature of 3 days with the 95th percentile of the average maximum temperature of the reference period (1985–2018) and (2) the acclimatization excess heat index (EHF_{accl}), which measures the difference between the average maximum temperature of three days and the average maximum temperature of the last 30 days. The first sub-index shows excess heat as a long-term anomaly (climate scale), and the second sub-index considers the heat stress amount as a short-term anomaly. The second sub-index is based on the logic that biological systems are less able to adapt to sudden increases in temperature (*Nairn* and *Fawcett*, 2013). These two sub-indexes and the *EHF* are calculated according The following equations (*Alexander* and *Herold*, 2016; *Nairn* and *Fawcett*, 2013).

$$EHF_{sig} = \frac{(T_i+T_{i+1}+T_{i+2})}{3} - T_{95}, \quad (1)$$

$$EHI_{accl} = \frac{(T_i+T_{i+1}+T_{i+2})}{3} - \frac{(T_{i-1}+ \ldots+T_{i-30})}{30}, \quad (2)$$

$$EHF = EHF_{sig} \times max(1, EHI_{accl}), \quad (3)$$

where T is the average maximum daily temperature and T_{95} is the 95th percentile of the average maximum temperature of the reference period (1985–2018). It should be noticed that the calculation basis of this index is based on the average daily air temperature (the average between the daily maximum and minimum temperatures). This study used the daily maximum temperature instead of the average daily air temperature.

When the *EHF* result is detected as positive, its value will be a quadratic measure of heat wave intensity that responds to both short-term and long-term anomalies. The measurement unit of this index is $°C_L^2$, where L refers to the local nature of the threshold and the *EHF* results. The *EHF* extracted the five different characteristics of heat waves including the HWN, HWD, HWF, HWM, and HWA. *Table 2* shows the definitions and measurement units of these five indicators.

Table 2. Aspects of heat wave analyzed based on *EHF* with their names, definitions, and units

Identifier	Heatwave aspect	Definition	Unit
HWN	Heat waves number	The annual number of summer heat waves that have the conditions of continuity for at least 3 consecutive days with positive *EHF* values.	Number of events
HWD	Heat waves duration	In terms of time, the longest heat wave of the summer season has the conditions of continuity for at least 3 consecutive days with positive *EHF* values.	Days
HWF	Heat waves frequency	The total number of days in the summer season that was involved in a heat wave and had the conditions of continuity for at least 3 consecutive days with positive *EHF* values.	Days
HWA	Heat waves magnitude	The hottest day of the hottest summer heat wave has continued for at least 3 consecutive days with positive *EHF* values.	$°C^2$
HWM	Heat waves average	The average magnitude of all summer heat wave days that have the conditions of continuity for at least 3 consecutive days with positive *EHF* values.	$°C^2$

It should be noted that two features of heat wave intensity such as HWA and HWM depend on the local temperature range changes, which are also different according to geographical latitude. Therefore, the annual values and the amount of change in HWA and HWM in different regions can only be compared with each other through the normalization of local heat wave intensity. To overcome this limitation, severity methodology based on *EHF* (EHF_{severity}) was incorporated by *Nairn et al.* (2018) to determine how severe a heat wave day is compared to the local climatology. Based on the normalization of the *EHF* daily intensity value by the 85th percentile (*EHF*85p) of a climatological period, the dimensionless index *EHF* severity is calculated based on Eq.(4), which is based on the extreme value theory. Here, *EHF* daily intensities are normalized by the 85th percentile for the climatological period 1985–2018:

$$EHF_{severity} = EHF \div EHF_{85p}. \tag{4}$$

In the analysis section of this study, instead of the normalized values of two characteristics of HWA and HWM (in $°C^{2)}$, their temperature equivalent (in °C) was used. It seems that using temperature equivalent instead of normalized values can provide a better understanding of the magnitude and intensity of heat waves in this region of Iran. All calculation steps of this index are programmed in MATLAB software environment.

4.2. The Sen's slope estimator nonparametric method

The Sen's slope estimator nonparametric test was used to analyze the trend of long-term changes in various characteristics of heat waves in the cental and southeastern parts of Iran. This method was first presented by *Theil* in 1950, and then developed and expanded by *Sen* in 1968. Like many other non-parametric methods such as Mann-Kendall, this method is based on analyzing the difference between the observations of a time series. This method can be used when the trend in the time series is a linear trend. This means that $f(t)$ can be expressed as:

$$f(t) = Qt + B \ , \tag{5}$$

where Q is the trend line slope and B is the constant coefficient value.

The slope between each pair of observational data must be first calculated using the following equation to calculate the trend line slope, i.e., Q:

$$Q_i = \frac{x_j - x_k}{j - k} \ , \tag{6}$$

where $j > k$. In this equation, x_j and x_k are observational data at times j and k, respectively. A slope is obtained for each pair of observational data by applying this relationship. In addition, a time series of calculated slopes is obtained by placing these slopes next to each other. That is, if there is an n number x_j in the time series (in this research, n=34), we will have an estimate of the slope (Q_i) equal to $N = n(n-1)/2$.

In the next step, the median of the studied time series should be obtained. For this purpose, N number of Q_i are sorted from small to large. Then, the median of the time series is determined using one of the following equations. If the number of observations of the studied time series is odd, Eq.(7) is used, and if it is even, Eq.(8) is used:

$$Q = Q_{[(N+1)/2]} \ , \tag{7}$$

$$Q = \frac{1}{2} = \left[Q_{N/2} + Q_{[(N+2)/2]}\right] . \tag{8}$$

The result of these equations is to obtain the trend line slope (Q_{med}). If the trend line slope is positive, it indicates an upward trend, and if it is negative, it indicates a downward trend.

The next step is to test the obtained slope in the confidence interval of α= 0.05. The following equatuion is used to perform this test:

$$C_a = Z_{1-\alpha/2}\sqrt{VAR(S)} \ , \tag{9}$$

where Z is the statistic of the standard normal distribution in a two-way test which is equal to $Z = 1.96$ for 95% confidence level, and $VAR(S)$ is the variance of the parameter S. The following steps must be followed to obtain the value of the parameter:

a) Calculating the difference between each sentence in a series and applying the sign function (sgn) and extracting the parameter *S*:

$$S = \sum_{k=1}^{n-1} \sum_{j=k+1}^{n} sgn(x_j - x_k) \ , \tag{10}$$

where n is the number of serial observations (in this research it is 34 years), and x_j, x_k are the data of the jth and kth series, respectively.

b) Calculating the sign function (sgn) which can be calculated as follows:

$$sgn(x) = \begin{cases} +1 if(xj - xk) > 0 \\ 0 if(xj - xk) = 0 \\ -1 if(xj - xk) < 0 \end{cases} . \tag{11}$$

c) Calculating the variance S using one of the following relationships. If the number of time series data is greater than ten, Eq.(12) is used, and if it is less than nine, Eq.(13) is used:

$$VAR(S) = \frac{n(n-1)(2n+5) - \sum_{i=1}^{m} t(t-1)(2t+5)}{18} \ , \tag{12}$$

$$VAR(S) = \frac{n(n-1)(2n+5)}{18} , \tag{13}$$

where, *n* is the number of observational data, *m* is the number of series in which there is at least one repeated data, and *t* represents the frequency of data with the same value.

Finally, the upper and lower confidence limits are calculated through the following relationships:

$$\begin{cases} M_1 = \frac{n' + C_a}{2} \\ M_2 = \frac{n' - C_a}{2} \end{cases} , \tag{14}$$

where n' is the number of slopes obtained by the method of Eq.(8).

Now, the M_1th and M_{2+1}th slopes from among the calculated slopes are extracted. If the number zero is in the range between the two slopes extracted above, the null hypothesis is accepted, and the absence of a trend in the data series is confirmed. Otherwise, the null hypothesis is rejected, and the existence of a trend in the confidence level of the test is accepted.

Finally, *n* number of differences $x_i - Qt_i$ is calculated to obtain the value of *B* in Eq.(5). Then, the median of these values provides the estimate of *B* (*Alijani et al.*, 2012b).

5. Analysis and discussion

5.1. Heat waves climatology

For all the studied stations in the cental and southeastern parts of Iran, the different characteristics of heat waves including HWN, HWD, HWF, HWM, and HWA were extracted using the *EHF* index. The climatological mean (1985–2018) of each of these characteristics was calculated for the cental and southeastern parts of Iran (the long-term average of the numerical values of each of the characteristics of heat waves for all stations were added together and divided by the number of stations), and their results are given in *Table 3*.

Table 3. Climatic average (1996–2018) of different characteristics of heat waves for the cental and southeastern parts of Iran

Different characteristics of heat waves	**Annual average**
Heat waves number	2.5
Heat waves duration	8.0
Heat waves frequency	14.6
Heat waves mean	41.2
Heat waves magnitude	43.4

The climatic average of HWN for the cental and southeastern parts of Iran was 2.5 events per year (*Table 3*). Minab station with 2.9 and Sirjan station with 1.2 occurrences per year have the highest and lowest station average values of this feature of heat wave, respectively (*Fig. 3a*). The spatial distribution map of this feature of the heat wave in the cental and southeastern parts of Iran shows that its lowest values are observed in the western and the highest in the southern (northern

coasts of the Oman Sea and the Persian Gulf) parts of the study area (*Fig. 3a*). In terms of the duration, the climatic average of the HWD in this part of Iran was equal to 8 days (*Table 3*). The southern part of the studied area has the lowest and the western part has the longest heat wave duration (*Fig. 3b*). Jask station with 5.5 days and Sirjan station with 11.5 days had the longest and shortest heat waves duration on a station scale, respectively (*Fig. 3b*). The HWF (the number of days involved in the occurrence of a heat wave) was the third feature of heat waves, whose climatic mean was analyzed for the cental and southeastern parts of Iran. The climatic average of this index for this part of Iran was 14.6 days (*Table 3*). Its spatial distribution in the cental and southeastern parts of Iran indicated the existence of low values in the southern half and high values in the western and central parts of the studied region (*Fig. 3c*). Jask station with 11.1 days and Sirjan station with 18 days have the lowest and highest heat waves frequency, respectively, in a station scale (*Fig. 3c*). The climatic average of HWM (average temperature of all heat waves) for the cental and southeastern parts of Iran was equal to 41.2 °C (*Fig. 3*). The highest values of this feature were observed in the northwest, east, center of Sistan and Baluchistan province, and south of Kerman province, and the lowest values were observed in the southeastern part of the study area (*Fig. 3d*). Iranshahr station with 44.2 °C and Chabahar station with 35.2 °C had the highest and lowest values of this heat waves characteristic, respectively (*Fig. 3d*). Finally, the average calculated for the heat waves magnitude was equal to 43.4 °C (*Table 3*). The spatial pattern of this feature is almost similar to the intensity feature of heat waves. The highest value of this feature was observed in the northwestern, eastern, and central parts of Sistan and Baluchistan province and south of Kerman province, and the lowest value was observed in the southeast ern part of the study area (*Fig. 3e*). Chabahar station with 38.6 and Minab station with 48.2 °C have the highest and lowest values of this feature in the cental and southeastern parts of Iran, respectively (*Fig. 3e*).

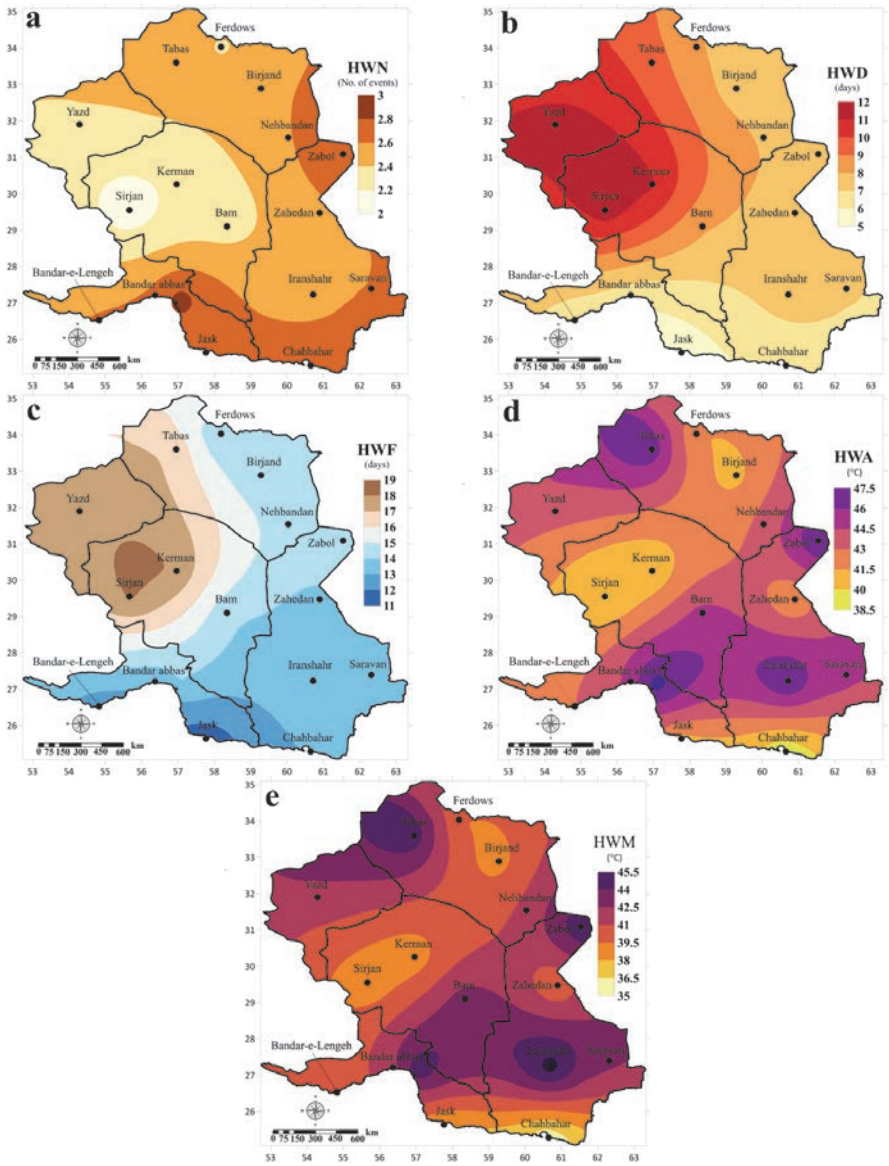

Fig. 3. Different characteristics of heat waves in the cental and southeastern parts of Iran including (a) HWN, (b) HWD, (c) HWF, (d) HWM, and (e) HWA using the *EHF* index in 1986–2018.

The distribution of the total frequency of heat waves in different months of the year was also considered. As it is presented in *Table 4*, the highest frequency

of heat waves in the studied stations in the cental and southeastern parts of Iran was concentrated in July, June, and August, respectively. In these three months, all the studied stations have experienced the maximum number of heat waves. Among the studied stations, Chabahar station was the only station that experienced heat waves in April and October. On April 1 and September 6, heat waves occurred at this station during the 34 years studied (1985–2018).

Table 4. Distribution of the total frequency of heat waves in the 7 months of the warm period of the years 1985–2018

Station	April	May	June	July	August	September	October
Zahedan	0	3	30	39	8	0	0
Bam	0	2	33	30	6	0	0
Bandar abbas	0	11	26	21	16	7	0
Bandar Lengeh	0	5	14	23	18	3	0
Birjand	0	2	29	39	11	0	0
Chabahar	1	31	36	10	2	2	6
Ferdows	0	0	28	34	12	2	0
Iranshar	0	3	43	31	5	1	0
Jask	0	14	40	17	9	0	0
Kerman	0	1	28	35	8	0	0
Minab	0	15	31	19	17	7	0
Sirjan	0	0	20	38	9	0	0
Tabas	0	0	25	40	15	0	0
Yazd	0	0	21	36	15	0	0
Zabol	0	3	24	35	12	1	0

5.2. Analysis of the trend of long-term changes in different characteristics of heat waves

This section presents the results of the trend analysis of long-term changes in five characteristics of heat waves in the cental and southeastern parts of Iran. The

HWN was the first feature of the heat waves that was noticed in the cental and southeastern parts of Iran. This feature of the heat waves is obtained by counting the number of heat waves that occur each year. The trend of long-term changes in the HWN on a regional scale for the cental and southeastern parts of Iran shows a significant increasing trend at the 95% probability level (*Table 5*). Based on this increasing trend, it is observed that 0.5 cases have been added to the heat waves number in the cental and southeastern parts of Iran in each decade (*Table 5*). In addition, the results of trend analysis at a station scale show an increasing trend for all studied stations except Sirjan station in Kerman province. Among the stations with an increasing trend, the two stations of Bandar-e Lengeh and Zabul have the highest values of the increasing trend in the heat waves number with an increasing trend of 1.04 and 0.93 in each decade, respectively (*Fig. 4a*). In terms of spatialdistribution, the highest change trend slope has been generally observed in the western half of Hormozgan province, southern part of Kerman province, central, and northern parts of Sistan and Baluchistan province (*Fig. 4a*). It should be noted that the trends of these changes were not significant for all the studied stations at the 95% probability level, and only Bandar Abbas, Iranshahr, Gorgan, Minab, Bam, Yazd, Bandar-e Lengeh, Zabul, and Zahedan stations were significant, the locations of which are shown in *Fig. 4b*. In line with the results of this part of the study, *Namroodi et al.* (2021) reported an increasing trend in the heat wave number in Iran. In that study, they showed that about 85% of the studied stations in Iran had an increasing trend in the heat wave number. In addition, *Esmailnejad et al.* (2014) confirmed the same increasing trend in the heat wave number for Iran. It should be noted that the indicators used in these two studies to identify Iran's heat waves were very different from the present study.

Table 5. The average trend slope of the change of different characteristics of heat waves in a decade for the regional scale of the cental and southeastern parts of Iran

Different characteristics of heat waves	The average slope trend changes in a decade
Heat waves number	0.52
Heat waves duration	0.91
Heat waves frequency	2.61
Heat waves mean	0.1
Heat waves amplitude	0.4

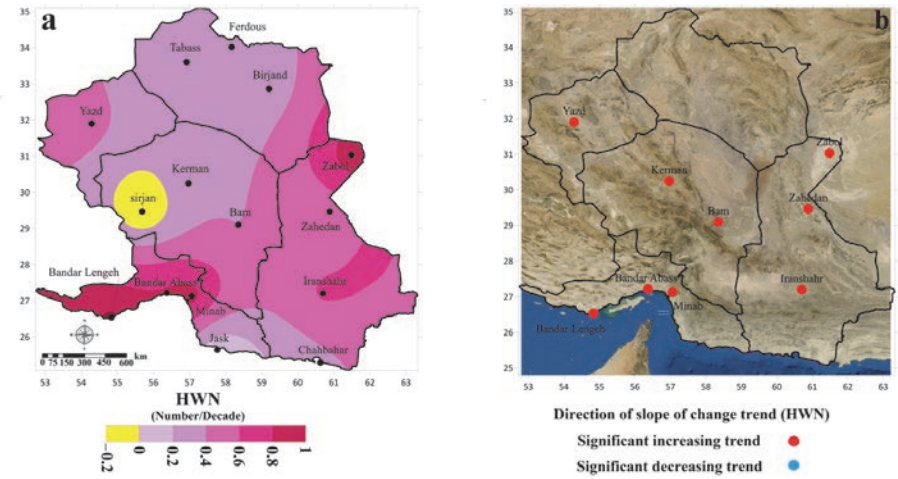

Fig. 4. (a) Spatial distribution of trend slope values of HWN changes in the cental and southeastern parts of Iran in terms of number per decade (1985–2018), and (b) the name and geographical location of the stations with significant trends at the probability level of 95% for the HWN in the cental and southeastern parts of Iran in terms of number per decade.

Another feature of heat waves is the heat wave duration, which is indicated by the abbreviation HWD. In this feature, the longest heat wave of each year is defined as the heat wave duration. A significant increasing trend is observed in this feature of the heat wave in the regional average of the cental and southeastern parts of Iran. Based on this increasing trend, 0.91 days will be added to the heat wave duration in the cental and southeastern parts of Iran every decade (*Table 5*). At the station scale, except for the Jask station, whose long-term change trend has been decreasing, the rest of the studied stations have had an increasing trend (*Fig. 5a*). All these trends, both decreasing and increasing ones, were not significant at the 95% probability level. Stations of Zabul (2.23 days per decade), Kerman (2.06 days per decade), Iranshahr (1.46 days per decade), Bam (1.33 days per decade), Tabas (1.3 days per decade), Bandar-e Lengeh (1.15 days per decade), and Chabahar (1.03 days per decade) were the seven stations whose changes were significant at the 95% probability level. The spatial distribution of these seven stations is shown in *Fig. 5b*. In addition, the spatial distribution map of trend slope values of this feature of the heat wave changes in the cental and southeastern parts of Iran does not show a specific spatial pattern, but the northern part of Sistan and Baluchistan province and the northern part of Kerman province can be named as two important centers of increasing changes, while the west coast of the Oman Sea is the most important center of decreasing changes (*Fig. 5a*).

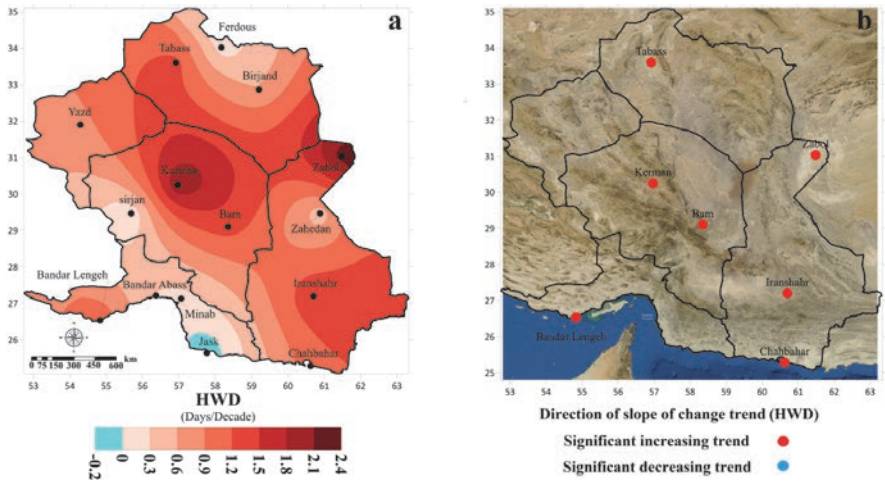

Fig. 5. (a) S Spatial distribution of trend slope values of HWD changes in the cental and southeastern parts of Iran in terms of day in the decade (1985–2018) and (b) the name and geographical location of the stations at the probability level of 95% probabilities for the duration of heat waves (HWD) in the cental and southeastern parts of Iran in terms of day in the decade

The HWF is the third feature of the heat waves whose long-term changes trend in the cental and southeastern parts of Iran were considered. HWF refers to the total number of days involved in the occurrence of various heat wave events in a year. The trend analysis of this feature of the heat waves on a regional scale for the cental and southeastern parts of Iran shows an increasing trend of 2.61 days per decade. This increasing trend has been significant at the 95% probability level (*Table 5*). The trends analysis at the station scale also shows that out of 15 stations studied, 13 stations have an increasing trend and 2 stations have a decreasing trend. The two stations, Ferdous and Jask, whose long-term changes trend has been decreasing, are not significant at the 95% probability level. Among the 13 stations with an increasing trend, the increasing trends of 11 stations have been significant at the probability level of 95%. In *Fig. 6b*, the geographical location of these stations is shown on a map of the cental and southeastern parts of Iran. The most observed changes among the studied stations belong to the stations of Zabul (5.23 days per decade), Bandar-e Lengeh (5.09 days per decade), Minab (4.52 days per decade), and Iranshahr (4.35 days per decade). *Fig. 6a* shows the spatial distribution of the slope values of the trend of the long-term change in HWF for the study area. According to this map, no specific spatial pattern of changes can be observed in the cental and southeastern parts of Iran, but two centers of decreasing changes can be observed in the southern and northern parts of the studied area, and several centers of increasing changes in the central and western parts of Hormozgan province, in the northern and central parts of Sistan and Baluchistan province (*Fig. 6a*).

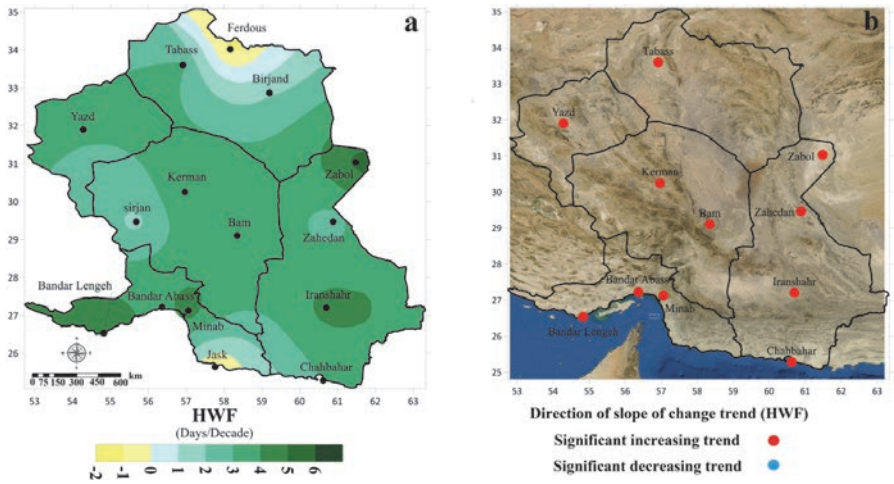

Fig. 6. (a) Spatial distribution of trend slope values of HWF changes in the cental and southeastern parts of Iran in terms of day in the decade (1985–2018), and (b) the name and geographic location of the stations with significant trends at the probability level of 95% for the heat waves frequency (HWF) in the cental and southeastern parts of Iran in terms of days per decade.

The long-term changes trend of HWM (average temperature of all heat wave events in one year) was analyzed both at a regional scale and at a station scale for the cental and southeastern parts of Iran. As mentioned, the regional average of this feature of the heat wave for the cental and southeastern parts of Iran was 41.2 °C (*Table 4*). At the regional scale, a significant increasing trend has been observed at the 95% probability level with a slope value of 0.1 °C in each decade. In other words, 0.1 °C is added every decade to the HWM in the cental and southeastern parts of Iran (*Table 5*). At the station scale, it was also observed that the trend of the long-term change in this feature of the heat wave was decreasing at the three stations of Sirjan, Bandar-e Lengeh, and Ferdous. The decreasing trend of these three stations also was not significant at the 95% probability level. Among the remaining 12 stations with increasing trends, 6 stations have confirmed their increasing trends at a probability level of 95%. *Fig. 7b* shows the location and geographical distribution of these 6 stations with a significant increasing trend. Stations of Bandar Abbas (0.15 °C per decade), Yazd (0.15 °C per decade), Zabul (0.15 °C per decade), Minab (0.12 °C per decade), Kerman (0.11 °C per decade) and Bam (0.11 °C per decade) had the highest values of the trend slope change among the studied stations. The spatial distribution map of trend slope values of this feature of the heat wave change was also drawn for the cental and southeastern parts of Iran (*Fig. 7a*). Based on this map, three main centers of increasing changes were observed in the northern part of Sistan and Baluchistan province, in the northern half of Yazd province, the central part of

Hormozgan province, and the cental part of Kerman province (*Fig. 7a*). The centers of decreasing changes can also be identified in the northern part of South Khorasan province, the western part of Kerman province, and the western part of Hormozgan province.

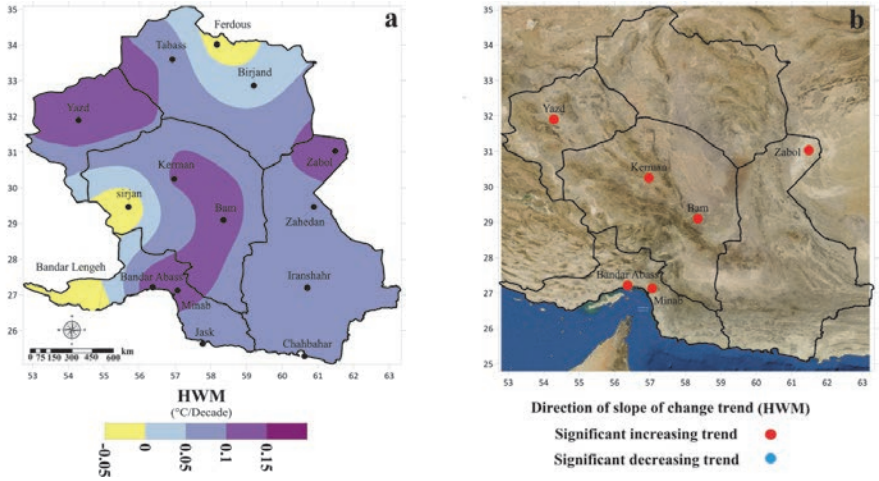

Fig. 7. (a) Spatial distribution of trend slope values of HWM changes in the cental and southeastern parts of Iran in terms of days per decade (1985–2018), and (b) the name and geographic location of the stations with significant trends at the probability level of 95% for the heat wave mean (HWM) in central and southeastern Iran in terms of days per decade.

HWA was the last feature of the heat wave whose long-term changes trend were analyzed. HWA is defined as the highest temperature and the hottest heat wave event in a year. Its regional average was previously calculated for the cental and southeastern parts of Iran, which is equal to 43.4 °C (*Table 4*). The trend analysis results of long-term changes in this feature of the heat waves on a regional scale show a trend slope of 0.4 °C in each decade for the cental and southeastern parts of Iran, which was also significant at the 95% probability level (*Table 5*). On a station scale, 14 stations have an increasing trend and one station has a decreasing trend. The stations of Bandar Abbas, Iranshahr, Kerman, Minab, Zahedan, and Zabul have significant trends for this characteristic of the heat waves at the probability level of 95% (*Fig. 8a*). Among all the studied stations, the highest trend slope change belongs to the three stations of Bandar Abbas (0.81 °C per decade), Minab (0.72 °C per decade), and Zabul (0.63 °C per decade). The spatial distribution of trend slope values of this feature of heat waves change indicates the existence of a specific spatial pattern in the cental and southeastern parts of Iran. In such a way, the trend slope changes are increasing from the

northwest to the southeast. Two very distinct spatial centers of the increasing change trend can be observed in the central part of Hormozgan province (Bandar Abbas and Minab stations) and in the northern parts of Sistan and Baluchistan province (Zabul station) (*Fig. 8b*).

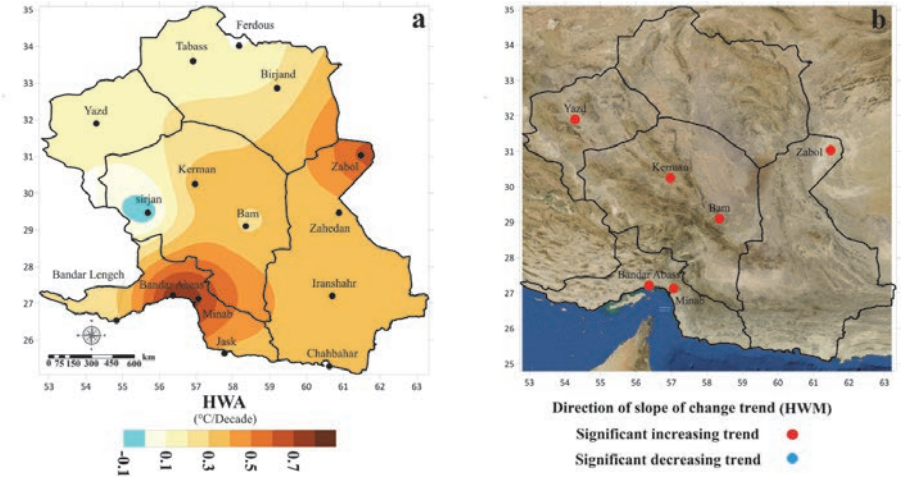

Fig. 8. (a) Spatial distribution of trend slope values of HWA changes in the cental and southeastern parts of Iran in terms of day per decade (1985–2018), and (b) the name and geographic location of the stations with significant trends at the probability level of 95% for HWA in central and southeastern Iran in terms of days per decade.

6. Conclusion

In this study, the climatology and long-term change trends of five different characteristics of heat waves in the cental and southeastern parts of Iran were analyzed using the EHF. The average of the highest number of heat wave events, and at the same time, the shortest average of their duration were observed in the stations located 492nt he coasts of the Oman Sea and the Persian Gulf, and on the Sistan plain in the eastern part of the studied area. The lowest average of heat wave number events and at the same time, the longest average of their duration was observed in the west of the studied area, which includes the two provinces of Kerman and Yazd. The average of the most intense heat waves did not follow specific spatial patterns in this region, and the average of the most intense heat waves in the northeastern (Tabas station), eastern (Zabul station), southeastern (Minab station), and central parts of Sistan and Baluchistan province (Iranshahr station) were observed in the point form. The high potential of this climatic hazard

for this part of Iran has been well shown due to the climatological results of the different characteristics of heat waves in the cental and southeastern parts of Iran.

In addition, the trend analysis of long-term changes in five different characteristics of heat waves in the cental and southeastern parts of Iran has indicated the intensifying of all these five characteristics for this part of Iran. On a regional scale, in each decade, 0.5 events have been added to the HWN in the cental and southeastern parts of Iran from 1985–2018. The long-term trend changes in the HWD also indicated an increase of 0.91 days per decade. The HWF has shown more drastic changes than other characteristics of heat waves. In every decade, 61.2 days have been added to the frequency of days contributing to the event of heat waves. This increase in HWF can be a serious warning for the occurrence of more and longer heat waves in the cental and southeastern parts of Iran. The regional average of HWM for the cental and southeastern parts of Iran is 41.2 degrees Celsius, which has increased by 0.1 °C every decade from 1985–2018. The average regional HWA for the studied area was about 43.4 degrees Celsius, and its long-term trend changes indicate an increase of 0.4 °C every decade.

The most drastic changes in the characteristics of heat waves in a station scale were observed in Zabul, Minab, Bandar Abbas, Bandar-e Lengeh, Yazd, Kerman, and Iranshahr stations, respectively. In the meantime, Zabul station in the northern part of Sistan and Baluchistan province has a more dangerous situation than other stations. The most important environmental factors in intensifying the various characteristics of heat waves in this part of Iran are the drying up of three international Hamon lakes, severe and long-term droughts, and the loss of vegetation. Stations located on the southeast coast of the study area such as Minab, Bandar Abbas, and Bandar-e Lengeh also experience the same situation as Zabul. Therefore, politicians and planners should pay special attention to the eastern and southeastern regions of the studied area, because they are the important centers of change in the characteristics of heat waves

These findings show the importance of choosing a suitable index for monitoring different characteristics of heat waves. The *EHF* index is a composite index based on minimum and maximum daily temperatures, which can be one of the suitable indices in this regard. Finally, it is necessary to consider the relationship of these changes with large-scale atmospheric forcing in future studies to gain a deeper understanding of the changes that occurred in the various characteristics of heat waves. In addition, it is necessary to study energy consumption and human health in this part of Iran, which has a dry and super-dry climate.

References

Alexander, L. and *Herold, N.*, 2016: ClimPACT2 Indices and Software University and of S. Wales. Sydney, Australia. https://climpact-sci.org/get-started/

Alijani, B., Mahmoudi, P., and *Kalim, D.M.*, 2015: Statistical Analysis of Climatic Histories of Desertification in Iran. *Geogr. Space 15*(51), 19–32.

Alijani, B., Mahmoudi, P., Salighe, M., and *Rigi Chahi, A.*, 2012a: Study of annual maximum and minimum temperature changes in Iran. *Geogr. Res. 26*, 101–122 (In Persian)

Alijani, B., Mahmoudi, P. and *Chogan, A.J.*, 2012b: A Study of annual and seasonal precipitation trends in Iran using a nonparametric method (Sen's slope estimator). *J. Climate Res. 3*(6), 23–42.

Alizadeh, A. and *Kamali, G.*, 2002: Effect of climate change of agricultural water use in Mashhad valley. *Geogr. Res. 2–3*,189–201.

AMS, 2000: Glossary of Meteorology, 2nd ed. Ed. *T. Glickman*. American Meteorological Society: Boston, MA.

Bidokhti, A.A. and *Ranjbar, A.A.*, 2003: Study of climatic effect of heat island for Tehran. In Third regional and first national conference on climate change, 21–23 October, Isfahan, Iran.

Choi, J. and *Meentemeyer V.*, 2002: Climatology of persistent positive temperature anomalies for the contiguous United States (1950–1995). *Phys. Geogr. 23*(3), 175–195. https://doi.org/10.2747/0272-3646.23.3.175

Darand, M., 2014: Recognition and Spatial-Temporal Analysis of Heat Waves in Iran. *Geogr. Develop. 12*(35), 167–180.

De Martonne, M., 1909: Traité de géographie physique – Climat – Hydrographic – Relief du sol – Biogéographie. Paris: Li-brairie Armand Colin. (In France)

Esmailnejad, M., Khosravi, M., Alijani, B. and *Masoodian, S.A.*, 2014: Identification heat waves of Iran. *Geogr. Develop. 11*(33), 39–53.

Field, C.B., 2012: Managing the risks of extreme events and disasters to advance climate change adaptation: Special report of the intergovernmental panel on climate change. Cambridge University Press. https://doi.org/10.1017/CBO9781139177245

Halabian, A.H., Poorshahbazi, J. and *Soltanian, M.*, 2017: Evaluation of the seasonal maximum and minimum temperature change of Iran. *Geogr. Plann. Space, 7*(23), 1–10.

Hatvani-Kovacs, G., Belusko, M., Pockett, J. and *Boland, J.*, 2016: Can the Excess Heat Factor Indicate Heatwave-Related Morbidity? A Case Study in Adelaide, South Australia. *EcoHealth 13*, 100–110. https://doi.org/10.1007/s10393-015-1085-5

Höppe, P., 1999: The physiological equivalent temperature - a universal index for the biometeorological assessment of the thermal environment. *Int. J. Biometeorol. 43*(2), 71–75. https://doi.org/10.1007/s004840050118

IPCC, 2013, Summary for Policymakers, In: Climate change 2013: the physical science basis. Contribution of Working Group I to the Fifth Assessment Report of the Intergovernmental Panel on Climate Change. (eds. *T.F. Stocker, D. Qin, G.-K. Plattner, M. Tignor, S.K. Allen, J. Boschung, A. Nauels, Y. Xia, V. Bex, P.M. Midgley*), Cambridge University Press, Cambridge, United Kingdom and New York, NY, USA, 3–29.

Jahanbaksh, S., Mohammadi, G., Rashedi, S. and *Hoseini Sadr, A.*, 2018: Study of the Cold Period Monthly Minimum Temperature Trend in Northwest of Iran. Geogr.Plann. 21(62), 79–96.

Jegasothy, E., McGuire, R., Nairn, J., Fawcett, R. and *Scalley, B.*, 2017: Extreme climatic conditions and health service utilisation across rural and metropolitan New South Wales. *Int. J. Biometeorol. 61*, 1359–1370. https://doi.org/10.1007/s00484-017-1313-5

Khoshakhlagh, F., Gharibi, E., and *Shafiei, Z.*, 2011: The study of the lowest temperature changes in Iran. *Geogr. Environ. Plann. J. 42*(2), 199–216.

Li, X-X., Yuan, C., and *Hang, J.*, 2022: Heat Wave Trends in Southeast Asia: Comparison of Results from Observation and Reanalysis Data. *Geophys. Res. Lett. 49*(4), 1–11. https://doi.org/10.1029/2021GL097151

Mahmoudi, P. and *Rigi Chahi, A.*, 2019: Climate Change Impact on Spatial and Temporal Distribution of Precipitation in Iran. 6th International Regional Conference of Climate Change, Nov. 18–19, Tehran, Iran.

Mahmoudi, P., Kalim, D.M., and *Amirmoradi, M.R.*, 2011: Investigation of Iran Vulnerability Trend to Desertification with Approach of Climate Change. International Conference on Environmental Science and Development—ICESD, January 7–9, Mumbai, India.

Mahmoudi, P., Mohammadi, M. and *Daneshmand, H.*, 2019: Investigating the trend of average changes of annual temperatures in Iran. *Int. J. Environ. Sci. Technol. 16*, 1079–1092. https://doi.org/10.1007/s13762-018-1664-4

Masoudian, S.A., 2004: Temperature trends in Iran the last half century. *Geogr. Develop 2*, 89–106.

Montazeri, M., 2014: Time-Spatial Investigation of Iran's Annual Temperatures During 1961-2008.*Geogr. Develop. 12*(36), 12–36. https://doi.org/10.1176/ps.12.1.36

Nairn, J.R. and *Fawcett, R.J.B.*, 2013: Defining heatwaves: heatwave defined as a heat- impact event servicing all community and business sectors in Australia. Technical Report 060, Collaboration for Australian Weather and Climate Research (CAWCR), 2013.

Nairn, J., Fawcett, R., and *Ray, D.*, 2009: Defining and predicting excessive heat events, a national system. Proceedings of the CAWCR Modelling.

Nairn, J., Ostendorf, B., and *Bi, P.*, 2018: Performance of Excess Heat Factor Severity as a Global Heatwave Health Impact Index. *Int. J. Environ. Res. Publ. Health*. *15*(11), 2494. https://doi.org/10.3390/ijerph15112494

Namroodi, M., Hamidianpour, M., and *Poodineh, M.*, 2021: Spatio-temporal analysis of changes in heat and cold waves across Iran over the statistical period 1966–2018. *Arabian J. Geosci. 14*, 857. https://doi.org/10.1007/s12517-021-07161-9

Oliveira, A., Lopes, A. and *Soares, A.*, 2022: Excess Heat Factor climatology, trends, and exposure across European Functional Urban Areas. *Weather Climate Extr. 36*, 100455. https://doi.org/10.1016/j.wace.2022.100455

Perkins, S.E. and *Alexander, L.V.*, 2013: On the Measurement of heatwaves. *J. Climate 26*, 4500–4517. https://doi.org/10.1175/JCLI-D-12-00383.1

Perkins-Kirkpatrick, S.E. and *Lewis, S.C.*, 2020: Increasing trends in regional heatwaves. *Nat. Commun. 11*, 3357. https://doi.org/10.1038/s41467-020-16970-7

Robinson, P., 2001: On the definition of a heat wave. *J. Appl Meteorol 40*, 762–775. https://doi.org/10.1175/1520-0450(2001)040<0762:OTDOAH>2.0.CO;2

Rousi, E., Kornhuber, K., Beobide-Arsuaga, G., and Luo, F. and Coumou, D. (2022) Accelerated western European heatwave trends linked to more-persistent double jets over Eurasia. *Nat. Commun. 13*, 3851. https://doi.org/10.1038/s41467-022-31432-y

Sari Sarraf, B., Khorshiddoust, A.M., Mahmoudi, P., and *Daraei, M.*, 2018: Impacts of climate change on the growing season in the Iran. *Italian J. Agrometeorol. 3*, 15–30.

Scalley, B.D., Spicer, T., Jian, L., Xiao, J., Nairn, J., Robertson, A. and *Weeramanthri, T.*, 2015: Responding to heatwave intensity: Excess Heat Factor is a superior predictor of health service utilisation and a trigger for heatwave plans. *Australian New Zealand J. Publ. Health 39*, 582–587. https://doi.org/10.1111/1753-6405.12421

Sen, P.K., 1968: Estimates of the Regression Coefficient Based on Kendall's Tau. *J. Amer. Stat. Assoc. 63*(324), 1379–1389. https://doi.org/10.1080/01621459.1968.10480934

Statistical Center of Iran, 2016: Census 2016 - General Results. https://www.amar.org.ir/english/Population-and-Housing-Censuses/Census-2016-General-Results

Stocker, T.F., Qin, D., Plattner, G-K., Tignor, M., Allen, S.K., Boschung, J., Nauels, A., Xia, Y., Bex, V. and *Midgley, P.M.*, 2013: Climate change 2013: The physical science basis. Intergovernmental Panel on Climate Change, Working Group I Contribution to the IPCC Fifth Assessment Report (AR5)(Cambridge Univ Press, New York).

Tavosi, T., Mahmoudi, P., and *Moghadam, F.S.*, 2010: Comparison of spatial spreading of arid and semi-arid climates in Iran during 1976-2005, *Iranian J. Range Desert Res. 17*(1), 94–105.

Theil, H. (1950) A rank-invariant method of linear and polynomial regression analysis. Indagationes Mathematicae, 1(2), 85–89.

Yin, G., Yang, Y., Chen, X., Yue, X., Liu, Y. and *Xin, Y.*, 2022: Changes in global heat waves and its socioeconomic exposure in a warmer future. *Climate Risk Manage. 38*, 100459. https://doi.org/10.1016/j.crm.2022.100459

Zare, A., Hasheminejad, N., Elahi Shirvan, H., Hemmatjo, R., Sarebanzadeh, K. and *Ahmadi, S.*, 2018: Comparing Universal Thermal Climate Index (UTCI) with selected thermal indices/environmental parameters during 12 months of the year. *Weather Climate Extremes, 19*, 49–57. https://doi.org/10.1016/j.wace.2018.01.004

IDŐJÁRÁS

VOLUME 128 * 2024

BUDAPEST, HUNGARY

AUTHOR INDEX

TABLE OF CONTENTS

I. papers

SUBJECT INDEX

U

V

W

Y

Z

Z

INSTRUCTIONS TO AUTHORS OF *IDŐJÁRÁS*

The purpose of the journal is to publish papers in any field of meteorology and atmosphere related scientific areas. These may be

- research papers on new results of scientific investigations,
- critical review articles summarizing the current state of art of a certain topic,
- short contributions dealing with a particular question.

Some issues contain "News" and "Book review", therefore, such contributions are also welcome. The papers must be in American English and should be checked by a native speaker if necessary.

Authors are requested to send their manuscripts to

Editor-in Chief of IDŐJÁRÁS
P.O. Box 38, H-1525 Budapest, Hungary
E-mail: journal.idojaras@met.hu

including all illustrations. MS Word format is preferred in electronic submission. Papers will then be reviewed normally by two independent referees, who remain unidentified for the author(s). The Editor-in-Chief will inform the author(s) whether or not the paper is acceptable for publication, and what modifications, if any, are necessary.

Please, follow the order given below when typing manuscripts.

Title page should consist of the title, the name(s) of the author(s), their affiliation(s) including full postal and e-mail address(es). In case of more than one author, the corresponding author must be identified.

Abstract: should contain the purpose, the applied data and methods as well as the basic conclusion(s) of the paper.

Key-words: must be included (from 5 to 10) to help to classify the topic.

Text: has to be typed in single spacing on an A4 size paper using 14 pt Times New Roman font if possible. Use of S.I. units are expected, and the use of negative exponent is preferred to fractional sign. Mathematical formulae are expected to be as simple as possible and numbered in parentheses at the right margin.

All publications cited in the text should be presented in the *list of references*, arranged in alphabetical order. For an article: name(s) of author(s) in Italics, year, title of article, name of journal, volume, number (the latter two in Italics) and pages. E.g., *Nathan, K.K.,* 1986: A note on the relationship between photosynthetically active radiation and cloud amount. *Időjárás 90,* 10–13. For a book: name(s) of author(s), year, title of the book (all in Italics except the year), publisher and place of publication. E.g., *Junge, C.E.,* 1963: *Air Chemistry and Radioactivity.* Academic Press, New York and London. Reference in the text should contain the name(s) of the author(s) in Italics and year of publication. E.g., in the case of one author: *Miller* (1989); in the case of two authors: *Gamov* and *Cleveland* (1973); and if there are more than two authors: *Smith et al.* (1990). If the name of the author cannot be fitted into the text: *(Miller,* 1989); etc. When referring papers published in the same year by the same author, letters a, b, c, etc. should follow the year of publication. DOI numbers of references should be provided if applicable.

Tables should be marked by Arabic numbers and printed in separate sheets with their numbers and legends given below them. Avoid too lengthy or complicated tables, or tables duplicating results given in other form in the manuscript (e.g., graphs). *Figures* should also be marked with Arabic numbers and printed in black and white or color (under special arrangement) in separate sheets with their numbers and captions given below them. JPG, TIF, GIF, BMP or PNG formats should be used for electronic artwork submission.

More information for authors is available: journal.idojaras@met.hu

Published by the HungaroMet Hungarian Meteorological Service

Budapest, Hungary

ISSN 0324-6329 (Print)

ISSN 2677-187X (Online)